Computer based Simulation of Optical Wireless Communications for the Development of Optimized Error Protection and Correction Schemes

Bernhard Epple

München 2017

Computer based Simulation of Optical Wireless Communications for the Development of Optimized Error Protection and Correction Schemes

Bernhard Epple

Dissertation
an der Fakultät für Mathematik, Informatik und Statistik
der Ludwig–Maximilians–Universität München

vorgelegt von
Bernhard Epple
aus Lindau

München, den 21. Dezember 2017

Erstgutachter: Prof. Dr. Hans Jürgen Ohlbach
Zweitgutachter: Christopher C. Davis
Tag der mündlichen Prüfung: 15. Oktober 2018

Eidesstattliche Versicherung

(Siehe Promotionsordnung vom 12.07.11, § 8, Abs. 2 Pkt. .5.)

Hiermit erkläre ich an Eidesstatt, dass die Dissertation von mir selbstständig, ohne unerlaubte Beihilfe angefertigt ist.

Epple, Bernhard

Name, Vorname

München, 30.11.2017

Ort, Datum

Bernhard Epple

Unterschrift Doktorand/in

Formular 3.2

Contents

List of Figures

List of Tables

Nomenclature

${}_1F_2$	A generalized hypergeometric function
A	On-axis amplitude
α	parameter of gamma-gamma distribution OR smoothing factor for calculation of $SRTT$ in Karn's algorithm
B_{Rx}	ARQ-SR receive buffer size
B_{Tx}	ARQ-SR transmit buffer size
β	parameter of gamma-gamma distribution OR smoothing factor for calculation of RTO in Karn's algorithm
C_{n}^2	Refractive Index Structure Constant
D_{Rx}	Diameter of the receiving aperture
δ	number of correctable symbols within an FEC code word
Δt_{ACK}	Time between reception of ACK frames in EPC for OWC
Δt_{max}	Maximum delay
Δt_{tx}	Time between transmission of data frames in EPC for OWC
$\boldsymbol{e}$	error (vector)
e_{rel}	relative error
$e_{\mathrm{RTT},i}$	prediction error for RTT
$\mathrm{erf}\,(x)$	Gauss error function of x
$\exp(x)$	natural exponential function of x (e^x)
F_0	Phase front curvature radius at transmitter
f_{c}	(Bessel) Filter cut-off frequency
f_{s}	Sampling frequency
FER_{res}	residual frame erasure rate
$\gamma(a, x)$	lower incomplete gamma function
$\Gamma(z)$	gamma function
h	height above ground
h_l	height above ground at position l
i	$\sqrt{-1}$
I	On-axis irradiance
k	parameter of gamma distribution OR Wave number of beam wave ($= 2\pi/\lambda$) OR

	number of data symbols in an FEC code word
$\mathrm{K}_n(x)$	Modified Bessel function of the second kind and order n
L	Link distance between transmitter and receiver in m
l	Position within the beam l meter away from transmitter OR length of user data inside a frame
l'	Protocol overhead within one frame
l_0	Inner scale of turbulence in m
L_0	Outer scale of turbulence in m
l_B	Position of beam waist in m
λ	Wavelength of a beam in m
Λ_IG	Shape parameter of the inverse Gaussian distribution function
Λ	Fresnel ratio of Gaussian beam
Λ_0	Fresnel ratio of Gaussian beam at transmitter
$\ln(x)$	natural logarithm of x
μ	mean value OR parameter of Gaussian distribution function OR parameter of log-normal distribution function OR parameter of inverse Gaussian distribution function
n	(Bessel) Filter order OR code word length of FEC code
N	maximum number of retransmissions in EPC for FSO
Ω_f	Focusing parameter
P	Optical power
P_Rx	Optical received power
P_T	Threshold parameter used within the gamma-gamma CDF
r	ratio β/α for the gamma-gamma distribution parameters
RTT	Round trip time
$\mathrm{Re}(x)$	real part of the complex number x
σ	variance OR parameter of the log-normal distribution function
σ_I^2	Scintillation index
σ_IG^2	Scintillation index for Gaussian beam wave
σ_P^2	Power scintillation index
σ_R^2	Rytov variance
σ_RG^2	Rytov variance for Gaussian beam wave
s	symbol size of FEC code
s_i	sample of RTT measurement

$\widehat{s_i}$	estimated value of RTT
$\Phi(x)$	Gaussian distribution function
$\dot{\widehat{s_i}}$	first derivative of $\widehat{s_i}$ over time
$\ddot{\widehat{s_i}}$	second derivative of $\widehat{s_i}$ over time
$SRTT_i$	smoothed RTT in Karn's algorithm OR predicted RTT in EPC for OWC
$\dot{SRTT}_i$	first derivative of $SRTT_i$ over time
$\ddot{SRTT}_i$	second derivative of $SRTT_i$ over time
t	simulation time
$t_{\mathrm{ACK},i}$	Timestamp for reception of i-th ACK frame in EPC for OWC
t_{f}	Duration of a fade
t_{s}	Duration of a surge
$t_{\mathrm{tx},i}$	Timestamp for transmission of i-th data frame in EPC for OWC
θ	parameter of gamma distribution
θ_{B}	Beam divergence ($1/e^2$ half) angle in rad
θ_{3dB}	Beam divergence full width half maximum angle in rad
Θ	Curvature parameter of Gaussian beam
Θ_0	Curvature parameter of Gaussian beam at transmitter
V	Visibility in m
v_{w}	root mean squared orthogonal wind velocity along propagation path in m/s
W_0	Beam radius at the transmitter in m
W_{B}	Beam radius in free-space at the waist in m

Abbreviations

ACK	Acknowledgment (of a received ARQ frame)
AMS-IX	Amsterdam Internet Exchange
ARQ	Automatic Repeat reQuest
ARQ-SR	selective-repeat ARQ
BEP	Bit error probability
BER	Bit error ratio
CDF	Cumulative distribution function
COTS	Commercial off the shelf
CWEP	Code word error probability
CRC	Cyclic redundancy check
DES	Discrete event simulation
DLR	German Aerospace Center (Deutsches Zentrum für Luft- und Raumfahrt e.V.)
DSL	Digital subscriber line
ECDF	Empirical cumulative distribution function
EDFA	Erbium-doped fiber amplifier
EPC	Error protection and correction
EPDF	Empirical probability distribution function
FEC	Forward error correction
FER	Frame erasure rate
FMT	Fading mitigation technique
FPS	Frames per second
FSOC	Free-space optical communications
FWHM	Full width half maximum
G	Gamma distribution
GG	Gamma-gamma distribution
$HV_{5/7}$	Hufnagel-Valley 5/7 model
IETF	The Internet Engineering Task Force
IG	Inverse Gaussian distribution
IM/DD	Intensity modulation with direct detection
ITU	International Telecommunication Union
KS-test	Kolmogorov-Smirnov test

LDPC	Low-density parity check (code)
LN	Log-normal distribution
LPC	Link parameter calculation
MAC	Media access control
N	Normal (or Gaussian) distribution
NACK	Negative acknowledgment (of a lost ARQ frame)
NRZ-OOK	Non return to zero on-off keying
OGS-OP	Optical Ground Station Oberpfaffenhofen, operated by DLR
OOK	On-off keying
OSI	Open System Interconnection
OWC	Optical wireless communications
PDF	Probability density function
PSD	Power Spectral Density
QoS	Quality of service
RFC	Request for comments
rms	root mean squared
RF	Radio frequency
RS	Reed-Solomon (code)
Rx	(optical) Receiver
SCP	Secure Copy (Protocol)
SEP	Symbol error probability (for an FEC symbol)
SN	Sequence number
SWaP	Size, weight, and power
TCP/IP	Transmission Control Protocol/Internet Protocol
TEM_{00}	Transverse electromagnetic mode of the lowest order
TDD	Time delayed diversity
Tx	(optical) Transmitter
UAV	Unmanned aerial vehicle
VLAN	Virtual local area network
VLC	Visible light communications

Acknowledgements

First of all I would like to express my very great appreciation to Prof. Dr. Hans Jürgen Ohlbach for supervising this thesis and giving me the opportunity to realize this work as external PhD student. My grateful thanks are also extended to Prof. Christopher C. Davis for his guidance and encouragement of my research work. The many discussions we had helped me to understand the key elements of turbulence theory and to structure this work.
My special thanks go to my former colleagues from German Aerospace Center (DLR), Hennes Henniger, Florian Moll, Martin Brechtelsbauer, Alexandra Ludwig, Dr. Giuliano Garrammone, Dr. Nicolas Perlot, Dr. Markus Knapek, Joachim Horwath. Thank you for everything we experienced together when setting up experimental free-space optical links through out Europe and publishing the results together.
From this group I especially want to thank Hennes for the continued joined work on optical communications after my time at DLR and everything you taught me about hardware development and forward error correction. In that context I also want to thank Dr. Hubertus Haan for the opportunity to take additional measurements during commercial demonstration campaigns of optical free-space communications.
Finally I want to thank my wife Silke for her support during times I was working on this thesis and her willingness to proof read this work.

Abstract

Commercial application of optical wireless communications is currently limited to the area of short range near ground connections, like networks between buildings over a few kilometers. For other areas of application, like data downlinks from flying platforms, demonstrations have been done, but commercial systems for long range communications over many kilometers are not yet available for general usage. The biggest challenge for reliable optical communications is to mitigate the fading of the received optical signal. A possible solution is to implement error protection and correction mechanisms for securing transmitted data. In this dissertation a simplified channel model is developed which can be used for computer based simulation. This simplified channel model is then used for the evaluation of error protection and correction mechanisms applied to the optical wireless channel. Finally generally proposed communication scenarios are evaluated if optical wireless communication is possible, based on the developed channel model. The results show that the combination of forward error correction and selective repeat automatic repeat request protocols can be used to realize reliable optical communication links in all proposed scenarios, even the most challenging ones. The back channel traffic for automatic repeat request protocols leads to a significant reduction of the transmittable user data rate in worst-case scenarios and has to be taken into account for the system design. The developed simulation approach can be used to optimize protocols for the optical wireless channel in order to reduce the load on the back channel and the over all required memory.

Zusammenfassung

Die kommerzielle Anwendung der optischen Freiraumkommunikation ist gegenwärtig auf den Bereich der bodennahen Kurzstreckenverbindungen mit wenigen Kilometern Länge begrenzt, beispielsweise Netzwerkverbindung zwischen Gebäuden. In anderen Anwendungsbereichen, z.B. Datendownlinks von fliegenden Plattformen, wurden zwar Technologiedemonstrationen durchgeführt, jedoch sind für solche Langstreckenverbindungen keine alltagstauglichen kommerziellen Systeme verfügbar. Die größte Herausforderung für zuverlässige optische Kommunikation ist die Kompensation der Signalschwankungen des empfangenen optischen Signals. Eine mögliche Lösung für dieses Problem ist die Implementierung von Fehlersicherungs- und Fehlerkorrekturmechanismen, um die Datenübertragung abzusichern. In dieser Dissertation wird ein vereinfachtes Kanalmodell entwickelt, welches für die Simulationen mittels Computern geeignet ist. Dieses vereinfachte Modell wird anschließend für die Bewertung von Fehlersicherungs- und Fehlerkorrekturmechanismen für den optischen Kanal verwendet. Abschliessend wird basierend auf dem entwickelten Kanalmodell der mögliche Einsatz von optischer Freiraumkommunikation in häufig vorgeschlagenen Szenarien untersucht. Die Ergebnisse zeigen, dass die Kombination von Vorwärtsfehlerkorrektur und Protokollen mit selektiver Wiederholung und automatischer Wiederholungsanfrage geeignet ist, um zuverlässige optische Kommunikationsverbindungen in allen vorgeschlagenen Szenarien zu realisieren, selbst in den anspruchsvollsten. Die Datenübertragung auf dem Rückkanal von Protokollen mit automatischer Wiederholungsanfrage führt im schlechtesten Fall zu einer signifikanten Reduzierung der übertragbaren Nutzdatenrate und muss bei der Systemauslegung berücksichtigt werden. Mit dem entwickelten Simulationsansatz können Protokolle für den optischen Funkkanal optimiert werden, um die Belastung des Rückkanals zu reduzieren und um den allgemeinen Speicherbedarf zu reduzieren.

Chapter 1

Introduction

1.1 Optical Wireless Communications

Optical wireless communications (OWC), also called free-space optical communications (FSOC), is an ongoing research topic since the invention of the laser in the 1960s. While optical communications had great success using optical fibers, OWC was often proposed to be the next big thing in communications, but also often disappointed expectations. The reason why interest in OWC never settled down is that it has several advantages over radio frequency (RF) based communications. The most important ones are:

- larger available bandwidth (over ten times in commercial systems)
- smaller size, weight and power (SWaP) footprint
- no regulation of optical frequencies
- less interference problems
- hard to jam for attackers
- allows for hidden communications
- more secure against eaves dropping

But these advantages come with additional cost as the performance of OWC is limited by weather conditions like fog, snow or clouds as well as by atmospheric effects. These limitations are the main reason why commercial application of OWC is currently limited to the field of the so called last-mile connections. In this area, cost-effective components, originally developed for optical fiber communications, can be used to establish OWC links over the

distance of a few kilometers. Most of these systems use intensity modulation with direct detection (IM/DD) and on-off keying (OOK) where a binary 1 is encoded as turning the optical source on, and a binary 0 is encoded as turning the optical source off. The practical application of OWC is not limited to the last mile terrestrial links. Other often proposed scenarios include links between flying platforms, e.g. satellites, high altitude platforms (HAP) or unmanned aerial vehicles (UAV), and from flying platforms to ground based platforms. Recent research activities are focused on extending the achievable communication range of OWC systems to over several tens to hundreds of kilometers, as it already has been done within some projects. For example in LCT-Marine [1] a link between a mobile terminal at the shore and a ship was established over 20 km, in CAPANINA [2] a link between a transportable ground station and a stratospheric balloon was established over a distance of up to 63 km, in ARGOS [3], IRON-T2 [4] and ORCA [5] links between ground terminals and aircrafts were demonstrated with link distances of over 100 km and in KIODO [6] a downlink from a low Earth orbiting satellite to ground was established for link distances greater 2000 km. In these projects several measurements concerning the propagation of the optical beam through the atmosphere were conducted and these measurements have shown that the biggest challenge for long-range OWC links using IM/DD is to mitigate the fading of the received optical signal. A brief overview on the current state of OWC technology and commercial projects is given in [7].

1.2 Fading Mitigation for the Optical Wireless Channel

Random variations in the refractive index of the turbulent atmosphere along the propagation path cause strong fluctuations in the received optical power, called scintillation. For long-range links these fluctuations can have a peak-to-peak amplitude of over 40 dB [4, 5], where especially the drops in received power (fades) result in an increase of the bit error ratio (BER) at the receiver or even a complete loss of the communication signal. Although similar effects are known from RF based communications, some special characteristics of the optical wireless channel do not allow for a reuse of already developed fading mitigation techniques (FMT). On the optical channel, fades can have durations of over 100 ms and affect thousands of bits for the commonly used high data rates of several Gbit/s. Most often it is tried to solve the fading problem on the physical layer [8]. One common approach is to create multiple channels with statistically independent fading behavior, so called diversity

techniques. The diversity can be achieved by using different wavelengths [9], multiple transmitters [10], multiple receivers [11], or combination of these approaches. The combined usage of statistically independent channels can reduce the occurrence probability of fades, but it is not possible to guarantee an error free channel due to some technical limitations. Most often SWaP constraints limit the number of transmitters and receivers as well as the spatial separation between the components. Another FMT approach is aperture averaging [12]. When the optical signal is collected by the aperture of the receiver, the scintillation of the incoming signal is averaged out over the whole area of the aperture. With an increase of the size of this aperture, the averaging effect increases and the scintillation of the received signal is reduced; but again SWaP constraints limit the implementable size of the receiving aperture. Due to the limitation of FMT on the physical layer it is necessary to address the fading problem also on higher communication layers. For the higher layers, there are two different approaches possible. The first approach is the application of coding to the transmitted data. Commonly used coding techniques are forward error correction (FEC) [13, 14] or time delayed diversity (TDD) [15]. TDD is a simple retransmission technique were the transmitted data is buffered at the sender and retransmitted after a certain time interval. Because the number of retransmissions and the retransmit time interval are fixed for every system, this scheme has two major disadvantages. First, this transmission scheme becomes inefficient if the channel experiences less fading than expected and second it will not give good performance if the channel conditions are worse than expected. For FEC the transmitted data is split into small blocks and some redundant data is added to this block for transmission. The added data allows to recover some errors in the data block at the receiver. If there are more errors in the received data than the chosen code can recover, the whole data block is lost. Because of the long fades there will be strong error burst in the received data, so that the decoding of the data will often fail [13]. For this reason FEC should be implemented on the packet layer, where it is possible to build longer blocks based on packets instead of bits. The generation of long coded blocks introduces a fixed delay into the communication flow which might not be acceptable for some services. The second technique asides coding is the application of Automatic Repeat reQuest (ARQ) protocols [16, 17]. Implementation of ARQ requires bidirectional communication on the channel. Each transmitted data packet is labeled with an identifier. This identifier can be used by the receiver to signal lost packets back to the transmitter and the transmitter then can retransmit the lost packets. ARQ protocols are a very efficient way to deal with lost data because only the lost data is retransmitted, and if the channel does not corrupt any data, the protocol automatically adjusts to the good chan-

nel conditions and no retransmissions are done at all. Also hybrid systems, where coding and ARQ are combined can be used. The main advantage of coding and ARQ over physical layer mitigation techniques is that these mitigation techniques have only little influence on the SWaP footprint of the communication terminals.

1.3 Dissertation Contributions

As mentioned in the previous sections, there have been many projects, demonstrating the feasibility of optical long-range links. For these prototyped links it was observed that the mitigation of the signal fading has major impact on communications. Because these projects focused on showing the technical feasibility, they were focused on the development of the physical layer and only used physical layer mitigation techniques. Higher communication layers were not implemented and the feasibility was proven by providing information about the BER of the physical layer. In this dissertation focus is laid on FMT on higher layers, especially on ARQ protocols because of their higher efficiency. For the evaluation of higher layer FMT it is necessary to use a channel model that can be applied to a wide range of scenarios, which is simple in its application and which does not require too much processing time. Existing channel models are mainly characterized by a large number of required input parameters for modeling the atmosphere and a long processing time when used for simulation. This is because the propagation of the laser beam is calculated in an iterative, time consuming split step approach [18, 19, 20]. With the split step approach only a few, well defined links can be simulated within a limited time frame and no general analysis is possible. To be able to analyze FMT in a more general way, several measurements have been done in various scenarios, and a simplified channel model is derived from these in this work. Based on the derived channel model and its given parameterization simulations of a wide range of OWC links can be done in real-time or faster. The proposed model is used in this work to develop a FMT scheme optimized for OWC long-range systems. The analysis of FMT in the following is limited to the field of inner atmospheric links, like inter-aircraft links or aircraft-to-ground links, using IM/DD. Other applications of OWC like inter-satellite links or the emerging field of indoor visible light communications (VLC) are not taken into account, although the presented results should be extendable into these areas.

1.4 Dissertation Organization

The remainder of this dissertation is organized as follows.

Chapter 2 accumulates the theory for laser beam propagation through the atmosphere. Based on this information it is possible to calculate all important link characteristics for OWC links.

For Chapter 3, the theory from Chapter 2 is used to develop a simplified channel model for OWC. For this a general description of OWC systems is given before results from several measurement campaigns are used to derive the simplified channel model.

In Chapter 4 a simulation system is described, which incorporates formulae from Chapter 2 and the channel model from Chapter 3. The results produced by this simulation system are validated against the original measurements used for development of the channel model. Finally, parameterization for several communication scenarios is given at the end of Chapter 4.

Chapter 5 focuses on error protection for OWC. First an overview on state of the art error protection and correction mechanisms are given, and then the required adaptation of these methods for the optical wireless channel are discussed based on the findings from the previous chapters.

Chapter 6 describes the implementation of a simulator that is based on the results from Chapter 4 and Chapter 5. This simulator can be used for simulation of any type of higher layer communication over optical wireless channels.

Chapter 7 evaluates the scenarios where OWC can be successfully deployed. For this OWC simulations for all scenarios described in Chapter 4 are done and evaluated against link layer requirements given by the International Telecommunication Union (ITU).

The dissertation is then concluded in Chapter 8 with the summary of the results from the described evaluation and a discussion about its application for OWC systems, including potential future work on this field.

Most of the underlying research done for this thesis has previously been published. Table 1.1 gives an overview of these publications and associates them with the appropriate chapters. Within each chapter the relevant findings of this preparational work is referenced accordingly.

Table 1.1: Listing of previously published work

Title	Chapter	Reference
Impact of Ground Profile on Scintillation Index for High-Altitude Optical Wireless Links	2	[21]
Rural Optical-Propagation Measurements	3	[22]
Simplified Channel Model for Simulation of Free-Space Optical Communications	3	[23]
Optical Satellite Downlinks to Optical Ground Stations and High-Altitude Platforms	3	[24]
Discussion on Design Aspects for Free-Space Optical Communication Terminals	3	[25]
Performance Analysis of Optical Wireless Communications on Long-Range Links	3	[26]
Maritime Mobile Optical-Propagation Channel Measurements	3	[1]
Broadband Communications for Aeronautical Networks: The ATENAA Outer Optical Link Validation	3	[27]
Optical High-Capacity Satellite Downlinks via High-Altitude Platform Relays	3	[28]
Broadband Backhaul Communication for Stratospheric Platforms: The Stratospheric Optical Payload Experiment (STROPEX)	3	[2]
Performance optimization of free-space optical communication protocols based on results from FSO demonstrations	4	[29]
A Cross-Layer Approach to mitigate Fading on Bidirectional Free Space Optical Communication Links	5	[30]
Coding Techniques to mitigate Fading on Free-Space Optical Communication Links	5	[31]
An Error Protection Protocol for user-transparent bridging of Fast Ethernet data transmission over the optical fading channel in an Aeronautical environment	5	[16]
Implementation concepts for a bridging protocol for the high data rate slow-fading Free-Space Optical Channel	5	[17]
Mobil FSO activities in Europe and fading mitigation approaches	5	[32]

Chapter 2

Laser Beam Propagation

In this chapter the theory for laser beam propagation through the atmosphere is accumulated. Based on the given information and formulae it is possible to calculate all important link characteristics for OWC links. In the first subsection a quick overview on beam models is given together with relevant formulae to calculate the most important beam characteristics. In the following subsections more information about the propagation of the laser beam and the impact of the atmosphere is given.

2.1 Laser Beam Models

For describing the propagation of laser beams different beam models have been developed. The most often used ones are plane wave, spherical wave and Gaussian beam waves [33, 34, 35].
The plane wave model describes the optical beam as an unbounded wave with constant amplitude and phase and is often used by astronomers for describing the light from stars arriving on the Earth's surface. The wave front is modeled for this as infinite parallel planes that propagate orthogonal to the phase velocity vector.
The spherical wave model uses an unbounded wave propagating in all directions from a single point. The amplitude decreases with the propagation distance from the point source. For very large propagation distances the spherical wave at a receiver can be approximated by a plane wave. The spherical wave model is often used to describe optical transmitters that use small transmit apertures for emitting beams with relatively large divergence angles in the orders of a few milliradians.
The third often used wave model is the Gaussian beam model, also called the transverse electromagnetic mode of lowest order (TEM_{00}) where the prop-

agating beam is described by a wave front whose amplitude is Gaussian distributed around the phase velocity vector. The beams emitted from most lasers are very well approximated by this model, but plane and spherical waves are often preferred for simplicity of the associated equations. In this work all evaluations are done using the Gaussian beam model if available, but it is mentioned if one of the two simpler models would be sufficient.
A Gaussian beam wave is described by its characteristic parameter Λ (Fresnel ratio), which describes the amplitude change due to focusing, and Θ (curvature), which describes the amplitude change due to diffraction [33, 34]. By setting $\Theta = \Lambda = 0$ the Gaussian beam wave model reduces to a plane wave and by setting $\Theta = 1$ and $\Lambda = 0$ it is reduced to a spherical wave. Therefore the results obtained from Gaussian beam wave calculations can be transfered to other beam models. Θ and Λ are beam properties that change with link distance L between transmitter and receiver, as it can be seen from (2.9) and (2.10). Therefore it is more practical to use the typically fixed parameters wavelength λ, divergence angle θ_B and the beam radius W_0 at the transmitter for characterizing the beam of a communication system. From these three parameters, all other properties of a Gaussian beam can be derived, as shown in the following.
W_0 is defined as the radius around the beam axis at the transmitter plane l_0, where the beam intensity has dropped by $1/e^2$ compared to the peak intensity located on the axis. An important measure of a Gaussian beam is the so called Rayleigh range l_R, which is the range from the position of the beam waist l_B to the position where the area of the beam cross section has doubled [36]:

$$l_\mathrm{R} = \frac{\pi W_\mathrm{B}^2}{\lambda} \tag{2.1}$$

For positions in the far-field ($l \gg l_\mathrm{B} + l_\mathrm{R}$) the beam radius increases linearly and the relation between divergence ($1/e^2$ half) angle θ_B in radians and the beam waist W_B in meters can be approximated by [36]:

$$\theta_\mathrm{B} = \frac{\lambda}{\pi W_\mathrm{B}} \tag{2.2}$$

W_B can be calculated by [34]:

$$W_\mathrm{B} = W_0 \sqrt{\frac{\Omega_\mathrm{f}^2}{1 + \Omega_\mathrm{f}^2}} \tag{2.3}$$

where Ω_f is the focusing parameter which gives the geometric focus of the beam and is defined by:

$$\Omega_\mathrm{f} = \frac{2F_0}{kW_0^2} \tag{2.4}$$

where F_0 is the phase front curvature of the beam at the transmitter and $k = 2\pi/\lambda$ is the optical wave number.
Equations (2.2) and (2.3) can be put together to form:

$$\theta_{\mathrm{B}} = \frac{\lambda}{\pi W_0 \sqrt{\frac{\Omega_{\mathrm{f}}^2}{1+\Omega_{\mathrm{f}}^2}}} \Leftrightarrow \frac{\Omega_{\mathrm{f}}^2}{1+\Omega_{\mathrm{f}}^2} = \left(\frac{\lambda}{\pi\theta_{\mathrm{B}} W_0}\right)^2 \Leftrightarrow \tag{2.5}$$

$$\Omega_{\mathrm{f}}^2 = \left(\frac{\lambda}{\pi\theta_{\mathrm{B}} W_0}\right)^2 + \left(\frac{\lambda}{\pi\theta_{\mathrm{B}} W_0}\right)^2 \Omega_{\mathrm{f}}^2 \Leftrightarrow \Omega_{\mathrm{f}}^2 = \frac{\left(\frac{\lambda}{\pi\theta_{\mathrm{B}} W_0}\right)^2}{1 - \left(\frac{\lambda}{\pi\theta_{\mathrm{B}} W_0}\right)^2}$$

using the above and Equation (2.4) F_0 can be calculated by:

$$\left(\frac{2F_0}{kW_0^2}\right)^2 = \frac{\left(\frac{\lambda}{\pi\theta_{\mathrm{B}} W_0}\right)^2}{1 - \left(\frac{\lambda}{\pi\theta_{\mathrm{B}} W_0}\right)^2} \Leftrightarrow \tag{2.6}$$

$$F_0 = \frac{kW_0^2}{2} \sqrt{\frac{\left(\frac{\lambda}{\pi\theta_{\mathrm{B}} W_0}\right)^2}{1 - \left(\frac{\lambda}{\pi\theta_{\mathrm{B}} W_0}\right)^2}}$$

As one can see from the previous formulae the practically used parameters lead to complicated formulae, so for calculations of the beam properties at position l, it is more convenient to describe the Gaussian beam by curvature parameter Θ_0 and Fresnel ratio Λ_0 at the input-plane ($l = 0$, transmitter) [33].

$$\Theta_0 = 1 - \frac{L}{F_0} \tag{2.7}$$

$$\Lambda_0 = \frac{2L}{kW_0^2} \tag{2.8}$$

where L is the distance between transmitter and receiver. Several parameters then can be calculated [34]:

$$\text{Curvature parameter at position } L: \quad \Theta = \frac{\Theta_0}{\Theta_0^2 + \Lambda_0^2} \tag{2.9}$$

$$\text{Fresnel ratio at position } L: \quad \Lambda = \frac{\Lambda_0}{\Theta_0^2 + \Lambda_0^2} \tag{2.10}$$

$$\text{Position of beam waist:} \quad l_\mathrm{B} = \frac{F_0}{1 + \Omega_\mathrm{f}^2} \tag{2.11}$$

$$\text{Spot size at position L:} \quad W = W_0 \sqrt{\Theta_0^2 + \Lambda_0^2} \tag{2.12}$$

$$\text{Radius of curvature at position L:} \quad F = \frac{F_0 \left(\Theta_0^2 + \Lambda_0^2\right)(\Theta_0 - 1)}{\Theta_0^2 + \Lambda_0^2 - \Theta_0} \tag{2.13}$$

$$\text{On-axis amplitude:} \quad A = \frac{1}{\sqrt{\Theta_0^2 + \Lambda_0^2}} \tag{2.14}$$

$$\text{On-axis irradiance:} \quad I = \Theta_0^2 + \Lambda_0^2 \tag{2.15}$$

2.2 Laser Beam Propagation in Vacuum

Without atmospheric effects, laser beam propagation can be characterized in the ideal case analogous to RF communications by the Friis equation [37]:

$$P_\mathrm{Rx} = P_\mathrm{Tx}\, G_\mathrm{Tx}\, \tau_\mathrm{Tx}\, \tau_\mathrm{fs}\, \tau_\mathrm{Rx}\, G_\mathrm{Rx} \tag{2.16}$$

where
P_Rx is the received optical power
P_Tx is the transmitted laser power
G_Tx is the transmitter antenna gain
τ_Tx is the transmitter transmittance
τ_fs is the free-space loss
τ_Rx is the receiver transmittance
G_Rx is the receiver antenna gain

The used parameters are defined as

$$G_\mathrm{Tx} = \frac{2.7675}{\theta_\mathrm{B}^2} = \frac{32}{\theta_{3\,\mathrm{dB}}^2} \tag{2.17}$$

where $\theta_{3\,\mathrm{dB}}$ is the full width half maximum (FWHM) divergence angle and θ_B is the $1/\mathrm{e}^2$ half divergence angle of the transmit beam in rad.

$$\tau_\mathrm{fs} = \left(\frac{\lambda}{4\pi L}\right)^2 \tag{2.18}$$

where λ is the optical wavelength in m and L is the link distance in m.

$$G_{\mathrm{Rx}} = \left(\frac{\pi D_{\mathrm{Rx}}}{\lambda}\right)^2 \tag{2.19}$$

where D_{Rx} is the diameter of the receiving aperture in m. All other parameters (P_{Tx}, τ_{Tx}, τ_{Rx}) used in (2.16) are system dependent values that have to be known from system design.

2.3 Laser Beam Propagation in Atmosphere

If light propagates through atmosphere, some of its energy is absorbed or scattered by molecules and particles. Therefore a factor τ_{ATM} for the atmospheric transmittance has to be inserted into (2.16) which then becomes

$$P_{\mathrm{Rx}} = P_{\mathrm{Tx}}\, G_{\mathrm{Tx}}\, \tau_{\mathrm{Tx}}\, \tau_{\mathrm{ATM}}\, \tau_{\mathrm{fs}}\, \tau_{\mathrm{Rx}}\, G_{\mathrm{Rx}} \tag{2.20}$$

2.3.1 Atmospheric Attenuation Factor α

It is common practice to define τ_{ATM} via an atmospheric attenuation factor α given in $\mathrm{dB\,km^{-1}}$

$$\tau_{\mathrm{ATM}} = 10^{-\alpha \frac{L}{10000}} \tag{2.21}$$

Where L is the distance between transmitter and receiver and the value for α depends on λ, altitude and especially on current weather conditions and therefore changes over time. In the literature various models are given to calculate α based on given weather conditions. To keep these models simple, it is generally assumed that for wavelengths relevant for OWC the absorption by atmospheric particles is negligible in comparison to the effect of scattering. Because the amount of atmospheric particles depends on altitude and weather conditions it is common practices to define α in relation to visibility V which is a simple and altitude independent measure for the amount of atmospheric particles. The technical definition of visibility V is the distance that light decreases to 2% of the original power, or qualitatively, visibility is the distance at which it is just possible to distinguish a dark object against the horizon [38]. The most often used models for calculation of α under different weather conditions is given in the following part.
For the estimation of α under general weather conditions without rain, fog or snow, the so called Kruse relation can be used. Kim et al. [38] have extended this relation to:

$$\alpha_{\mathrm{clear}} = \frac{3912}{V}\left(\frac{\lambda \times 10^9}{550}\right)^{-q} \tag{2.22}$$

where V is visibility in m and q is a parameter for the size distribution of the scattering particles given by

$$q = \begin{cases} 0 & V < 500\,\text{m} \\ V \times 10^{-3} - 0.5 & 500\,\text{m} < V < 1000\,\text{m} \\ 16V \times 10^{-5} + 0.34 & 1000\,\text{m} < V < 6000\,\text{m} \\ 1.3 & 6000\,\text{m} < V < 50\,000\,\text{m} \\ 1.6 & V > 50\,000\,\text{m} \end{cases} \tag{2.23}$$

For rain Atlas has given the relation as [39]:

$$\alpha_{\text{rain}} = 0.204R^{0.68} \tag{2.24}$$

where R is the rain fall rate in mm/h.
For the occurrence of snow an often used relation between attenuation and snowfall rate is [40]:

$$\alpha_{\text{snow}} = aS^b \tag{2.25}$$

where S is the snowfall rate in mm/h. a and b are two parameters depending on the type of snow. Commonly used values for these are:

$$a_{\text{dSnow}} = 54200\lambda + 5.4958776 \qquad b_{\text{dSnow}} = 1.38 \quad \text{(dry snow)} \tag{2.26}$$

$$a_{\text{wSnow}} = 102300\lambda + 3.7855466 \qquad b_{\text{wSnow}} = 0.72 \quad \text{(wet snow)} \tag{2.27}$$

In [40] several other values for a and b are given. The reason for this is that these are all derived from measurements and often there are additional weather conditions present, like fog, which influence the measurements.
For fog there are two different models given, valid for wave length from 650 nm to 1550 nm and a visibility from 50 m to 1000 m:

$$\alpha_{\text{aFog}} = \frac{11478 \times 10^7\lambda + 3836.7}{V} \qquad \text{(advection fog)} \tag{2.28}$$

$$\alpha_{\text{cFog}} = \frac{18126 \times 10^{15}\lambda^2 + 13709 \times 10^7\lambda + 3750.2}{V} \qquad \text{(convection fog)} \tag{2.29}$$

2.3.2 Deriving Rainfall and Snowfall Rate from Visibility

Most often it is difficult to estimate the rainfall rate R or the snowfall rate S, while it is easier to estimate the current visibility V. In [40] a fairly simple model is given to calculate S from V for the two given types of snowfall:

$$S_{\text{dry}} = \frac{2210}{V} \qquad \text{(dry snow)} \tag{2.30}$$

$$S_{\text{wet}} = \frac{18720}{V} \qquad \text{(wet snow)} \tag{2.31}$$

For deriving R from V, no model is given in literature. Therefore values for V and R given in [41] have been used to fit an exponential function to it for deriving a model. The result of this fit is:

$$R = 3 \times 10^6 V^{-1.6} \tag{2.32}$$

The Formulae (2.32) and (2.24) have been compared against the approximation

$$\alpha_{\text{rain}} = \frac{2900}{V} \tag{2.33}$$

given in [39] and show very good agreement. (2.33) has not been used in the first place because in the literature there are different variations of formulae (2.24) and (2.33) available, each derived from different measurements. By adding (2.32) to the set of formulae a solution has been found that agrees well with commonly given visibility values for different rainfall rates.

2.3.3 The Impact of Weather Conditions on Laser Beam Propagation

Using the equations given in the previous section, it is possible to calculate α based only on the current weather condition in conjunction with an estimation of the visibility. Figure 2.1 illustrates the impact of weather conditions on a laser beam with $\lambda = 1550\,\text{nm}$. For this plot it has to be mentioned that the equations for fog are only valid in the region from 50 m to 1000 m and should be used as rough approximation in the extended regions. In addition it is not likely to have all visibility ranges for all weather conditions. For example if in clear air condition the visibility is limited to a few hundred meters, this only can be due to small particles similar to fog. Therefore α_{clear} is more like α_{aFog} than α_{rain}. Another example is the difference in visibility between fog and snow. When fog is present, visibility is usually limited to a few hundred meters, while in case of light snowfall visibility can still be a few kilometers. For this reason even though the attenuation by snowfall seems to be more severe in Figure 2.1 than the one given for fog, in practice the occurrence of fog is usually assumed to make OWC impossible, while the occurrence of snow is accepted in many cases. Finally the y-axis is limited to $20\,\text{dB}\,\text{km}^{-1}$ as this value is assumed in this work to make OWC long-range links impossible, especially for link distances longer than 100 km.

To give a better overview on which values to expect for α in real world conditions, Table 2.1 to 2.4 give values for V and α for a wavelength of 1550 nm under common weather situations. Values for other wavelengths used for OWC can be expected to give results in similar ranges. Values for V used

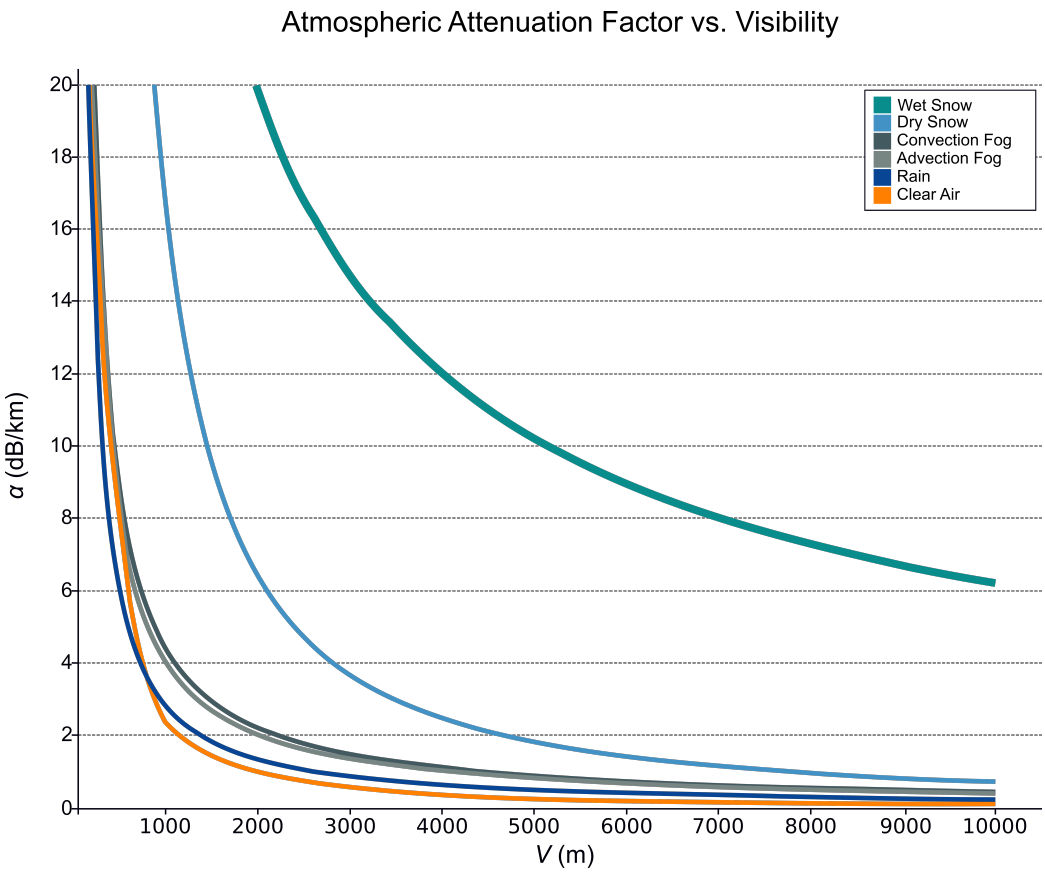

Figure 2.1: Atmospheric attenuation factor α versus visibility V. λ has been set to 1550 nm.

in the tables are taken from [41]. From these tables it can be seen that α is rather large for occurrences of snowfall, where the occurrence of moderate snow can pose problems for OWC. Since most optical links are deployed in regions where moderate to strong snowfalls are less likely, snowfall is often assumed to be acceptable for optical links. For fog the 20 dB km^{-1} limit occurs between moderate and thick fog, so for the occurrence of a limited amount of fog OWC links can be established, but since most often fog with a few hundred meters visibility occurs in most regions of interest, fog is generally assumed to pose severe problems for optical links. For the occurrence of rain Table 2.3 shows that only strong cloudburst pose a thread to OWC while links can be established under all other types of rain. In clear air condition OWC is rarely influenced by the additional attenuation from the atmosphere. Concluding this section it can be said that for designing optical communications systems a good research on the weather conditions in the targeted

deployment region should be done. Based on the information given here it is possible to limit the required data to visibility statistics, that are e.g. available from most air fields, and a statistics of the general weather situation which can be obtained from most meteorological data bases.

Clear Air		
Weather Condition	V(m)	α_{clear}(dB km^{-1})
Exceptionally Clear	100000	0.007
	50000	0.015
Very Clear	50000	0.015
	20000	0.051
Clear	20000	0.051
	10000	0.102

Table 2.1: Listing of α for common clear air situations. Calculations are done for $\lambda = 1550\,\text{nm}$.

Fog			
Weather Condition	V(m)	α_{aFog}(dB km^{-1})	α_{cFog}(dB km^{-1})
Light Haze	10000	0.4	0.4
	4000	1.0	1.1
Haze	4000	1.0	1.1
	2000	2.0	2.2
Thin Fog	2000	2.0	2.2
	1000	4.0	4.4
Light Fog	1000	4.0	4.4
	500	8.0	8.8
Moderate Fog	500	8.0	8.8
	200	20.1	22.0
Thick Fog	200	20.1	22.0
	50	80.3	88.0
Dense Fog	50	80.3	88.0
	1	4014.6	4398.2

Table 2.2: Listing of α_{aFog} and α_{cFog} for common occurrences of fog. Calculations are done for $\lambda = 1550\,\text{nm}$.

Rain		
Weather Condition	V(m)	α_{rain}(dB km^{-1})
Drizzle	23000	0.09
	10000	0.23
Light Rain	10000	0.23
	4500	0.55
Medium Rain	4500	0.55
	2000	1.33
Heavy Rain	2000	1.33
	1000	2.82
Cloudburst	1000	2.82
	100	34.52

Table 2.3: Listing of α_{rain} for common occurrences of rain. Calculations are done for $\lambda = 1550\,\text{nm}$.

Snow			
Weather Condition	V(m)	α_{dSnow}(dB km^{-1})	α_{wSnow}(dB km^{-1})
Light Snow	6000	1	9
	1000	17	33
Moderate Snow	1000	17	33
	500	43	54
Heavy Snow	500	43	54
	10	9592	895

Table 2.4: Listing of α_{dSnow} and α_{wSnow} for common occurrences of snow. Calculations are done for $\lambda = 1550\,\text{nm}$.

2.3.4 Scintillation

Scintillation of the received optical signal is caused by turbulence inside the atmosphere. Wind and solar heating cause inhomogeneities in temperature and pressure of the air and create air cells (eddies) with different index of refraction values. These differences in the refractive index of the air lead to disturbances in the optical beam which then is experienced by the optical receiver as scintillation of the received signal. A detailed description of scintillation and other atmospheric effects can be found in [34]. In this work only the most important formulae and models are given, which are required for developing a simplified channel model. As for the attenuation, also the scintillation is influenced by weather conditions. For example, rain reduces the strength of turbulence along the optical path and therefore reduces the

scintillation of the optical signal. Unlike for attenuation there is no single measurable value for predicting the strength of scintillation in scenarios of OWC.

Refractive Index Structure Constant C_n^2

A common measure for the strength of optical turbulence is the refractive index structure constant C_n^2, given in $m^{-2/3}$. C_n^2 can be understood as a quantitative measure of the strength of turbulence within the atmosphere. The strongest turbulence is observed a few meters above ground, where C_n^2 has an average value in the order of $10^{-14}\,m^{-2/3}$. The exact value of the ground level C_n^2 heavily depends on environmental parameters like daytime, surface type, relative humidity and wind speed. With increased height above ground, the value of C_n^2 decreases by a few orders of magnitude up to a height of about 10 km. In the region between 10 km to 15 km the present jet streams cause an increase of turbulence. The most often used model for C_n^2 is the Hufnagel-Valley 5/7 ($HV_{5/7}$) model [33]:

$$C_n^2(h) = 0.00594\left(\frac{v_w}{27}\right)^2\left(10^{-5}h\right)^{10}\exp\left(\frac{-h}{1000}\right) + 2.7\times10^{-16}\exp\left(\frac{-h}{1500}\right) + C_n^2(0)\exp\left(\frac{-h}{100}\right) \tag{2.34}$$

Where h is the height above ground in m, $C_n^2(0) = 1.7\times10^{-14}\ m^{-2/3}$ is the ground level value of C_n^2 and $v_w = 21$ m/s is the root mean squared orthogonal wind velocity along the propagation path. For the estimation of v_w altitude dependent models exist like the Bufton Wind Model [34] which can be used to further refine the model. As mentioned before, $C_n^2(0)$ depends on the condition on the ground and should be adjusted to the ground composition, e.g water, woods, sand, etc., for more accurate results. For the presented analysis the $HV_{5/7}$ model with fixed $C_n^2(0)$ and v_w is used to keep the analysis more simple. But it should be kept in mind that the parameter dependence on altitude and surface type also influences the optical turbulence along the path.
C_n^2 is sometimes used to categorize the atmospheric turbulence as weak ($C_n^2 \leq 10^{-17}\ m^{-2/3}$) or strong ($C_n^2 \geq 10^{-13}\ m^{-2/3}$) [33], were strong turbulence will be experienced rarely in nature, e.g. only close to heated concrete or a heated roof top. The terms weak and strong turbulence are sometimes confused with the term weak and strong scintillation. Weak and strong scintillation is defined by the Rytov variance which is explained in the next section. Since the Rytov variance characterizes the scintillation of the laser beam

at the end of the propagation path, integrating all the turbulence present along this path, it is possible to have weak turbulence all along the path, but to experience strong scintillation at the receiver. This differentiation is important in order to use the available theory correctly. Because C_n^2 is typically less than 10^{-14} $\mathrm{m}^{-2/3}$ it is sufficient in most cases to use a theory that is only valid under weak turbulence, which leads to simpler formulations.

Rytov Variance σ_R^2

One of the first measures developed to characterize the optical turbulence along a propagation path was the Rytov Variance. Originally it was developed for the propagation of a plane wave under weak scintillation conditions (i.e. $\sigma_\mathrm{R}^2 \ll 1$) along a horizontal path with homogeneous turbulence [34]

$$\sigma_\mathrm{R}^2 = 1.23 C_\mathrm{n}^2 k^{\frac{7}{6}} L^{\frac{11}{6}} \tag{2.35}$$

Where $k = 2\pi/\lambda$ is the optical wave number and L is the distance between sender and receiver in m. If turbulence is not homogeneous, the turbulence has to be integrated along the path, which leads to [34]:

$$\sigma_\mathrm{R}^2 = 2.25 k^{\frac{7}{6}} L^{\frac{5}{6}} \int_0^L C_\mathrm{n}^2 (h_l) \times \left(1 - \frac{l}{L}\right)^{\frac{5}{6}} dl \tag{2.36}$$

Where h_l is the height above ground at link distance l from the transmitter. For slant-paths (2.36) is usually given by using the zenith angle and assuming a constantly increasing altitude above ground for the propagation path of the beam. As shown in [21, 42], the ground profile can have a reasonable impact on the Rytov variance because of the altitude dependence of C_n^2. Therefore (2.36) is given in a form where the integration is done along the propagation path, instead of integrating along the path altitude. For a Gaussian beam the above formula has to be extended by several terms to form the (on-axis) Rytov variance for a Gaussian beam [34]:

$$\sigma_\mathrm{RG}^2 = 3.86\, \sigma_\mathrm{R}^2 \times \mathrm{Re}\left[i^{\frac{5}{6}}\, {}_2F_1\left(-\frac{5}{6}, \frac{11}{6}; \frac{17}{6}; \overline{\Theta} + i\Lambda\right) - \frac{11}{16}\Lambda^{\frac{5}{6}} \right] \tag{2.37}$$

Where $i = \sqrt{-1}$, $\overline{\Theta} = 1 - \Theta$, ${}_2F_1\,(a, b; c; z)$ is the Gaussian hypergeometric function and Re denotes the real part.

Scintillation Index σ_{I}^2 and Power Scintillation Index σ_{P}^2

In order to describe temporal and spatial fluctuations of the intensity field of the laser beam, the (on-axis) scintillation index σ_{I}^2 is generally used:

$$\sigma_{\mathrm{I}}^2 = \frac{\langle I^2 \rangle - \langle I \rangle^2}{\langle I \rangle^2} \tag{2.38}$$

Where I denotes the intensity (irradiance) of the laser beam and $\langle\rangle$ denotes the ensembled average. In other words, σ_{I}^2 is the normalized variance of I. For approximation of σ_{I}^2 for the different beam models, the Rytov variance can be used. For weak turbulence the (on-axis) scintillation index of a Gaussian beam σ_{IG}^2 equals σ_{RG}^2, but to also include strong turbulent conditions, (2.37) has to be extended to [34]:

$$\sigma_{\mathrm{IG}}^2 = \exp\left\{ \frac{0.49\sigma_{\mathrm{RG}}^2}{\left[1 + 0.56\,(1+\Theta)\,\sigma_{\mathrm{RG}}^{\frac{12}{5}}\right]^{\frac{7}{6}}} + \frac{0.51\sigma_{\mathrm{RG}}^2}{\left[1 + 0.69\sigma_{\mathrm{RG}}^{\frac{12}{5}}\right]^{\frac{5}{6}}} \right\} - 1 \tag{2.39}$$

Because σ_{IG}^2 is defined for a receiver consisting of a single point placed directly on the beam propagation axis (point receiver), it is not valid for IM/DD OWC systems, where collecting apertures are used for reception of the beam. These apertures collect optical power across their whole area, averaging out intensity variations that affect only smaller areas on the receiver plane. This effect is called aperture averaging. For characterizing communication links, the power scintillation index σ_{P}^2 is defined in analogy to (2.38), but using received power at the receiver P_{Rx} instead of I and therefore describes the normalized variance of P_{Rx}. Based on σ_{RG}^2 and taking aperture averaging into account, σ_{P}^2 for a Gaussian beam can be approximated by [34]:

$$\begin{aligned}\sigma_{\mathrm{P}}^2 = \exp\Bigg[& \frac{0.49\left(\frac{\Omega_{\mathrm{G}}-\Lambda}{\Omega_{\mathrm{G}}+\Lambda}\right)^2 \sigma_{\mathrm{RG}}^2}{\left(1 + \frac{0.4\left(2-\overline{\Theta}\right)\left(\frac{\sigma_{\mathrm{R}}}{\sigma_{\mathrm{RG}}^2}\right)^{12/7}}{(\Omega_{\mathrm{G}}+\Lambda)\left(\frac{1}{3}-\frac{1}{2}\overline{\Theta}+\frac{1}{5}\overline{\Theta}^2\right)^{6/7}} + 0.56\,(1+\Theta)\,\sigma_{\mathrm{RG}}^{12/5}\right)^{7/6}} \\ & + \frac{0.51\sigma_{\mathrm{RG}}\left(1 + 0.69\sigma_{\mathrm{RG}}^{12/5}\right)^{-5/6}}{1 + \frac{1.20\left(\frac{\sigma_{\mathrm{R}}}{\sigma_{\mathrm{RG}}}\right)^{12/5} + 0.83\sigma_{\mathrm{R}}^{12/5}}{\Omega_G+\Lambda}} \Bigg] - 1\end{aligned} \tag{2.40}$$

With:

$$\Omega_{\mathrm{G}} = \frac{16L}{kD_{\mathrm{Rx}}^2} \tag{2.41}$$

Where D_{Rx} is the diameter of the receiving aperture. As previously mentioned, by setting $\Theta = \Lambda = 0$, (2.40) reduces to a plane wave and by setting $\Theta = 1$ and $\Lambda = 0$ it reduces to a spherical wave. At this point it has to be mentioned that the given formulae assume fixed values for inner scale ($l_0 = 0$) and outer scale ($L_0 = \infty$). These two scale sizes represent the smallest and the largest air cells affecting the propagation of the beam. In theory these two sizes act as band pass filter on the scintillation spectrum, blocking very high and very low frequencies. For IM/DD OWC systems only the higher frequencies (inner scale) affect the transmission quality of the link. In Figure 2.2 the effect of the inner scale on the development of σ_{P}^2 along a horizontal path is shown by fixing L_0 to ∞ and setting l_0 to different values. The approximation formulae used for these plots can all be found in [34]. For correct application of these approximations from [34] to real world problems, one has to understand the way how these approximations were derived and which assumptions have been made on this way. Therefore they are not given as quick reference within this work.

Because L_0 should not have much effect on σ_P^2, it has been fixed to infinity. l_0 is generally assumed to be in the range of several millimeters [34]. Recently a model has been published that results in values of up to 5 cm for altitudes of approximately 7500 m above ground [5]. Therefore l_0 has been set to values between 0 and 5 cm. The red line in each plot shows the results for the approximation done by using (2.39), where the orange line shows the results for the approximation done by using (2.40). From this series of plots one can clearly see that l_0 has a significant impact on σ_P^2. Nevertheless (2.39) and (2.40), which both do not take inner and outer scale into account, are used within this work for the following reasons.
First, all formulae taking l_0 and L_0 into account assume homogeneous turbulence conditions along the propagation path, i.e constant C_{n}^2, l_0, L_0, v_{w}, h_l, ground composition and weather conditions. It is not very likely that these conditions can be fulfilled for link distances of several kilometers in a natural environment. Secondly, there is no common model for inner and outer scale that the scientific community has agreed on. Up to now the presented models are based on different measurements with different results. This indicates that taking inner and outer scale into account would render the goal of giving a generally valid characterization of the OWC channel impossible. Finally, it has been shown in [21] and [42], that for the characterization of long-range links the ground profile or even just the Earth curvature can not be ignored. The uncertainty introduced into the approximations by using

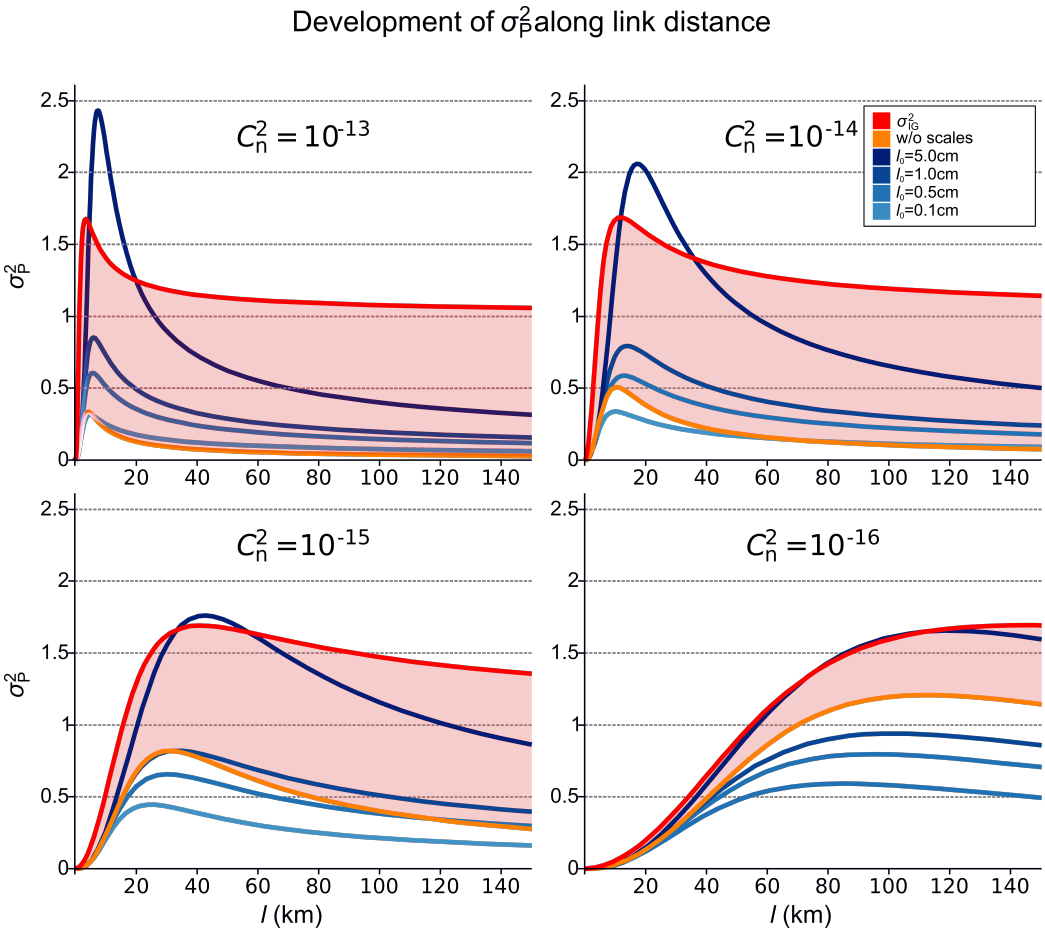

Figure 2.2: Development of σ_{P}^2 along link distance for a typical OWC scenario ($W_0 = 2.5$ cm, $\theta_{\mathrm{B}} = 500$ µrad, $D_{\mathrm{Rx}} = 10$ cm). C_{n}^2 has been assumed fixed along the path with values between 10^{-13} m$^{-2/3}$ and 10^{-16} m$^{-2/3}$ as annotated on top of each plot. The red shaded area shows the range between best and worst-case link conditions as assumed within this work.

(2.39) and (2.40) seems to be less than it would be by assuming a constant link altitude. Finally, in this work (2.39) is only used to derive an estimate of the maximum value for σ_P^2 to expect in various OWC scenarios (i.e. for the worst-case always a point receiver is assumed) and (2.40) to derive an estimate of σ_P^2 for average link conditions. In this case l_0 can be taken into account by adding a safety margin on top of the calculated values. This has to be done anyway, because of all the uncertainties and simplification contained in the given approximations.

2.3.5 Probability Density Function of Received Optical Power

The received optical power at the receiver can be seen as a continuous random variable, whose value is varied by the optical turbulence along the transmission path. The probability density function (PDF) is generally used to describe the relative likelihood for such a randomly distributed variable to take on a certain value. As long as the receiving aperture is small enough, the received power is equal to the received intensity (point receiver) and therefore the distribution of the received intensity can be used to characterize the received power. Under weak scintillation conditions, the log-normal (LN) distribution is widely accepted as the characterizing distribution [35, 43] for received intensity. Under moderate to strong turbulence the LN distribution was also widely accepted before some work had shown evidence, that the LN assumption has some limitations especially under strong turbulence [44, 45]. For the occurrence of strong turbulence, the K, gamma (G) and gamma-gamma (GG) distributions are given as suitable PDFs [46, 35, 43]; where the GG distribution is a generalization of the K distribution and should be valid under all scintillation conditions. Therefore the K distribution is not considered any further within this work.
For the case of aperture averaging, i.e. when apertures with several centimeters of diameter are used and the point receiver assumption is no longer true, which is generally the case for IM/DD OWC systems, the LN distribution is proposed as the PDF of P_{Rx} [47, 43].
Scientists also often assume an LN distribution of P_{Rx} in situations where other distributions should be expected, just to simplify the models, and accept the inaccuracies contained in this simplification [48]. Another distribution recently proposed for a simplified model of P_{Rx} is the Inverse Gaussian (IG) distribution [49]. This distribution is not derived from propagation theory, but has been chosen because of its similarity to the LN distribution. Therefore it should be applicable for the same atmospheric conditions, especially, weak scintillation and the presence of aperture averaging.
In the following, the formulae for the most commonly used distribution functions are given. At this point within this work, these distributions are given purely as reference, but they are used for channel modeling of the OWC channel later on. For the visualization of a distribution, it is common practice to use the PDF. For statistical tests and data analysis the cumulative distribution function (CDF) is more appropriate. In order to derive an empirical PDF (EPDF) from a measurement vector, the histogram of this measurement has to be normalized by its area, to obtain an integral of 1 for the EPDF. The calculation of this integral is inaccurate, since it can only be done by

estimating the area of a bar representation of the histogram, where the width of the bars influences the final result. The calculation of the empirical CDF (ECDF) is not subject to this problem, because all data points of the ECDF have to be normalized only by the maximum value of a step function for correct representation. Both representations of the distributions are given in the next part.

Log-normal Distribution (LN)

The log-normal distribution is given by:

$$\text{PDF: } f_{LN}(P_{\text{Rx}};\mu,\sigma^2) = \frac{1}{P_{\text{Rx}}\sqrt{2\pi\sigma^2}} e^{\frac{(\ln(P_{\text{Rx}})-\mu)^2}{2\sigma^2}} \tag{2.42}$$

$$\text{CDF: } F_{LN}(P_{\text{Rx}};\mu,\sigma^2) = \frac{1}{2} + \frac{1}{2}\text{erf}\left(\frac{\ln(P_{\text{Rx}})-\mu}{\sqrt{2\sigma^2}}\right) \tag{2.43}$$

where μ is the mean and σ^2 is the variance of the natural logarithm of the received power. $\text{erf}\,(x)$ is the Gauss error function and $\ln(x)$ is the natural logarithm of x. μ and σ^2 are related to σ_P^2 by:

$$\sigma^2 = \ln(\sigma_P^2 + 1) \tag{2.44}$$

$$\mu = \ln(\langle P_{\text{Rx}}\rangle) - \frac{\sigma^2}{2} \overset{\langle P_{\text{Rx}}\rangle=1}{\Longrightarrow} -\frac{\sigma^2}{2} \tag{2.45}$$

Gamma Distribution (G)

The Gamma distribution is given by:

$$\text{PDF: } f_G(P_{\text{Rx}};k,\theta) = {P_{\text{Rx}}}^{k-1} e^{\frac{-P_{\text{Rx}}}{\theta}} \frac{1}{\theta^k \Gamma(k)} \tag{2.46}$$

$$\text{CDF: } F_G(P_{\text{Rx}};k,\theta) = \frac{\gamma\left(k, \frac{P_{\text{Rx}}}{\theta}\right)}{\Gamma(k)} \tag{2.47}$$

where $\gamma(a,x)$ is the lower incomplete gamma function, $\Gamma(z)$ is the gamma function and the parameters $k > 0$ and $\theta > 0$ are related to σ_P^2 by:

$$\theta = \sigma_P^2 \tag{2.48}$$

$$k = \frac{1}{\sigma_P^2} \tag{2.49}$$

Gamma-Gamma Distribution (GG)

The Gamma-Gamma distribution is given by [50]:

$$\text{PDF: } f_{GG}(P_{\text{Rx}};\alpha,\beta) = \frac{2\left(\alpha\beta\right)^{\frac{\alpha+\beta}{2}}}{\Gamma\left(\alpha\right)\Gamma\left(\beta\right)} P_{\text{Rx}}^{\frac{\alpha+\beta}{2}-1} \mathrm{K}_{\alpha-\beta}\left(2\sqrt{\alpha\beta P_{\text{Rx}}}\right) \tag{2.50}$$

$$\begin{aligned}\text{CDF: } F(P_{\text{Rx}};\alpha,\beta) =& \frac{\pi}{\sin\left[\pi\left(\alpha-\beta\right)\right]\Gamma\left(\alpha\right)\Gamma\left(\beta\right)} \\ &\times \left\{ \frac{\left(\alpha\beta P_T\right)^{\beta}}{\beta\Gamma\left(\beta-\alpha+1\right)} \times {}_1F_2\left(\beta;\beta+1,\beta-\alpha+1,\alpha\beta P_T\right)\right. \\ &- \left.\frac{\left(\alpha\beta P_T\right)^{\alpha}}{\alpha\Gamma\left(\alpha-\beta+1\right)} \times {}_1F_2\left(\alpha;\alpha+1,\alpha-\beta+1,\alpha\beta P_T\right)\right\}\end{aligned} \tag{2.51}$$

where α and β are shape parameters, P_T is a threshold parameter, ${}_1F_2$ is a generalized hypergeometric function and $\mathrm{K}_n(x)$ is the modified Bessel function of the second kind and order n. As it can be seen from (2.51) the closed form CDF of the GG distribution has a rather long and complex formulation that leads to numerical inaccuracies if implemented on a computer. In most cases it is more accurate to obtain the CDF by numerical integration of the PDF. The GG distribution has been developed by modeling effects from inner and outer scale on the laser beam as two independent processes that follow each a G distribution [46]. Although α and β are related in the model to physical effects, they can not be directly related to σ_P^2. In [23] the following relation has been used to fit the GG distribution to measurement values:

$$\sigma_P^2 = \frac{1}{\alpha} + \frac{1}{\beta} + \frac{1}{\alpha\beta} \tag{2.52}$$

In conjunction with the observation that α and β have symmetrical effects in Eq. (2.50) and (2.52) the calculation of α and β can be reduced to a search for a ratio r that fulfills:

$$\beta = r\alpha, \quad 0 \leq r \leq 1 \tag{2.53}$$

$$\sigma_{\text{P}}^2 = \frac{1}{\alpha} + \frac{1}{r\alpha} + \frac{1}{r\alpha^2} \tag{2.54}$$

For the analysis presented in [23] it has been observed that the best fits were achieved using values for r between 0.9 and 1.0. Similar observations have been reported in [51, 52]. For this reason α and β can be derived from σ_{P}^2 by assuming $\alpha = \beta$ and using (2.52):

$$\alpha = \beta = \frac{\sqrt{\sigma_{\text{P}}^2 + 1} + 1}{\sigma_{\text{P}}^2} \tag{2.55}$$

Inverse Gaussian Distribution (IG)

The inverse Gaussian distribution is given by:

$$\text{PDF: } f_{IG}(P_{\text{Rx}};\mu,\lambda_{\text{IG}}) = \sqrt{\frac{\lambda_{\text{IG}}}{2\pi P_{\text{Rx}}^3}} e^{-\frac{\lambda_{\text{IG}}(P_{\text{Rx}}-\mu)^2}{2\mu^2 P_{\text{Rx}}}} \tag{2.56}$$

$$\begin{aligned}\text{CDF: } F_{IG}(P_{\text{Rx}};\mu,\lambda_{\text{IG}}) = & \quad \Phi\left(\sqrt{\frac{\lambda_{\text{IG}}}{P_{\text{Rx}}}}\left(\frac{P_{\text{Rx}}}{\mu}-1\right)\right) \\ & + e^{\frac{2\lambda_{\text{IG}}}{\mu}} \Phi\left(-\sqrt{\frac{\lambda_{\text{IG}}}{P_{\text{Rx}}}}\left(\frac{P_{\text{Rx}}}{\mu}+1\right)\right)\end{aligned} \tag{2.57}$$

Where $\Phi(x)$ is the standard Gaussian distribution, μ is the mean value and λ_{IG} is the shape parameter. The parameters are related to σ_P^2 by:

$$\mu = \langle P_{\text{Rx}} \rangle = 1 \tag{2.58}$$

$$\lambda_{\text{IG}} = \frac{1}{\sigma_P^2} \tag{2.59}$$

2.3.6 Spectral Characteristics of the Received Optical Power

The previously given parameters like σ_P^2 only describe the distribution of P_{Rx}, but do not give any information about the temporal behavior of an OWC link. Measurements presented in 3.2 have shown, that there is no correlation between σ_P^2 and the temporal fluctuations of P_{Rx}, respectively the power spectral density (PSD) of P_{Rx}. A simple description for the PSD of P_{Rx} for a point receiver has been given in [34]. Based on the work of Tatarskii [53] and Ishimaru [54], Andrews and Phillips used Taylor's frozen turbulence hypothesis [55] to describe the PSD. According to their work, a characteristic frequency f_t exists that splits the shape of the PSD into two parts. For frequencies smaller than f_t, the PSD has a constant value. Starting at f_t, the PSD then decays with a constant slope of $f^{-\frac{8}{3}}$. The value of f_t can be approximated for a point receiver by:

$$f_t = \frac{v_{\text{w}}}{\sqrt{L/k}} \tag{2.60}$$

where v_{w} is again the root mean squared transverse wind speed, L the propagation distance and k the wave number ($= 2\pi/\lambda$). v_{w} represents the speed of the air masses moved through the laser beam. In fixed scenarios this speed is truly just the wind speed. In mobile scenarios, where at least one partner

is moving and therefore the laser beam has to be tracked, this speed is the sum of wind and the moving speed of the lase beam. For non point receivers, which is typically the case for OWC systems, a deviation from the theoretical spectrum should be visible [34]. The aperture averaging effect filters out some higher frequencies and increases the power contained within the lower frequencies. Therefore f_t is shifted towards lower frequencies and the decay is steeper than $f^{-\frac{8}{3}}$. Nevertheless, (2.60) gives an estimate of the upper bound for f_t and the shape of the PSD; which is useful as long as no exact values are required.

Chapter 3

Modeling the Optical Wireless Communication Channel

In order to design, evaluate and optimize error protection schemes for the optical wireless channel, a computer implementable model of the optical wireless communication path is required. That model should allow for discrete event simulation (DES). DES is a simulation methodology often used by protocol and communication system designers, where simulations are done based on timed events and not in a time continuous way. This approach allows to simulate processes inside a communication system faster than in reality. The existing split-step approach [18, 19, 20] for simulation of OWC does not fulfill this requirement. For the split-step method, the propagation path is separated into several shorter sections. For each section, a phase screen is calculated, which represents the wave front exiting this section. This phase screen is then used as input for the next section, in order to calculate the phase screen for the next section. By splitting the propagation path into shorter sections, simplified formulae can be used for calculations done for each section. Nevertheless, numerically solving these simplified equations is a computational complex task which has to be done on thousands of segments for long range links just to calculate the channel conditions for a single moment in time. Given this complexity, which increases linearly with the time resolution of the simulation, it is not well suited to be used for DES. In this work a stochastic based channel model is proposed for the optical communications channel, which has a low computational complexity and is suitable for the fast generation of time series of channel conditions for use in DES systems.

3.1 Model of Optical Wireless Communications Systems

Figure 3.1 shows a schematic overview of the elements of an OWC system. The main elements of an OWC system are the optical transmitter (Tx), the

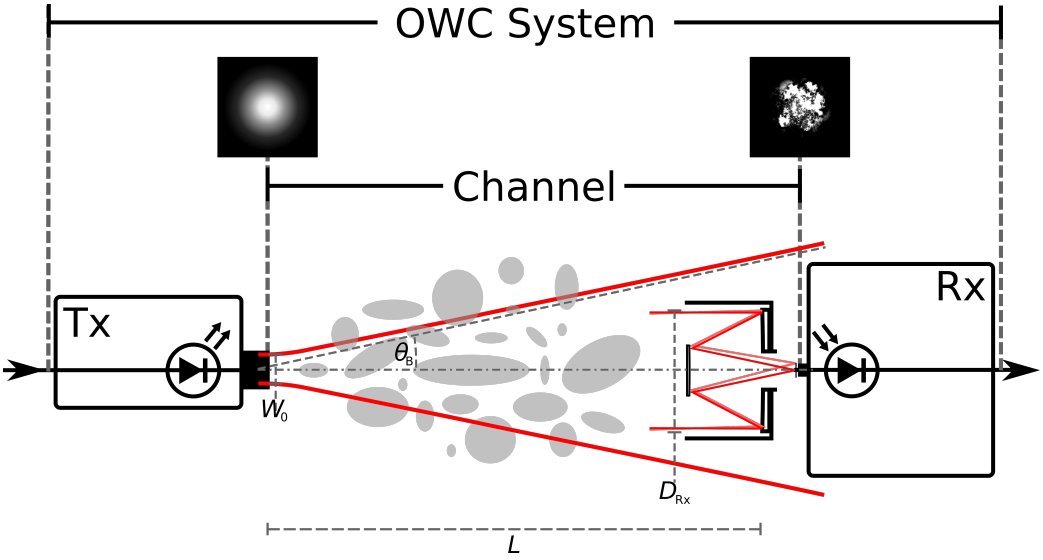

Figure 3.1: Schematic overview on the elements of an OWC system. The main elements are the optical transmitter (Tx), the atmospheric channel and the optical receiver (Rx). The two images above Tx and Rx show the cross section of the laser beam at these points. The image above Tx shows the intensity pattern of a Gaussian beam, while the image above Rx shows the speckled intensity pattern of the beam after propagation through the atmosphere. The gray blobs on the propagation path between transmit and receive telescope symbolize the atmospheric eddies.

atmospheric channel and the optical receiver (Rx). For the simulation of wireless communications systems it is common practice to model the system by a time series of the bit error probability (BEP). The BEP of an optical communication system is determined by the received power P_{Rx} at Rx and its distribution. Tx can be assumed to have no effect on BEP and therefore it can be neglected in the model, but its characteristic parameters mean transmission power $\langle P_{\mathrm{Tx}} \rangle$, diameter of the beam at its aperture W_0 and the beam divergence angle θ_{B} are input parameters for calculations about the optical propagation path. For optical IM/DD receivers a model already exists that allows for the conversion from P_{Rx} to BEP [56]. To fit the atmospheric channel into this framework, a model is required, that uses the characteristic

parameters of Tx and the formulae given in Chapter 2 as input and is able to produce time series of P_{Rx} that can be passed to the Rx model. From Chapter 2 it is possible to calculate $\langle P_{\mathrm{Rx}} \rangle$ and σ_{P}^2 at Rx. For a complete model of the optical communication system a stochastic description of P_{Rx} is required for modeling the channel. Based on this stochastic description and the input parameters $\langle P_{\mathrm{Rx}} \rangle$ and σ_{P}^2, time series of P_{Rx} can be generated. This stochastic description of the channel is given in the following sections based on results from several measurement campaigns.

3.2 Measurements

In order to obtain parameters for a stochastic description of P_{Rx}, several measurements of P_{Rx} have been conducted in three areas where FSO links are currently deployed. The first set of measurements originates from mobile near ground links, the second set are measurements in the marine environment and the third set is derived from airborne downlinks from a satellite and an aircraft. For each measurement, an optical power meter has been added to the optical path at the receiver side in order to record time series of P_{Rx}. A detailed description of each measurement campaign is given in the following subsections. Beside information about the optical communication system and the link conditions required for channel modeling, also some additional information about the link system, e.g. user data and error protection, is given for completeness.
Over all, the analyzed data has been collected on 23 days of successful trials totaling over 13 hours of valid measurements after post processing. The post processing of the data has been done in the following way. First, the measurements were analyzed for portions were only background light was recorded by the power meter. These parts of the measurements were used to determine the level of background light, in order to separate the received signal from background noise, and then removed from the analysis. These background light recordings were purposely created during the trials by blocking the transmit beam or switching it off and on again from time to time. Since most measurements were taken in mobile scenarios where the value of background light can change rapidly, only measurements were kept in which several background light measurements were contained. The measured background light was then subtracted from the measured signal. After this processing step, measurements were filtered out that had a bad link margin compared to the background light level. To remove measurement errors caused by changes of channel conditions like variation of the link distance, tracking errors or similar, the mean value of each measurement was generated by using a slid-

ing average filter of 1 s. Finally, the measurements were normalized by the sliding mean value and split into blocks of 1 s duration for analysis.

3.2.1 ATENAA

In ATENAA a short horizontal near ground link was demonstrated in February 2007 [27]. The goal of this European Union funded project was to demonstrate the applicability of optical wireless communications for airborne links. Nevertheless the measurements were taken during ground tests of the communication system and therefore this measurement belongs to the group of mobile near-ground scenarios. The optical link was established between the optical ground station (OGS-OP) of the German Aerospace Center (DLR) in Oberpfaffenhofen, Germany and a plane emulating vehicle on the taxiway of the nearby airport. The system parameters are given in Table 3.1.

Table 3.1: Parameters of the communication system for the ATENAA measurements.

ATENAA	
L	1.2 to 1.4 km
$\langle P_{\mathrm{Tx}} \rangle$	0.5 W
λ	808 nm
$\theta_{3\,\mathrm{dB}}$	15 mrad
W_0	2.5 cm
D_{Rx}	8.5 cm
v_{w}	1 to 5 m/s
V	>10 000 m
Modulation Format:	NRZ-OOK
Data Rate:	125 Mbit/s
Error Protection:	Packet layer FEC
User data:	User datagram protocol based video stream
General weather conditions:	Overcast, partly sunny, relative humidity 81%, temperature -2 to 7 °C, area was partly covered by snow, some light rain showers

3.2.2 Ellwangen

These measurements were taken in the vicinity of Ellwangen, Germany, during one day in June 2010 [22]. As transmitter the Laser Communication Terminal for Marine Environment (LCT-Marine) provided by Carl Zeiss Optronics was placed on a hill top. As receiver a power meter with a 300 mm focal length refractive receiving telescope was used. The receiver was setup at four different locations within one day. At each location measurements with four different aperture plates in front of the receiving optics were taken in order to evaluate aperture averaging effects. The system parameters are given in Table 3.2.

Table 3.2: Parameters of the communication system for the Ellwangen measurements.

Ellwangen	
L	3.8, 7.3, 11.9, 16.6 km
$\langle P_{\mathrm{Tx}} \rangle$	0.1 W
λ	1550 nm
$\theta_{3\,\mathrm{dB}}$	1.1 mrad
W_0	1.0 cm
D_{Rx}	2.5, 5.0, 7.5, 9.0 cm
v_{w}	1 to 5 m/s
V	>10 000 m
Modulation Format:	NRZ-OOK
Data Rate:	125 Mbit/s
Error Protection:	none
User data:	randomly generated data
General weather conditions:	Overcast, partly sunny, relative humidity 65%, temperature 20 °C, stable conditions over the whole day

3.2.3 KIODO

The project Kirari's Optical Downlink to Oberpfaffenhofen (KIODO), was a joint project between the Japan Aerospace Exploration Agency (JAXA) and DLR in Summer 2006 and Summer 2009 [6, 57]. This project successfully demonstrated ten optical downlinks from the Japanese low Earth orbiting Optical Inter-orbit Communications Engineering Test Satellite (OICETS) to DLR's OGS-OP. For the whole campaign 18 downlinks were scheduled, but in eight tries weather conditions did not allow for closing the link. In eight of the ten successful downlinks, measurement data was recorded. OICETS had a Sun-synchronous orbit with an altitude of 610 km. All measurements were taken at night time between two and four o'clock local daylight savings time (UTC+2). The system parameters are given in Table 3.3.

Table 3.3: Parameters of the communication system for the KIODO measurements.

KIODO	
L	778 to 2542 km
$\langle P_{\mathrm{Tx}} \rangle$	0.1 W
λ	847 nm
$\theta_{3\,\mathrm{dB}}$	5.5 µrad
W_0	12 cm
D_{Rx}	5.0 and 40.0 cm with 13.0 cm obscuration
v_{w}	30 to 450 m/s
V	7000 to >10 000 m
Modulation Format:	NRZ-OOK
Data Rate:	49.3724 Mbit/s
Error Protection:	none
User data:	Pseudo random bit sequence
General weather conditions:	Night, clear to cloudy sky, relative humidity 72 to 97 %, temperature 12 to 18 °C

3.2.4 VABENE

In the project VABENE (**V**erkehrsm**a**nagement **b**ei Groß**e**reignissen u**n**d Katastroph**e**n), the successor of the project ARGOS (**A**irborne Wide A**r**ea Hi**g**h Altitude M**o**nitoring **S**ystem) [3], DLR develops a traffic monitoring and management system for disasters or major public events. For the transmission of high resolution imaging data from an aircraft, an optical link is installed. For the measurements, the aircraft equipped with the optical link was flying random paths around the OGS-OP. The measurements were taken on seven days in October 2010 and March 2011. Due to air traffic regulations the aircraft had to fly below an altitude of 3000 m. On days with cloud cover the flight altitude was even lower to avoid link blocking. The system parameters are given in Table 3.4.

Table 3.4: Parameters of the communication system for the VABENE measurements.

VABENE	
L	10 to 120 km
$\langle P_{\mathrm{Tx}} \rangle$	0.7 W
λ	1550 nm
$\theta_{3\,\mathrm{dB}}$	2.0 mrad
W_0	0.3 cm
D_{Rx}	0.3 cm
v_{w}	170 to 190 m/s
V	8000 to >10 000 m
Modulation Format:	NRZ-OOK
Data Rate:	125 Mbit/s
Error Protection:	Packet-layer Forward Error Correction
User data:	Ethernet Bridge
General weather conditions:	Sunny with clear sky to cloudy sky with some rain, relative humidity 41 to 88 %, temperature -1 to 22 °C

3.2.5 LCT-Marine

These measurements were taken during a demonstration campaign of the Laser Communication Terminal for Marine Environment (LCT-Marine) provided by Carl Zeiss Optronics [1] in June 2008. For this, the LCT-Marine was mounted on a vessel that was cruising around the Bay of Kiel at the Baltic Sea. The receiver was first placed in a building close to the coast line and later placed on a pier at the sea. The measurements were taken over the course of one day of this demonstration campaign. The system parameters are given in Table 3.5.

Table 3.5: Parameters of the communication system for the LCT-Marine measurements.

	LCT-Marine
L	6 to 24 km
$\langle P_{\mathrm{Tx}} \rangle$	0.2 W
λ	1550 nm
$\theta_{3\,\mathrm{dB}}$	1.5 mrad
W_0	1.0 cm
D_{Rx}	15 cm
v_{w}	2 to 5 m/s
V	>10 000 m
Modulation Format:	NRZ-OOK
Data Rate:	125 Mbit/s
Error Protection:	none
User data:	Ethernet Bridge
General weather conditions:	Cloudy sky with local drizzle at sea, relative humidity 38 to 56 %, temperature 20 to 24 °C

3.2.6 Eckernförde Bay

For these measurements the same setup as for the LCT-Marine measurements was used, but both communication partners were placed on piers and a static link across the Eckernförde Bay was established. The measurements were taken during one day in July 2010. The system parameters are given in Table 3.6.

Table 3.6: Parameters of the communication system for the Eckernförde Bay measurements.

Eckernförde Bay	
L	12.7 km
$\langle P_{\mathrm{Tx}} \rangle$	0.2 W
λ	1550 nm
$\theta_{3\,\mathrm{dB}}$	1.5 mrad
W_0	1.0 cm
D_{Rx}	15 cm
v_{w}	5 to 7 m/s
V	>10 000 m
Modulation Format:	NRZ-OOK
Data Rate:	125 Mbit/s
Error Protection:	none
User data:	Ethernet Bridge
General weather conditions:	Some clouds, relative humidity 49 to 64 %, temperature 18 to 20 °C

3.2.7 Naval Research Laboratory (NRL)

In November 2010 measurements were taken on the Lasercomm Test Facility (LCTF) at the Naval Research Laboratory's Chesapeake Bay Detachment. This facility has already been used in a variety of OWC experiments, e.g. [58, 59]. The measurements have been taken across Chesapeake Bay on two days, using a retro-reflected laser. The presence of a retro-reflector within the link changes the measured beam properties compared to a directly received signal, but using modulated retro-reflectors for OWC is quite common and therefore this type of link is also interesting for simulations. The system parameters are given in Table 3.7.

Table 3.7: Parameters of the communication system for the NRL measurements.

NRL	
L	32.4 km
$\langle P_{\mathrm{Tx}} \rangle$	0.2 W
λ	1550 nm
$\theta_{3\,\mathrm{dB}}$	0.15 mrad
W_0	10 cm
D_{Rx}	15 cm
v_{w}	1 to 10 m/s
V	1000 to >10 000 m
Modulation Format:	NRZ-OOK
Data Rate:	125 Mbit/s
Error Protection:	none
User data:	Ethernet Bridge
General weather conditions:	One day thin fog, the other day overcast with some rain and wet snow, relative humidity 55 to 98 %, temperature 3 to 15 °C

3.3 Statistical Description of P_{Rx}

In order to describe the statistical properties of a wireless communication channel, it is common practice to give the probability density function (PDF) and the power spectral density (PSD) of P_{Rx}. These two functions can then be used to generate time series from random numbers with the same statistical properties. These random numbers can then be interpreted as vector of P_{Rx} for computer based simulation of OWC. In the following, the measurements mentioned in Section 3.2 are analyzed in order to obtain a simple description of PDF and PSD. It is not the goal of this section to derive an exact mathematical description of P_{Rx}, but to derive a computer implementable description that can be used for discrete event simulations. Further the presented results will not give a description of solely the propagation of the laser beam. Because of the setup of the measurements, it will include all effects that are present for OWC systems like tracking errors, motion of the communication platform, and so on. A similar analysis has already been presented for some of the measurements in [23]. The results from this work have been used to refine the analysis done on the larger set of measurements presented here.

3.3.1 Distribution Function of P_{Rx}

In this subsection, the PDFs given in Section 2.3.5, which are LN, G, GG and IG are compared against the measurements from Section 3.2. The work done within this subsection is a follow up of the work previously published in [23]. In order to check the validity of the measurements, the normal distribution (N) is included in the analysis. In [23] the relative error e_{rel} has been used for evaluating the match between the distribution of measured values and a distribution function. e_{rel} is defined as:

$$\boldsymbol{e} = \mathrm{F_M}(P_{\mathrm{Rx}}) - \mathrm{F}\left(P_{\mathrm{Rx}}\right) \tag{3.1}$$

$$e_{\mathrm{rel}} = \left\langle \frac{|\boldsymbol{e}|}{\mathrm{F}\left(P_{\mathrm{Rx}}\right)} \right\rangle \tag{3.2}$$

where $\mathrm{F_M}\left(P_{\mathrm{Rx}}\right)$ denotes the ECDF of the measurement and $\mathrm{F}\left(P_{\mathrm{Rx}}\right)$ the CDF of the fitted distribution. e_{rel} had to be used in [23] for the goodness-of-fit evaluation, because a search for the parameters of GG was implemented. This search used the measurement values as input and therefore linked the distribution parameters statistically to the measured values. Statistical tests like the Kolmogorov-Smirnov test (KS-test) [60], which test for equality of two distributions can be used to compare measured values against distribution functions. In general, such statistical tests require that the measured

values and the distribution function under evaluation are statistically independent. This requirement is violated by the search of best fitting α and β values. As mentioned before, it had been observed for the previously done analysis that α and β most often were close to equal, so by setting $\alpha = \beta$ the need for a parameter search for GG can be avoided and it is valid to conduct the KS-test as rejection test. Before doing the analysis with the new values for α and β, it had to be evaluated if the assumption $\alpha = \beta$ would change the results obtained in [23]. Obviously, by removing the search, e_{rel} increases for all cases were α and β are not equal. For example in the ATENAA measurements, e_{rel} for GG increased in average by 0.05. By looking closer on the results, it can be seen that most of this degradation originates from measurements were GG is anyway not the best-fitting distribution. E.g. for the ATENAA measurements GG is still in 25 % of the measurements the best-fitting distribution as it is if the parameters are determined by the search algorithm. This investigation shows that it is valid to set $\alpha = \beta$ without penalizing the GG distribution. Since the KS-test can only be used to reject distributions and not to evaluate the quality of a fit, e_{rel} will be used as metric to evaluate the goodness-of-fit.
For the analysis, the measurements from Section 3.2 are grouped together by the scenario which they belong to. These scenarios are: Near Ground (ATENAA, Ellwangen), Maritime (LCT-Marine, Eckernförde Bay, NRL) and Airborne (KIODO, VABENE). To derive the results for each scenario, the results from each measurement campaign are normalized by the number of available data blocks, in order to give each measurement campaign equal weight. Table 3.8 shows the results of the KS-test, done with a significance level of 0.05. The KS-test shows that the proposed distributions are frequently rejected by

Table 3.8: Rejection percentage for each CDF for the KS-test with significance level = 0.05

CDF	Near Ground	Maritime	Airborne	
LN	86	94	13	%
IG	87	97	84	%
G	93	100	94	%
GG	96	100	100	%
N	100	100	100	%

the KS-test. This is not surprising, because the distributions are derived from theory which assumes a clean system without additional error sources. In measurements there are a lot of error sources that influence the distribu-

tion of P_{Rx}. Examples for such error sources are the resolution of discrete sampling devices, detector noise, vibrations of moving platforms, tracking errors, changes in link distance, varying wind speeds, fast changes in background light, thermal effects on structures and so on. This variety of possible error sources makes it impossible to completely remove their effects in post processing of measurements. Nevertheless, the KS-test results in Table 3.8 favor LN and IG as possible distributions. In Table 3.9 e_{rel} is used as metric to determine the goodness-of-fit. For the given evaluation the distribution resulting in the lowest value for e_{rel} was counted as the best-fitting distribution for each measurement. From Table 3.8 and 3.9 it can be seen that the

Table 3.9: Best-fitting CDF by e_{rel}

CDF	Near Ground	Maritime	Airborne	Overall	
IG	56	31	23	42	%
G	10	30	32	29	%
GG	16	16	24	16	%
LN	18	21	13	13	%
N	0	2	8	2	%

normal distribution was never accepted by the KS-test and that it rarely gave the best-fit by e_{rel}. This indicates that in post processing all invalid measurements, where the link was interrupted and only noise was recorded, were successfully removed from the data pool. The e_{rel} analysis shows that even though the KS-test favors LN and IG equally, the fitting-quality in terms of e_{rel} of IG seems to be better. IG was proposed in [49] as a replacement of LN in some cases where this simplifies calculations. From the shown evaluation it can be concluded that this substitution seems valid, but nevertheless LN with its theoretical justification should be favored. Another observation is that there is no single distribution that is clearly the best-fitting distribution in any of the scenarios. For an easy to use channel model a single CDF has to be selected to keep the parameterization simple. Therefore a decision has to be made to chose one of the proposed distribution functions. Because LN and GG are the two dominant distributions in theoretical work, in Table 3.10 only these two distribution functions are compared against each other using e_{rel}. That table clearly favors LN as best-fitting distribution and therefore LN will be the distribution of choice for a simplified channel model.

Table 3.10: Comparison of the fitting quality of LN and GG by e_{rel}. The values give the percentage how often the distribution was best-fitting in each scenario.

CDF	Near Ground	Maritime	Airborne	Overall	
LN	75	75	50	66	%
GG	25	25	50	34	%

3.3.2 Power Spectral Density Function of P_{Rx}

In this section the measurements from Section 3.2 are evaluated against well known filter functions in order to reproduce the atmospheric spectrum from random numbers. Equation (2.60) or the more complicated formulae given in [34] can be used to filter a set of random numbers to obtain the desired spectrum, but this approach would require to generate vectors of P_{Rx} in advance to each simulation run and the input (channel) parameters could not be changed on-the-fly. For simulation of the time varying atmospheric optical channel this is an essential feature. By using common filter functions which are part of most signal processing frameworks it is possible to filter a set of random numbers in a sequential way, or number by number. This sequential approach allows to change the filter between the processing of two numbers, thus the channel parameters can be changed on-the-fly. In order to determine a filter function suitable to describe the PSD of P_{Rx}, the methodology given in [23] is followed. The exact algorithm how the signal for this evaluation is generated is given later in Section 3.4. In a first step the digital Bessel, Butterworth, Chebyshev Type 1 and 2, elliptic and FIR filters have been used to generate series of random numbers with a PSD similar to the measured ones. In this initial analysis it has been observed (as it also had been observed in [23]) that the Bessel filters gave best results for all scenarios. Therefore a closer look on the parameterization of the Bessel filters is taken here (in respect to order n and cut-off frequency f_{c}).
For each measurement power vectors have been generated using the algorithm specified in Section 3.4 and using different orders and cut-off frequencies for the Bessel filter. For evaluating the fit between measurement and generated power vector the CDF of fade duration (t_{f}:=Duration where $P_{\mathrm{Rx}} < \langle P_{\mathrm{Rx}} \rangle$ continuously holds) and surge duration (t_{s}:=Duration where $P_{\mathrm{Rx}} \geq \langle P_{\mathrm{Rx}} \rangle$ continuously holds) has been obtained. Then the best fitting parameter set for n and f_{C} has been determined by the smallest RMS between measured and generated CDFs. In another step, the KS-test has been used to evaluate the hypothesis, that the measured and generated fade and surge durations

originate from the same distributions. Figure 3.2 shows the result of the evaluation for the best-fitting order of Bessel filter. It can be clearly seen that for each scenario a Bessel filter of order 3 gave best results, with order 2 as second best fit. For the Ellwangen measurements, several measurements had

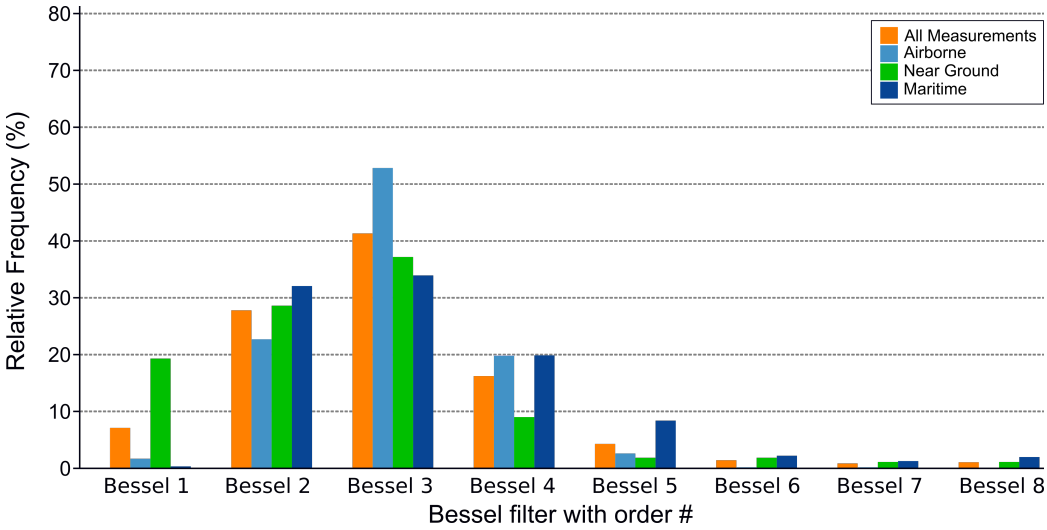

Figure 3.2: Histogram of best-fitting Bessel filters with order n, grouped by communication scenario.

been taken under the same link conditions but using different aperture sizes. The analysis of this measurement (Figure 3.3) does not show any correlation between filter order and aperture size. For the cut-off frequency of the filter the results are not so clear. In most scenarios the derived values for f_{c} span a range of several hundred Hertz, following no obvious distribution. For simulations this implies that a few frequency values from that span have to be selected as value for f_{c} for use in separate simulation runs. In Table 3.11 some statistics for the derived cut-off frequencies are given.

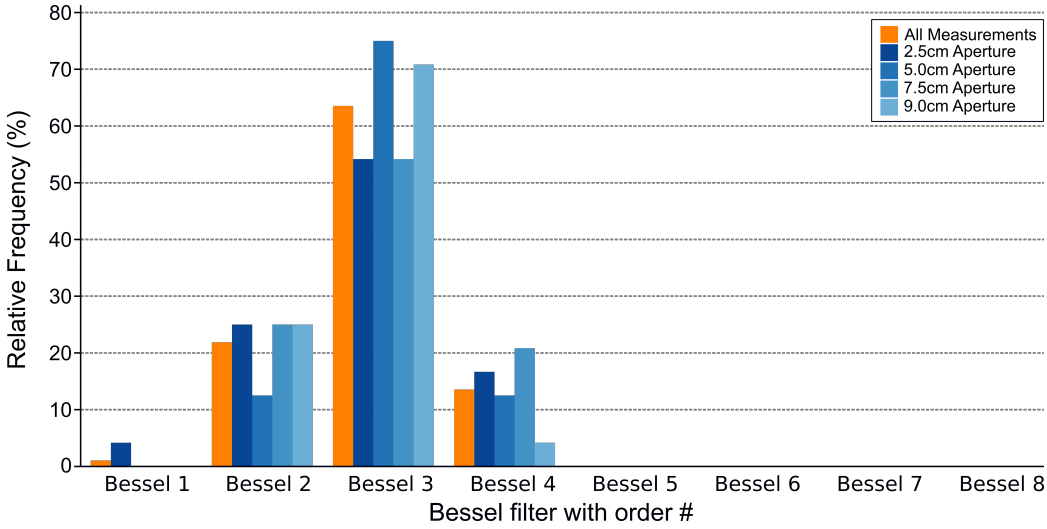

Figure 3.3: Histogram of best-fitting Bessel filters with order n for the different aperture sizes used in the Ellwangen measurements.

Table 3.11: Statistics of cut-off frequency f_c for a Bessel filter of order 3 derived from all measurements. The values in the cells give the minimum (Min.), median (Med.), average (Avg.) and maximum (Max.) value in Hz for f_c in each scenario.

Measurement	Min. f_c	Med. f_c	Avg. f_c	Max. f_c	
ATENAA	6	188	508	2461	Hz
Eckernförde	19	35	223	1168	Hz
Ellwangen	8	35	60	558	Hz
KIODO	1	293	332	1550	Hz
LCT Marine	1	15	17	1168	Hz
NRL	5	120	122	385	Hz
VABENE	1	184	207	6738	Hz

3.4 Simplified Channel Model

Results obtained in Section 3.3 confirm, that the simulation methodology proposed in [23] can be used for simulation of OWC. This methodology is commonly used for the simulation of log-normal rain or multipath fading in radio frequency communication systems and is based on three principles [61].

1. If a signal with a Gaussian distribution is put through a linear system, then the output is also Gaussian distributed (but with altered parameters μ and σ).

2. If a non-linear function with zero memory and a smooth characteristic is applied to a random signal, the PSD of the output signal will be much like the PSD of the input signal.

3. Random signals following a Gaussian distribution have a flat PSD over the whole frequency range (white Gaussian noise) and therefore can be used as basis to generate signals with a desired PSD if a suitable filter is applied.

Because an implementation of the Bessel filter proposed in section 3.3.2 can be seen as a linear device, it can be used to shape the PSD of a Gaussian signal to the desired shape of the PSD for P_{Rx} for OWC systems. The LN distribution proposed in Section 3.3.1 as PDF for P_{Rx} can be generated from a Gaussian signal by applying the exponential function, which has a smooth characteristic and zero memory. Therefore this transformation should change the PSD of the signal insignificantly. For the work presented in [26] several available random number generators had been analyzed for abnormalities in the power spectrum or the auto correlation function derived from large sets of generated numbers. None of the investigated sets of numbers gave evidence that the associated generator would produce samples with insufficient randomness. Therefore, for generating the Gaussian signal any state of the art pseudo random number generator can be used that outputs Gaussian (normal) distributed random numbers. By getting samples from the random number generator at a constant rate, the random numbers can be interpreted as values of a signal at time t and passed on to the Bessel filter. Figure 3.4 gives a schematic overview of this simplified channel model for OWC systems.

3.5 Receiver Model

In [33] it is well explained how optical receivers work. For direct detection systems, on which this work is focused, the most important element

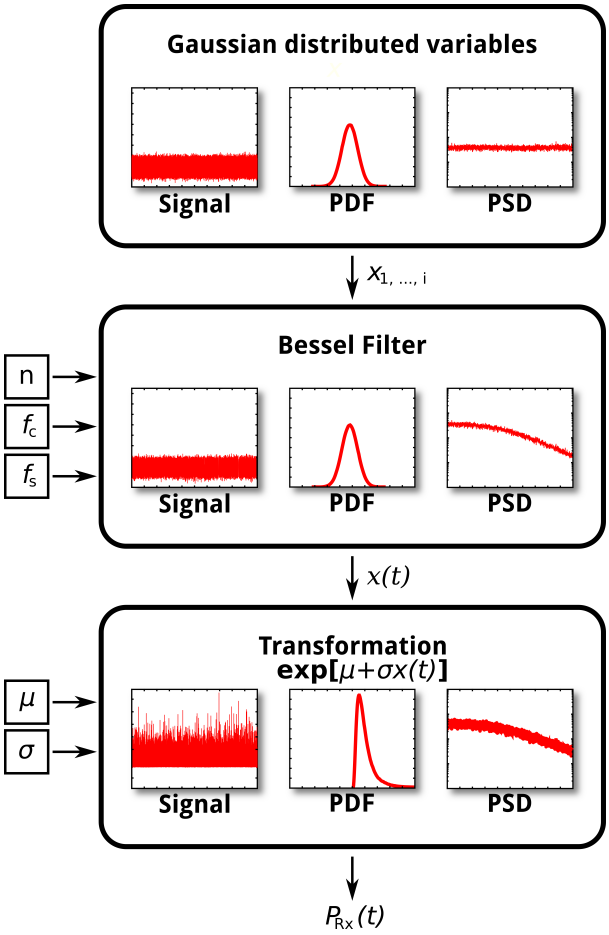

Figure 3.4: Schematic overview of the simplified channel model for OWC systems. The input parameters are limited to the filter parameters n, f_c, f_s and the parameters of the LN distribution μ and σ.

is a photo-detector, which converts the instantaneous power collected on the photo-detector surface into electrical power. This is illustrated in Figure 3.5. There is a direct relationship between the amount of optical received power and the output electrical power, but this relationship is not linear. In addition to converting optical power into electrical power, the receiver has to recover the information modulated onto the optical carrier signal. For IM/DD systems this means, that the receiver has to be capable of detecting the presence of a signal within the noise constantly received from background radiation. The power of the optical signal adds to the power of present noise, therefore the signal detection can be realized by setting a threshold value for the received power as shown in Figure 3.6.

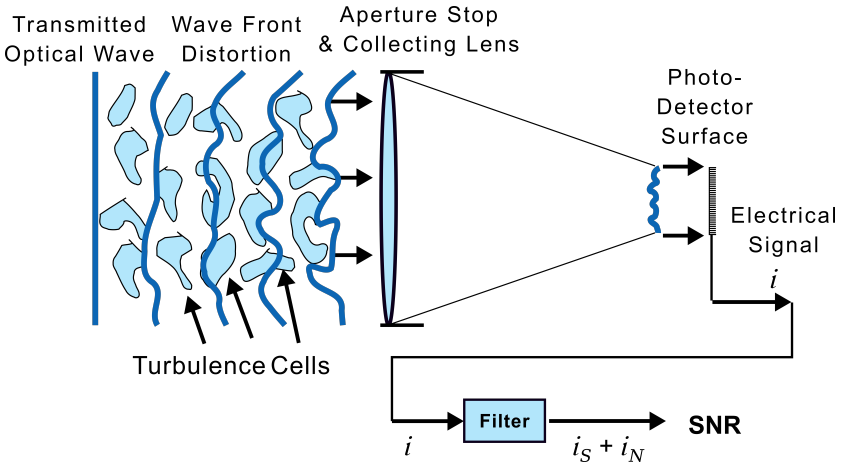

Figure 3.5: Direct detection system [33]

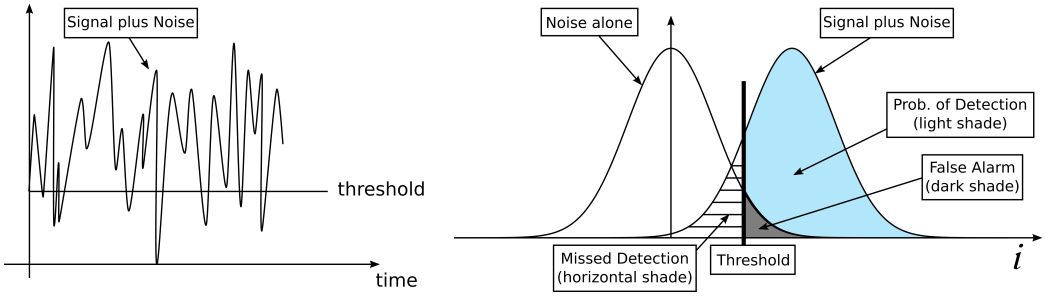

Figure 3.6: Impact of receiver threshold on detection probability [33]

The amount of received noise is varying over time and depends on many factors, like weather conditions, light emitting objects close to the optical path, position to the sun and other. Commonly a low pass filter is added to the receiver circuit which can only be passed by the higher frequencies of the intensity modulated signal and therefore eliminates most of the received noise. As there is no common way of setting the receiver threshold and designing the receiver circuit, all optical receivers have different performance characteristics. In [56] a receiver model has been developed for IM/DD systems to convert from P_{Rx} to BEP. This model will be used within this work to complete the presented OWC system model. The Rx model defines a Rx by its characteristic power P_0 and a form factor ξ. From these two parameters the BEP can be calculated by:

$$BEP\left(P_{\mathrm{Rx}}\right) = \frac{1}{2}\mathrm{erfc}\left(\frac{Q\left(P_{\mathrm{Rx}}\right)}{\sqrt{2}}\right) \tag{3.3}$$

with

$$Q\left(P_{\mathrm{Rx}}\right) = \frac{P_{\mathrm{Rx}}/P_0}{1+\sqrt{1+\xi P_{\mathrm{Rx}}/P_0}} \tag{3.4}$$

In [23] this has been rewritten to

$$Q\left(BEP\right) = \sqrt{2} \times \mathrm{erfc}^{-1}\left(2BEP\right) \tag{3.5}$$

and

$$P_{\mathrm{Rx}} = \left[\xi Q\left(BEP\right)^2 + 2Q\left(BEP\right)\right] P_0 \tag{3.6}$$

From Equation (3.6) the required P_{Rx} for achieving a desired BEP at the Rx can be calculated for the case when no turbulence is present. For the case when turbulence is present, two types of BEP have to be taken into account. The first one is the short-term BEP (BEP_{ST}). This is the bit error probability at the different power levels as calculated by (3.3). Due to the scintillation of P_{Rx} BEP_{ST} varies over time. The other type of BEP is the long-term BEP (BEP_{LT}) which is $\langle BEP_{\mathrm{ST}} \rangle$ and often used to characterize the communication performance of a link. Communication systems are generally designed to achieve a BEP_{LT} of 10^{-9} or less. If a Rx model is given as well as the PDF of P_{Rx}, then BEP_{LT} can be calculated by:

$$BEP_{\mathrm{LT}} = \int_0^\infty BEP\left(P_{\mathrm{Rx}}\right) f\left(P_{\mathrm{Rx}}\right) \mathrm{d}P_{\mathrm{Rx}} \tag{3.7}$$

Where (3.3) and (2.42) will be used as representations of $BEP\left(P_{\mathrm{Rx}}\right)$ and $f\left(P_{\mathrm{Rx}}\right)$ within this work. In order to give the channel performance in a more practical way than (3.7), e.g for including it in link budget calculations, a threshold BEP_{Th} for BEP_{ST} can be defined that divides the channel performance in a good state ($BEP_{\mathrm{ST}} \leq BEP_{\mathrm{Th}}$) and a bad state ($BEP_{\mathrm{ST}} > BEP_{\mathrm{Th}}$). This two state model is not accurate for receiver optimized for the optical wireless channel, where BEP is continuously increased with P_{Rx}, but it is valid for most commercial off the shelf (COTS) receivers for fiber based optical communications. These receivers provide near error free reception down to a certain power level (threshold). Below this power level the BEP increases until the receiver loses synchronization with the transmitted data. Resynchronization is only possible if P_{Rx} raises above the threshold again. The probability p_{bad} gives the probability for the channel to be in the bad state. The received power $P_{\mathrm{Rx,Th}}$ at least required for the channel good state can be derived from (3.6) and BEP_{Th}. If P_{Rx} is assumed to be LN distributed, then the CDF given in (2.43) can be used to calculate p_{bad} from given $\langle P_{\mathrm{Rx}} \rangle$, $P_{\mathrm{Rx,Th}}$ and σ_{P}^2:

$$p_{\mathrm{bad}} = \frac{1}{2} + \frac{1}{2}\mathrm{erf}\left\{\frac{\ln\left(P_{\mathrm{Rx,Th}}\right) - \ln\left(\langle P_{\mathrm{Rx}} \rangle\right) + \frac{\ln\left(\sigma_{\mathrm{P}}^2+1\right)}{2}}{\sqrt{2\ln\left(\sigma_{\mathrm{P}}^2+1\right)}}\right\} \tag{3.8}$$

Equation (3.8) can be solved for $\langle P_{\mathrm{Rx}} \rangle$ to get a value for the required $\langle P_{\mathrm{Rx}} \rangle$ to fulfill the channel requirements given by p_{bad} and $P_{\mathrm{Rx,Th}}$:

$$\langle P_{\mathrm{Rx}} \rangle = \exp\left[-\mathrm{erfinv}\left(2p_{\mathrm{bad}} - 1\right)\sqrt{2\ln\left(\sigma_{\mathrm{P}}^2 + 1\right)} + \ln\left(P_{\mathrm{Rx,Th}}\right) + \frac{\ln\left(\sigma_{\mathrm{P}}^2 + 1\right)}{2}\right] \tag{3.9}$$

where erfinv is the inverse error function. The additional required link margin τ_{Sci} to compensate for scintillation (also called scintillation loss) is the ratio between required received power for fulfilling the channel quality requirements without scintillation and with scintillation. For the case without scintillation the required received power is equivalent to $P_{\mathrm{Rx,Th}}$, for the case with scintillation $\langle P_{\mathrm{Rx}} \rangle$ from (3.9):

$$\tau_{\mathrm{Sci}} = \frac{P_{\mathrm{Rx,Th}}}{\langle P_{\mathrm{Rx}} \rangle} \tag{3.10}$$

In [23] three sets of parameters for receivers are given. These three receivers are CAPANINA Rx (APD, 1550 nm, 1250 Mbit/s), which is custom built by DLR, CDX RFE01b (APD, 1550 nm, 155 Mbit/s), a receiver available from Codex GmbH & Co. KG and Fujitsu FRM5W621KT/LT (APD, 1550 nm, 622 Mbit/s) which is available from Fujitsu. The parameters are given in Table 3.12.

Table 3.12: Rx model parameters for selected optical receivers

Receiver	$P_0(nW)$	ξ
CAPANINA RX	4.19	0.46
CDX RFE01b	0.92	0.78
Fujitsu FRM5W621KT/LT	1.35	0.80

Chapter 4

Simulation of Optical Wireless Communications

The results presented in Chapter 2 and 3 can be used to implement a simulation system for OWC. In Chapter 2 formulae are given for calculating important communication parameters, while in Chapter 3 it is shown how time series of P_{Rx} can be generated based on these calculated parameters. In the following section the developed simulation framework is presented and parameters for common OWC scenarios are given.

4.1 Simulation Model

The proposed methodology for simulation of OWC consists of three modules. The first module is the link parameter calculation (LPC). The LPC takes input parameters to describe the communication system, the communication scenario and the desired link quality and outputs an estimate of the expected link quality and distribution parameters for P_{Rx}. The second module is the simplified channel model which generates a time series of P_{Rx}. The required input parameters are the description of the used filter and the targeted distribution parameters for P_{Rx}. The last module is the implementation of the channel where the generated P_{Rx} time series is used to decide if a transmitted bit is corrupted or not. Figure 4.1 shows a schematic overview of the simulation methodology for OWC systems. In this figure the elements required for the LPC are marked green. The description of the OWC system consists of parameters for Tx and Rx. Tx is defined by mean transmission power $\langle P_{\mathrm{Tx}} \rangle$, wavelength λ, beam diameter at transmit aperture W_0 and beam $1/e^2$ half divergence angle θ_{B}. Rx is defined by receive aperture diameter D_{Rx}, its characteristic power P_0 and its form factor ξ. The description of the

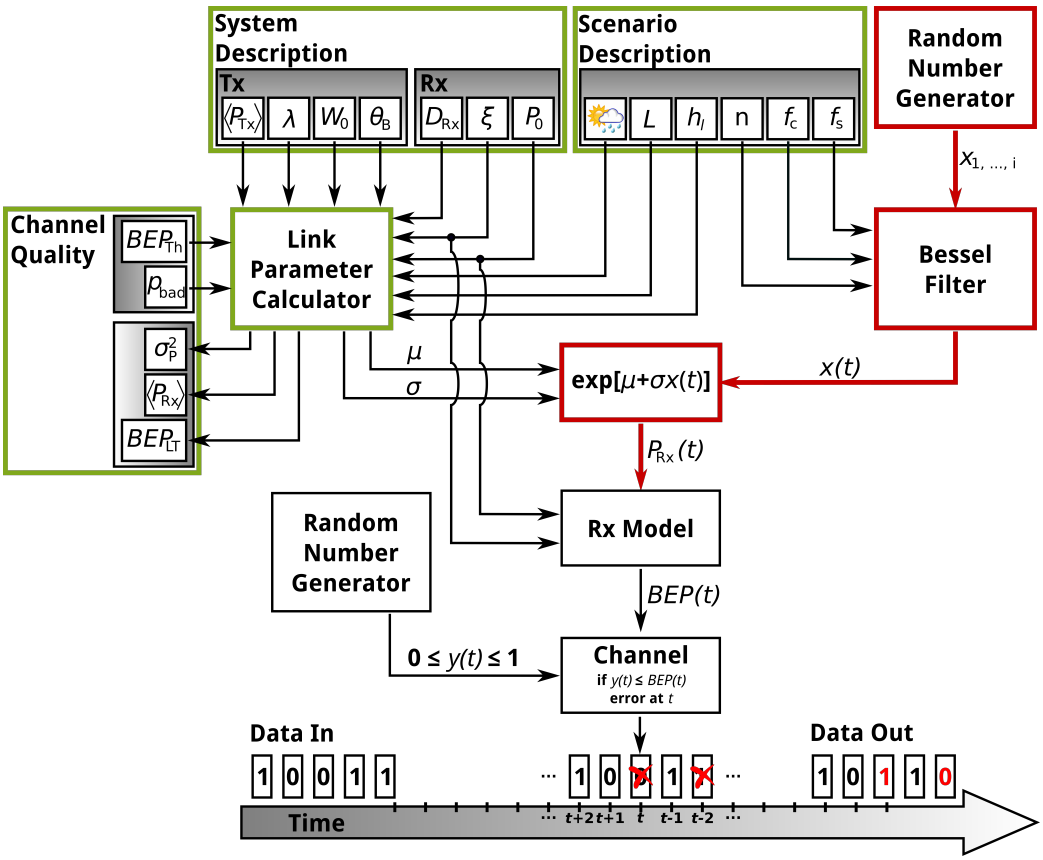

Figure 4.1: Schematic overview of the simulation methodology for OWC systems. The red marked elements are the components of the simplified channel model presented in Chapter 3. The green marked elements are the elements defining the optical link. These elements can also be used during the design phase of an OWC system to evaluate the effect of parameter changes on the final system. The second random number generator is used to decide if a bit is in error or not, based on the output of the Rx Model.

communication scenario consists of the weather conditions for which the link is designed (clear, rain, fog or snow and visibility V), the link distance L, hight profile along the link h_l, and a description of the filter (order n, cut-off frequency f_c and the sampling rate f_s used for the time interpretation of the generated samples). The input parameters from the channel quality class are bit error probability threshold BEP_th and the probability p_bad of having a BEP below BEP_th. Output of the LPC are the link quality parameters power scintillation index σ_P^2, mean received power $\langle P_\mathrm{Px} \rangle$ and an estimate of the long-term bit error probability BEP_LT. Additionally the parameters of

the LN distribution mean μ and variance σ are calculated from σ_{P}^2. The LPC can also be used during design of the communication system for evaluating the effect of changing the OWC system parameters on channel quality. The red marked elements are the elements of the simplified channel model as described in Section 3.4. This block takes n, f_{c} and f_{s} from the scenario description and μ and σ from the LPC as input parameters and produces a time series for P_{Rx}. It has to be noted that the filtering of the signal will affect the variance of the generated signal. The change in variance depends on n, f_{c} and f_{s}, but if n and f_{s} are fixed during the simulation, a formula for relating f_{c} and the change in variance can be derived. The lower half of Figure 4.1 shows the elements required for completing the simulation of OWC. The Rx model from Section 3.5 is used to convert a $P_{\mathrm{Rx}}(t)$ value to a value for the bit error probability $BEP(t)$. The input parameters P_0 and ξ are taken from the system description. With the given f_{s} from the scenario description the $P_{\mathrm{Rx}}(t)$ values are interpreted as P_{Rx} at time t and so is the calculated $BEP(t)$. For every bit arriving at the channel in the time interval $[t, t+1)$, a normal distributed number $y(t) \in [0, 1]$ can be generated by a random number generator to decide if the bit is in error or not. If $y(t) \leq BEP(t)$, then the bit is assumed to be in error.

4.2 Accuracy of the Simulation Model

In order to evaluate the accuracy of the simulation model, all measurements used for the analysis in Chapter 3 were compared against data generated by using the simulation methodology given in Section 4.1. As receiver for the analysis of generated error patterns, the CAPANINA RX from Table 3.12 has been used. In order to obtain the maximum expectable accuracy, the input parameters have not been derived from the LPC, but directly from each measurement. The values in Table 4.1 show that the simulation methodology

Table 4.1: Average e_{rms} for several CDFs of the features received power, fade time, surge time, error segments and no error segments derived from generated power series. The given results for e_{rms} in each cell are rounded to two decimal places (i.e. 0.00 is < 0.005).

Scenario	P_{Rx}	t_{f}	t_{s}	Error Segments	No Error Segments
Airborne	0.02	0.06	0.05	0.00	0.00
Near Ground	0.02	0.10	0.10	0.00	0.01
Maritime	0.09	0.11	0.10	0.00	0.00

is able to generate series of P_{Rx} with an e_{rms} of ≤ 0.09 for all three scenario groups. The accuracy of the generated t_{f} and t_{s} CDFs are up to e_{rms} of 0.11 off the targeted durations. When the measured and generated vectors are put through a receiver model for generating bit error sequences it can be seen that the CDFs for length of continuous segments of errors and no errors have an average e_{rms} of less than 0.01. When the feature vectors used for Table 4.1 are evaluated via KS-test to originate from the same distribution as the feature vectors derived from the measurements, a similar picture is drawn. In this case the null hypothesis is that the generated feature vector originates from the same, but unknown, distribution as the feature vectors derived from the measurements. The two-sample KS-test with a confidence level of 0.05 is used to evaluate if the null hypothesis can be rejected. The results from this evaluation are given in Table 4.2. If the null hypothesis is

Table 4.2: Rejection percentage of KS-test with significance of 0.05 for the null hypothesis that the generated feature series originates from the same distribution as the feature series obtained from measurement.

Measurement	P_{Rx}	t_{f}	t_{s}	Error Segments	No Error Segments	
Airborne	90	45	45	0	0	%
Near Ground	93	46	44	9	17	%
Maritime	95	22	10	1	7	%

always true, then the KS-test should falsely reject the hypothesis in 5 % of the tests done. The table shows that the generated P_{Rx} is rejected in over 90 %, so it can not be used for simulations requiring high accuracy for received power. When looking at the generated error segments the table shows that the generated vectors are in good agreement with the measurements.

4.3 Communication Scenarios

In the following some communication scenarios are given in which OWC is currently deployed. For each scenario all required parameters for the simulation of an IM/DD OWC system consisting of low-cost components are given as well as the output from the LPC. For simplicity reasons it is assumed that the same transmitter terminal is used in all scenarios. For IM/DD OWC systems, the most favorable wavelength is 1550 nm, which is also the most often selected wavelength from the demonstrations referenced in Section 3.2. There are three main benefits for selection of this wavelength. First, there is an atmospheric window at this wavelength, which means that the atmospheric

loss for this wavelength is less than for other wavelengths [34, 35]. Second, the human eye can not focus light of 1550 nm on the retina, thus allowing for much higher eye-safe power levels than wavelengths that can get focused on the retina like 850 nm. Third, 1550 nm are also used for fiber optical communications and therefore a wide range of commercial of the shelf products are available at this wavelength, especially SWaP optimized erbium-doped fiber amplifiers (EDFA) that can be used to get higher $\langle P_{\mathrm{Tx}} \rangle$ for long-range transmissions. Currently available small form factor EDFA offer $\langle P_{\mathrm{Tx}} \rangle$ of up to 500 mW. The SWaP footprint of these modules is small enough to fit in every type of optical terminal but the peak output power of 1 W would require special optics to spread the output beam in order to fulfill eye-safety regulations. For the base of the calculations presented here, $\langle P_{\mathrm{Tx}} \rangle$ of 150 mW and 300 mW will be used. By spreading these beams at the transmit aperture to W_0 =2.5 cm or larger, eye-safety requirements can be satisfied and the optics can be realized with a small size and weight footprint. In mobile scenarios θ_{B} should be around 0.5 mrad to allow for some errors by the tracking system. As Rx the CAPANINA receiver from Table 3.12, optimized for a data rate of 1 Gbit/s is used. D_{Rx} will vary between the scenarios as it is desirable to have an aperture as large as possible (limited by SWaP). For small OWC terminals, as they are used on planes or other airborne platforms, D_{Rx} is typically limited from 10 to 20 cm to keep the terminal footprint small for reduced additional drag on the aircraft. For optical ground stations, which are set up at a fixed location, a D_{Rx} in the range from 40 to 100 cm can be realized. In the following a D_{Rx} of 15 cm or 20 cm will be used for mobile terminals, depending on the type and load capabilities of the platform. 60 cm apertures will be used for fixed stations. For the calculation of $\langle P_{\mathrm{Rx}} \rangle$ in the LPC it will be assumed that the optical system has a loss of 3 dB because of beam splitting for tracking systems, tracking errors (vibration), component misalignment and absorption by components. The weather condition will be clear air with V=8 km in most scenarios, except for high altitude scenarios where much better visibility can be assumed. L will vary from scenario to scenario and h_l will be calculated assuming a spherical earth model. The validity of the spherical Earth model for calculations done on the presented long-range links, has been shown in [21]. The filter parameters for the channel model are selected according to the observations made in section 3.3.2. Because all system parameters are fixed by technological limitations, BEP_{th} and p_{bad} can not be used for adjusting these parameters, e.g. increase $\langle P_{\mathrm{Tx}} \rangle$ to meet the given channel quality. For each scenario the required mean received power $\langle P_{\mathrm{Rx}} \rangle_{\mathrm{th}}$ for achieving $BEP_{\mathrm{th}} = 10^{-6}$ and $p_{\mathrm{bad}} = 0.99$ will be given as additional information. For evaluating the expectable channel quality in each scenario, BEP_{LT} is calculated. In some scenarios the system

parameters will depend on the direction of the link, e.g. for links between a fixed and a mobile platform. In this case both link directions are given to show the asymmetry of the link. For the simulation of such a scenario, communications in both directions (up- and downlink) have to be simulated, to cover the effects of this asymmetry. In the proposed model the quality of the designed links is defined by p_{bad} and BEP_{th}. For the quality of service (QoS) in wireless 3G networks, the ITU defines requirements of a residual BER between 10^{-3} and 10^{-6} for all types of service [62]. In addition, all delay critical services can accept packet losses of up to 1%. In [63] it is stated that for Digital Subscriber Line (DSL) systems, a worst-case BER of 10^{-6} should be expected. From these reports it is derived that all communication services that are developed following the ITU recommendations should be able to operate over links with a residual BER of 10^{-6} in order to be available to a broad audience (all 3G and DSL users). Therefore this value will be used for BEP_{th}. With BEP_{th} set, p_{bad} can be used to evaluate if the channel fulfills the given QoS requirements. Using the assumption that all delay critical services can deal with 1% of loss and all other services implement their own mechanism to ensure error free transmission, the channel is assumed to be ok if $p_{\text{bad}} \leq 0.01$. If this condition is not fulfilled, additional mechanisms are required for improving the channel quality.

4.3.1 Near Ground and Maritime Links

For land-mobile near ground links, small terminals can be mounted on top of cars, rovers, vans, or similar. An example of such a terminal has been demonstrated in [64]. Other use cases are small terminals mounted on masts for communication between fixed locations or the use of OWC terminals for interconnection between ships. For long-range near ground links the biggest challenge is given by vegetation, ground formations and the Earth curvature that limit the length of the link. Therefore the terminals in this scenario will either be placed on a mast, an elevated position, or on top of some structures. In most cases these links will be limited to distances of about 20 km, where for links between large ships like aircraft carriers 50 km might be feasible. Application of this link type is e.g. the establishment of surveillance infrastructures along borders, around larger acreage, to offshore facilities, or the interconnection between temporary camps, auxiliary teams or tactical units. In the maritime use case turbulence affecting the communication beam will generally be less than in the near ground case [59], therefore the simulations will be done for near ground links with range up to 50 km as worst-case simulation.

NGND		
$\langle P_{\mathrm{Tx}} \rangle$	150	mW
λ	1550	nm
W_0	2.5	cm
θ_{B}	0.5	mrad
D_{Rx}	15	cm
P_0	4.19	nW
ξ	0.46	
Weather	clear air	
V	8	km
L	50	km
n	3	
f_{c}	100	Hz
f_{s}	10	kHz
σ_{P}^2	0.0 - 1.5	
$\langle P_{\mathrm{Rx}} \rangle$	100	nW
$\langle P_{\mathrm{Rx}} \rangle_{\mathrm{th}}$	80	nW
BEP_{LT}	1×10^{-8} - 1×10^{-2}	

Table 4.3: Simulation parameters for the near ground and maritime OWC scenario

4.3.2 UAV to Ground

A common use case for OWC is the connection between a UAV (or drone) and a control station. UAVs are often used for reconnaissance missions in case of disasters or military conflicts. UAVs are most often equipped with cameras for taking images of a target area and OWC can offer sufficient bandwidth for simultaneous transmission of several high definition or 3D video streams. It can be assumed that clouds should not pose a problem for OWC in this scenario as the presence of clouds would also prevent the use of cameras. The flying altitude of such UAVs is generally between 3 and 5 km (some military UAVs fly at higher altitudes, but these shall not be taken into account). The range in this scenario is mostly limited by the surroundings of the ground station, which might block the line of sight at lower elevation angles, but with thoughtful placement of the ground station, link distances up to 100 km should be realizable.

OGS-UAV/UAV-OGS			
	Uplink	Downlink	
$\langle P_{\mathrm{Tx}} \rangle$	300	150	mW
λ	1550	1550	nm
W_0	2.5	2.5	cm
θ_{B}	0.5	0.5	mrad
D_{Rx}	15	60	cm
P_0	4.19	4.19	nW
ξ	0.46	0.46	
Weather	clear air	clear air	
V	8	8	km
L	70	70	km
n	3	3	
f_{c}	300	300	Hz
f_{s}	10	10	kHz
σ_{P}^2	0.0 - 1.5	0.0 - 1.5	
$\langle P_{\mathrm{Rx}} \rangle$	60	490	nW
$\langle P_{\mathrm{Rx}} \rangle_{\mathrm{th}}$	80	80	nW
BEP_{LT}	6×10^{-5} - 4×10^{-2}	$< 1 \times 10^{-14}$ - 4×10^{-4}	

Table 4.4: Simulation parameters for the OWC ground to UAV link

4.3.3 Aircraft to Aircraft

Another airborne OWC scenario is the interconnection of commercial aircrafts to form a flying transatlantic network. Commercial aircrafts fly at altitudes between 9000 and 15 000 m. For flying by visible flight rules they keep a minimum distance of 1500 m to the cloud layer below. In general, cloud structures reaching up into this flight level can be assumed to be caused by severe weather conditions that will be avoided by the aircrafts. Therefore cloud blocking should only be a problem if the link distance between the aircrafts would require the OWC link to pass through the cloud layer below. Using a spherical Earth model, the presence of the cloud layer below should limit the link distance in this scenario to about 320 km. Due to the limited size of the assumed terminal, a reduced link distance of about 150 km seems feasible. At the given altitudes the thin atmosphere should be exceptionally clear, giving a visibility range greater 100 km.

AC-AC		
$\langle P_{\mathrm{Tx}} \rangle$	300	mW
λ	1550	nm
W_0	2.5	cm
θ_{B}	0.5	mrad
D_{Rx}	15	cm
P_0	4.19	nW
ξ	0.46	
Weather	exceptionally clear air	
V	100	km
L	150	km
n	3	
f_{c}	300	Hz
f_{s}	10	kHz
σ_{P}^2	0.3 - 0.6	
$\langle P_{\mathrm{Rx}} \rangle$	80	nW
$\langle P_{\mathrm{Rx}} \rangle_{\mathrm{th}}$	80	nW
BEP_{LT}	2×10^{-3} - 7×10^{-3}	

Table 4.5: Simulation parameters for the Aircraft to Aircraft OWC link

4.3.4 High Altitude Platforms

High Altitude Platforms (HAP) are quasi-stationary airborne platforms that are placed at altitudes between 17 and 25 km, above commercial air traffic flight levels. Equipped with microwave telecommunications technology such HAPs could service an area of several hundred square kilometers. Recently, companies like Google with Project Loon [65] and Facebook with its Connectivity Lab [66], have started to invest in this technology and are pushing the development of commercial systems. For HAP networks, OWC is predestined to be used for the interconnection of the nodes. At the altitude between 17 and 25 km, winds are reduced compared to lower altitudes which is favorable for the position keeping of HAPs. In addition, in some regions, especially close to the equator, cloud formations can reach altitudes up to 19 km, so for permanent connection, the optical link should be kept above this altitude. This altitude limit also prevents the optical links from interfering with commercial air traffic which uses altitudes below 15 km. Assuming a positioning altitude for HAPs of 23 km, the implementable link distance is limited to about 450 km, nevertheless, especially for robustness of the link and a good ground coverage, HAPs should be placed no further than 200 km from each other.

HAP-HAP		
$\langle P_{\mathrm{Tx}} \rangle$	300	mW
λ	1550	nm
W_0	2.5	cm
θ_{B}	0.5	mrad
D_{Rx}	20	cm
P_0	4.19	nW
ξ	0.46	
Weather	exceptionally clear air	
V	100	km
L	200	km
n	3	
f_{c}	50	Hz
f_{s}	10	kHz
σ_{P}^2	0.2 - 0.4	
$\langle P_{\mathrm{Rx}} \rangle$	70	nW
$\langle P_{\mathrm{Rx}} \rangle_{\mathrm{th}}$	80	nW
BEP_{LT}	1×10^{-3} - 4×10^{-3}	

Table 4.6: Simulation parameters for optical interconnection of HAPs

4.3.5 Ground to High Altitude Platform

The main use case of HAPs is the establishment of a flying backbone for offering radio frequency telecommunication services. For the connection of this backbone to ground based telecommunications infrastructure optical wireless links can be used. In this scenario cloud blocking poses definitely a problem. One concept for fighting this problem is the installment of several optical ground stations (OGS) which are distributed over a large enough area for uncorrelated weather conditions between the locations. In addition the placement of the OGSs relative to the HAPs can reduce the likeliness of cloud blocking. Because of geometric constraints the probability for a randomly placed cloud to block the link decreases with the increase of the elevation angle between OGS and HAP. Therefore in this scenario an OGS should be placed as close as possible to the perpendicular foot of a HAP for achieving a larger elevation angle (>45°). This consideration limits the link distance to about 35 km.

OGS-HAP/HAP-OGS			
	Uplink	Downlink	
$\langle P_{\mathrm{Tx}} \rangle$	150	150	mW
λ	1550	1550	nm
W_0	2.5	2.5	cm
θ_{B}	0.5	0.5	mrad
D_{Rx}	15	60	cm
P_0	4.19	4.19	nW
ξ	0.46	0.46	
Weather	clear air	clear air	
V	8	8	km
L	35	35	km
n	3	3	
f_{c}	100	100	Hz
f_{s}	10	10	kHz
σ_{P}^2	0.0 - 1.5	0.0 - 2.5	
$\langle P_{\mathrm{Rx}} \rangle$	600	5500	nW
$\langle P_{\mathrm{Rx}} \rangle_{\mathrm{th}}$	80	80	nW
BEP_{LT}	$< 1 \times 10^{-14}$ - 2×10^{-4}	$< 1 \times 10^{-14}$ - 1×10^{-6}	

Table 4.7: Simulation parameters for links between an OGS and a HAP

4.3.6 Aircraft to High Altitude Platform

Another use case for HAPs is the connection between HAP networks and commercial aircrafts. These links shall provide entertainment and communication services for the passengers as well as air traffic control services for flight safety. Commercial aircrafts usually fly above the cloud layer at altitudes between 9 and 15 km, HAPs should be positioned between 17 and 25 km of altitude. Using the given geometric constraints, link distances of up to 700 km are feasible. For a flexible network layout, the aircraft terminal should be able to connect to HAPs and other aircraft, so the same terminal should be used for both types of links. As mentioned before, the SWaP requirements given for adding OWC terminals to an aircraft allow only for smaller terminals with limited communication range.

AC-HAP/HAP-AC			
	Uplink	Downlink	
$\langle P_{\mathrm{Tx}} \rangle$	300	300	mW
λ	1550	1550	nm
W_0	2.5	2.5	cm
θ_{B}	0.5	0.5	mrad
D_{Rx}	20	15	cm
P_0	4.19	4.19	nW
ξ	0.46	0.46	
Weather	exceptionally clear air	exceptionally clear air	
V	100	100	km
L	150	150	km
n	3	3	
f_{c}	200	200	Hz
f_{s}	10	10	kHz
σ_{P}^2	0.3 - 0.6	0.3 - 0.5	
$\langle P_{\mathrm{Rx}} \rangle$	100	80	nW
$\langle P_{\mathrm{Rx}} \rangle_{\mathrm{th}}$	80	80	nW
BEP_{LT}	1×10^{-4} - 1×10^{-3}	2×10^{-3} - 6×10^{-3}	

Table 4.8: Simulation parameters for optical interconnection of commercial aircrafts and HAPs

Chapter 5

Error Protection for Optical Wireless Communications

For wireless links (RF and optical), the biggest challenge in establishing reliable communications is the fading of the received signal P_{Rx}. Although the cause of this fading is manifold, the result is always the same. The fading of P_{Rx} causes variation in BEP for the communication link, where strong fades cause P_{Rx} to drop down to levels where reliable communication is not possible due to the increased BEP. For OWC it is often tried to solve the fading problem on the physical layer [8]. Goal of these efforts is to reduce the fading of P_{Rx}, especially to reduce the occurrence of deep fades. On the transmitter side the simplest mitigation approach is to increase P_{Tx} to power levels, for which fading can not reduce P_{Rx} down to these bad levels. Unfortunately, SWaP requirements and eye-safety regulations limit the applicability of this approach. Instead of increasing P_{Tx} of a single link, a smarter approach is to utilize multiple, spatial separated communication beams (spatial diversity) that transmit the same data over statistical independent channels. At the receiver these beams are seen as a single beam with increased P_{Rx} and reduced fading due to the statistical independence [10]. It is also possible to create these statistical independent channels by using different wavelengths (wavelength diversity), but this leads to a higher complexity at the receiver side [9]. Because SWaP requirements limit the number of implementable channels in general, the diversity techniques can not completely remove the impact of fading. On the receiver side the most common approach to tackle the fading problem is to utilize the effect of aperture averaging [12], where the size of the receiving aperture is limited by size and weight constrains. The use of multiple receivers (receiver diversity) is also limited by SWaP [11]. The latest approach on the physical layer is the use of adaptive optics systems to predistort the emitted wavefront at the transmitter and to correct the incom-

ing wavefront at the receiver. Because of existing physical limitations this approach can only correct the distortions caused by a few kilometers of link distance and therefore its applicability is limited, especially for long-range links [67]. Concluding this section, although there exist several techniques to mitigate the fading problem on the physical layer, none of them alone and also no combination of these can guarantee a channel that does not suffer from fading. Therefore additional mechanisms have to be implemented on the communication layer to enable reliable communications for OWC systems.

5.1 Protection Schemes

For error protection and correction on communication layer there are three classes of schemes. The first one are the proactive schemes where precautionary measures are taken before data is transmitted to reduce the risk of losing data on the link. The second class are the reactive schemes were errors inside the communication are detected and actions are taken to correct them. The third class is the combination of techniques from both classes, the so called hybrid schemes. The dominant technique of the proactive schemes is forward error correction (FEC) and the most often used reactive technique are Automatic Repeat reQuest (ARQ) protocols. Both schemes will be discussed in the following and a hybrid cross-layer protection scheme tailored for OWC will be presented.

5.1.1 Forward Error Correction (FEC)

As a proactive scheme FEC is commonly used to protect data on simplex communication links and does not require a feedback channel. For FEC the data is encoded in a structured way, generating redundancy within the transmitted data. The added redundancy and the known structure of the data are used at the receiver for correctly decoding the data even if it got corrupted during transmission. The amount of added redundancy and the algorithm used to generate the redundant data determine the number of errors that can be tolerated by the used code. If more errors are contained within the received data than the code can deal with, the whole lot of data is lost. For FEC, all operations are done on symbols with size s. This means that s bit of transmitted data form one coded symbol. Since all operations are done on these symbols, it does not make any difference if just one bit within a transmitted symbol gets corrupted, or alls bits. In both cases the error counts as one symbol error. The application of FEC on the optical wireless physical layer [4, 68] as well as on the packet layer [14, 69] has already been demon-

strated for OWC. For the physical layer FEC demonstrations it has to be noted that in [4] there was an amplifier in the receiver chain that eliminated the fading behavior of the received signal. Therefore in this case FEC was not applied directly to the optical fading channel, it was used to compensate for the added signal noise by the amplifier. In [68] FEC was applied directly to the fading optical signal, but also an interleaver was used that introduced a delay of 1.25 s, which is a not acceptable delay for many types of communications. Nevertheless, these demonstrations have shown that available FEC codecs can be used at data rates of up to 10 Gbit/s.
The most often used types of FEC codes are so called block codes. For these codes the encoder splits the incoming data into blocks with k symbols and adds a given number of redundancy symbols to form a code word with length n. On the physical layer one symbol is usually one byte, while on the packet layer one symbol is usually one packet (with fixed length) or a larger block of data (e.g. 1000 B). For the physical layer, an often used code is the Reed-Solomon (RS) code RS(255, 236) with $n = 255$, $k = 236$, $s = 8$, and $\delta = 9$ or RS(255, 223) with $n = 255$, $k = 223$, $s = 8$, and $\delta = 16$. Where δ is the error correction capability of the code. This means that these codes can correct 9, respectively 16 erroneous transmitted bytes, no matter how many bit errors are contained within. Nevertheless, the 255 B of the code word take only 2.04 µs for transmission with typical data rate for OWC of 1 Gbit/s. Compared to the relatively large fade durations of up to several milliseconds experienced on OWC links, these codes can not be used on their own to set up a reliable channel. For implementing larger RS codes the decoding complexity increases heavily, making it difficult to process higher data rates in the Gbit/s order. Another group of codes that can be used to generate longer code words are low-density parity check (LDPC) codes, for example the LDPC code used for DVB-S2 works on code words with a length of 8100 B which would be 64.8 µs on a 1 Gbit/s link. But again, this duration is not long enough for the requirements given for reliable communications. By implementing the LDPC code from DVB-S2 on the packet layer and using s =1000 B, one can achieve a duration of 64.8 ms on the given link. This duration would be in a range suitable for reliable communications. The major drawback of this approach is that buffering, encoding and decoding introduce additional delay into the communication path. The buffering delay is proportional to k times the symbol size as this amount of data has to be buffered for generating the redundancy. The encoding delay depends on the encoding algorithm, but as some algorithms are capable of on-the-fly encoding while the data is buffered, the encoding delay can be neglected. Because the decoding complexity increases with code word size, the decoding process impacts the over all delay and is assumed to be above 100 ms for the given

code word size (some times over 500 ms are assumed) [31]. Because the decoded data has to be stored at the receiver until the final bit is decoded, additional buffering delay is added at the receiver. The sum of all delays can easily exceed 300 ms, especially if OWC is used as part of a communication network, where other segments also add delay to end-to-end communication. The International Telecommunication Union (ITU) suggests maximum delays for end-to-end one way communication of 400 ms, where some services might not tolerate delays over 100 ms [70, 62]. Therefore packet layer FEC can not be used as general error protection mechanism in OWC systems, but it is very well suited for delay tolerant services like file transfer.

5.1.2 Automatic Repeat reQuest (ARQ) Protocols

Since ARQ is a reactive error correction scheme it requires a feedback channel in order to signal data losses from receiver back to transmitter. For the implementation of this feedback, the transmitted data is split into frames where each frame is marked with a specific identifier. Based on this identifier the receiver can detect lost frames and inform the transmitter about this loss. The transmitter can then resend the missing frame for correcting this loss. The application of ARQ for OWC has been researched in [29, 16, 17, 30]. From the known ARQ protocol variants (stop-and-wait, go-back-n, selective-repeat), selective-repeat ARQ (ARQ-SR) is the most advanced version and should be used for error protection in OWC systems. In ARQ-SR, the transmitter is continuously transmitting data, even in case of lost data. The receiver is signaling received and lost data back to the transmitter using acknowledgment (ACK) or negative acknowledgement (NACK) information. This information can be embedded in data frames or transmitted in dedicated frames. Based on the received ACK and NACK information, the transmitter will mix retransmissions of lost data into its output in order to correct the signaled errors. In theory this approach guarantees that all frame losses on the transmission channel can be corrected by retransmissions, but for practical application there are two limiting constraints. The first one are the available buffer sizes in receiver and transmitter. In case of lost frames at the receiver, all incoming data has to be buffered until the frame is successfully received after any number of retransmissions. In case of larger BEP it is very likely that also the retransmitted frames get lost and have to be retransmitted again and again. Since new data will arrive in-between the retransmissions, the buffer at the receiver will fill up. At the transmitter side, all transmitted but not yet acknowledged data has to be buffered for retransmission. So also on the transmitter side the buffer will fill up if a frame subsequently fails to arrive at the receiver. Besides filling up

buffers, the retransmissions also consume some time and increase the delay for the transmitted data. Therefore the second limiting constraint are delay requirements given by the transported services which limit the number of retransmissions for a single frame. These two practical limitations prevent ARQ-SR protocols from correcting all errors and some amount of residual errors has to be accepted. Nevertheless, the adaptation of the redundancy to the link conditions (no retransmission in best case, maximum number of retransmissions in worst-case) give ARQ-SR advantage over FEC in terms of efficiency, because FEC always has a fixed amount of redundancy contained within the transmitted frames. This advantage comes with additional cost for the configuration of the protocol. The buffer sizes have to be set in order to allow for the number of required retransmissions and the maximum number of retransmissions has to be limited to meet delay requirements of the transported services. Because also frames transmitting acknowledgment information can get lost, timers have to be implemented that trigger retransmissions of unacknowledged frames at the sender and also for giving frames finally lost at the receiver in order to continue transmission of correctly received frames. In dynamic scenarios with changing link distance these timer values have to be adjusted to the changing propagation delay between Tx and Rx. At the Tx, badly configured timers lead to early retransmissions, if the timer runs out just before the ACK arrives or late retransmissions, if the retransmission of a frame is triggered a while after a lost ACK should have arrived. At the Rx bad timers lead to unnecessary lost data if a frame is given lost just before it arrives (early timeout) and unnecessary delay if the Rx keeps waiting for a frame that has been finally lost (late timeout).

5.2 Error Protection and Correction (EPC) Protocol for Optical Wireless Communications

In this section a hybrid EPC approach on data link and physical layer is suggested that improves communication quality on optical wireless channels to be suitable for telecommunication services. The main design goal is to develop a link that meets the requirements given by the ITU [70, 62]. These requirements are a residual packet loss rate of less than one percent for any size of packets and a maximum end-to-end delay of 100 ms. Because well designed, delay-critical services prevent fragmentation of packets on the Ethernet layer, it is legitimate to assume that higher layer packets are equivalent to Ethernet frames and therefore the higher layer packet loss rate will be

equivalent to the frame erasure rate (FER) on the physical layer. In order to shadow the added EPC protocol from higher layers and to avoid side effects with other protocols, the proposed protocol shall guarantee in-order delivery. As there are currently no standards defined covering the interfaces and the physical layer of OWC devices, most available devices use Gigabit-Ethernet as standard interface and include an internal media converter for access of the OWC physical layer. These media converters take the parallel transmitted Ethernet signal and serialize it to an amplitude modulated binary signal. This serial signal is then used to modulate a laser diode for the optical wireless transmission. The developed protocol should fit into this system architecture without requiring changes on higher communication layers, i.e. the connecting interface to the optical link should still be Gigabit-Ethernet. The wireless LAN standard IEEE 802.11 [71] integrates ARQ and FEC into the wireless physical layer, but is not suitable for OWC for the following reasons. First, the standard is tailored for short range radio frequency links and implements a stop-and-wait ARQ, which has been shown to be inefficient for long-range OWC links [29]. Additionally, the timeout values for the ARQ protocol are fixed to values too low for long-range links. Second, the FEC is integrated into the physical layer together with coherent modulation schemes that can not be applied to optical IM/DD systems.
The ITU has published the recommendation G.9960 [72] for home networks, in particular for smart grid power line communications, which implements ARQ-SR and FEC on the physical layer. Like IEEE 802.11, the recommendation is tailored for short range links and specifies coherent modulation schemes for the FEC enhanced physical layer. In addition, the recommendation only describes ways to implement ARQ-SR and additional features, but does not give specific details e.g. how to determine the required timeout values or the amount of required memory. Therefore vendors optimize their products for short range links, as this is the intended area of application by this recommendation. For the given reasons available hardware based on the two standards can not be used for EPC in OWC and a different way of integrating the required mechanisms into OWC systems is needed. For the implementation of FEC the used media converters have to be extended to add FEC to the serialized signal before the signal is modulated on the laser diode. For the implementation of ARQ-SR, an additional device can be developed that adds ARQ-SR to the Ethernet layer before the Ethernet frames are passed to the media converters. Later, the proposed EPC protocol can also be integrated into the media converters. The proposed protocol stack for OWC systems is given in Figure 5.1.

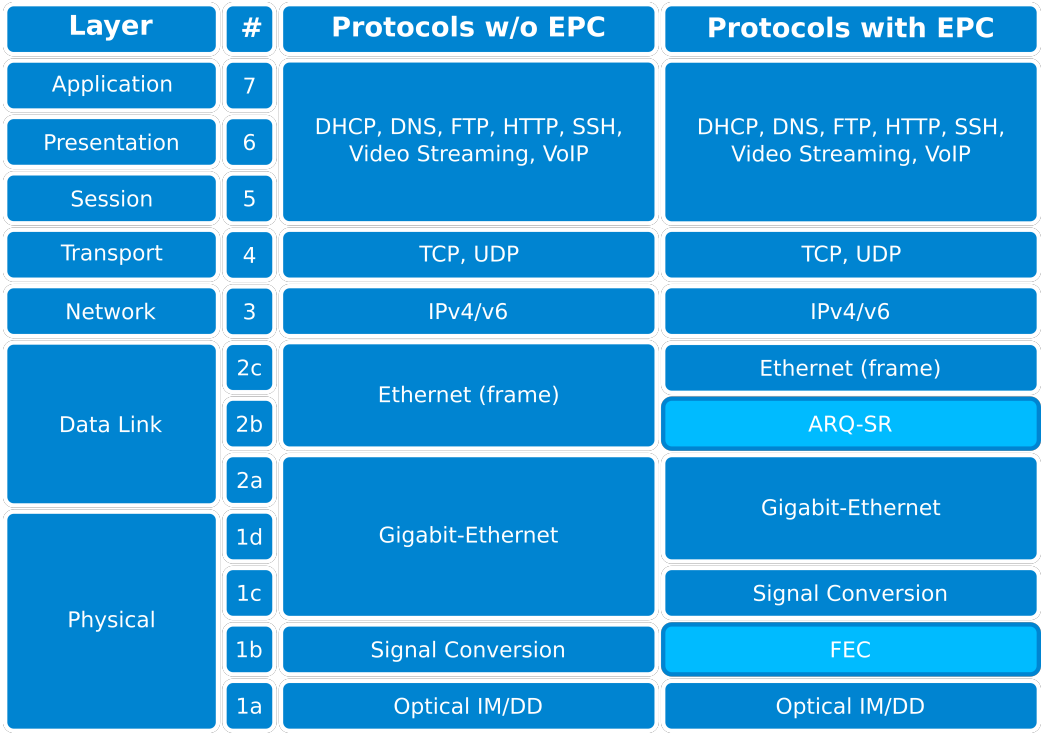

Figure 5.1: The protocol stack of OWC systems as it is currently implemented (w/o EPC) and with the proposed addition of EPC mechanisms.

5.2.1 Functional Requirements

- The protocol shall allow for transparent bridging of Ethernet traffic over OWC links.
- The protocol shall be functional for a wide range of OWC links, especially the links given in Section 4.3.
- For the implementation no modifications to layers from the OSI model higher than layer 2 shall be done.
- The protocol shall guarantee in-order delivery.
- The residual frame erasure rate for transmission in the selected scenarios shall be lower than one percent.
- The maximum delay for transmissions over the OWC link shall not exceed 100 ms.

5.2.2 Characterization of Bit Errors

Prior to designing an optimized EPC for OWC long-range links, the expected errors on these links have to be characterized in more detail. For this, bit error vectors for the links given in Section 4.3 have been generated, using the methodology given in Chapter 4. From these vectors the FER for frame sizes between 1 and 1518 B have been derived. The results for selected frame sizes are given in Tables 5.1 to 5.3. This analysis shows that links between OGS and HAP and the UAV downlink already fulfill the given requirements for most situations. For all other links FER indicates severe frame loss which requires the implementation of EPC mechanisms in order to meet the QoS requirements. Looking at the maximum number of errors in the frames, it can be seen that in some situations EPC would have to correct several thousand erroneous bits for successful transmission. Using solely FEC as error protection would introduce a lot of unnecessary overhead to the communication for the majority of frames were zero or just a few errors are occurring. On the other hand, in some situations FER raises up to 0.7 which would require an average of 12 retransmissions per frame in order to reduce FER below 0.01. This number of retransmissions introduces non acceptable delay into the data flow and therefore ARQ-SR is also not suitable as a stand alone EPC mechanism for OWC. This short investigation confirms the decision to implement a combined FEC and ARQ-SR EPC protocol.

Table 5.1: Error statistics for the links between aircrafts (AC-AC) and between aircrafts and HAPs (AC-HAP, HAP-AC).

Link	Condition	Size	FER	Bit Errors per erroneous Packet			
				Min.	Med.	Avg.	Max.
AC-AC	typical	1	0.02	1	1	1	6
		64	0.20	1	3	6	115
		1518	0.41	1	11	65	2222
	worst-case	1	0.04	1	1	1	8
		64	0.29	1	5	11	176
		1518	0.48	1	27	163	3646
AC-HAP	typical	1	0.00	1	1	1	4
		64	0.03	1	1	3	42
		1518	0.09	1	3	17	679
	worst-case	1	0.00	1	1	1	6
		64	0.09	1	2	7	121
		1518	0.20	1	9	69	2301
HAP-AC	typical	1	0.01	1	1	1	6
		64	0.19	1	2	5	104
		1518	0.40	1	10	57	1928
	worst-case	1	0.04	1	1	1	7
		64	0.27	1	4	10	171
		1518	0.47	1	24	144	3344

Table 5.2: Error statistics for the links between HAPs (HAP-HAP) and between HAPs and a ground station (HAP-OGS, OGS-HAP).

Link	Condition	Size	FER	Bit Errors per erroneous Packet			
				Min.	Med.	Avg.	Max.
HAP-HAP	typical	1	0.01	1	1	1	7
		64	0.17	1	2	4	79
		1518	0.43	1	7	39	1380
	worst-case	1	0.03	1	1	1	8
		64	0.26	1	3	8	147
		1518	0.49	1	16	103	2783
HAP-OGS	typical	1	0	0	0	0	0
		64	0	0	0	0	0
		1518	0	0	0	0	0
	worst-case	1	0.00	1	1	1	1
		64	0.00	1	1	1	5
		1518	0.00	1	2	4	38
OGS-HAP	typical	1	0	0	0	0	0
		64	0	0	0	0	0
		1518	0	0	0	0	0
	worst-case	1	0.00	1	1	1	6
		64	0.01	1	3	9	113
		1518	0.03	1	7	91	2154

Table 5.3: Error statistics for the links near ground (NGND) and between UAVs and a ground station (UAV-OGS, OGS-UAV).

Link	Condition	Size	FER	Bit Errors per erroneous Packet			
				Min.	Med.	Avg.	Max.
NGND	typical	1	0.00	1	1	1	1
		64	0.00	1	1	1	1
		1518	0.00	1	1	1	1
	worst-case	1	0.08	1	1	2	8
		64	0.31	1	8	24	246
		1518	0.46	1	68	398	5198
OGS-UAV	typical	1	0.00	1	1	1	2
		64	0.03	1	1	1	4
		1518	0.48	1	1	1	9
	worst-case	1	0.18	1	1	2	8
		64	0.54	1	18	37	264
		1518	0.69	1	210	688	5588
UAV-OGS	typical	1	0	0	0	0	0
		64	0	0	0	0	0
		1518	0	0	0	0	0
	worst-case	1	0.00	1	1	1	6
		64	0.02	1	3	7	124
		1518	0.05	1	9	78	2341

5.2.3 Forward Error Correction for Protection on Physical Layer 1b

In order to keep Ethernet as interface to the OWC physical channel (i.e. the media converters), FEC has to be implemented between serialization and electrical-optical conversion (i.e. below Ethernet, inside the media converters). The reason for this is the use of cyclic redundancy check (CRC) in Ethernet frames for error detection. Most Ethernet hardware will drop frames with an invalid CRC. If the content of the frame is protected by FEC, the checksum is invalid even if just one bit is corrupted. This will cause the frame to get dropped on Ethernet layer and the frame will not be passed to a higher layer. If FEC is implemented above Ethernet, the frame will be dropped before decoding is done. If FEC is implemented below Ethernet layer, the checksum is evaluated after the FEC decoding and thus the frame will only get dropped if the checksum is invalid after decoding of the frame. For the design of the FEC portion of the EPC protocol the data from Tables 5.1 to 5.3 gives valuable information. The values for frames of size 1 B show that it is most likely for 8 bit symbols from FEC codes to carry one error. Therefore, as worst-case assumption, the FEC code has to be able to correct as many symbol errors as bit errors are contained within one frame. In order to use available codes like RS(255, 223) with data of arbitrary length zero-padding can be used. Because the encoders typically do not mix data symbols with parity symbols, one does not have to transmit known portions of the transmitted data together with the parity symbols. When data shorter than the required number of data symbols for the code should be encoded, the beginning of the data can be padded with zeros in order to achieve the required data length. This zero-padded data can then be used for code word generation. For transmission, these leading zeros can be removed from the code word and later added back in by the decoder. For example, if a RS(255, 223) code is used and 200 B of data should be transmitted, one can add 23 bytes of zeros at the beginning of the data and encode this zero-padded data to a 255 B code word. For transmission, the padded zeros can be removed from the code word, forming an RS(232,200) code word. On reception the decoder expects code words of length 255. If shorter code words are received, the missing bytes are zero-padded to the beginning of the received code word to reconstruct the original RS(255, 223) code word. After decoding, the padded zeros have to be removed again from the data. In order to apply this approach and to use the available RS(255, 223) codecs, larger blocks can be split into blocks of 223 B where the last block is zero-padded to the required length. Each block is encoded to form a 255 B code word. For transmission, the padding from the last block is removed and the blocks are transmitted

as a contiguous block of data. At this point, the only assumption about the physical layer is that the layer is able to transmit blocks of contiguous data. If additional features are added, e.g. line codes for better clock recovery, it has to be ensured that these modifications do not weaken the FEC. On reception, the receiver can split the data blocks of arbitrary length into several blocks of 255 B and decode each of them. The last data block will most likely be less than 255 B long, so zero-padding has to be added before decoding and removed again afterwards. The decoded blocks can then be reassembled to reconstruct the original frame. Using this method, a maximum Ethernet frame of length 1518 B is transmitted as 1742 B (6 blocks with 255 B and one with 212 B) were in each block 16 errors can be corrected, or in the best case, 112 errors in the whole frame. The effect of this FEC scheme on FER is given in Tables 5.4 to 5.6. These tables show that FEC reduces FER, but especially under worst-case conditions it does not achieve the required FER < 0.01. It can also be seen that FEC is most effective for bad channel conditions. For example, if the FER is rather high without FEC (> 0.2), FEC is able to reduce FER by 20 to 30 %. If FER is already low without FEC (< 0.1), the reduction of FER by FEC is just a few percent and an error free channel is not always achieved.

Table 5.4: FER for the links between aircrafts (AC-AC) and between aircrafts and HAPs (AC-HAP, HAP-AC) without and with the proposed FEC scheme. The analysis is done for the shortest Ethernet frames (64 B) and the largest Ethernet frames (1518 B) allowed by IEEE definitions 5.2

Link	Condition	Size	FER w/o FEC	FER with FEC	Change
AC-AC	typical	64	0.20	0.02	-0.18
		1518	0.41	0.09	-0.32
	worst-case	64	0.29	0.08	-0.21
		1518	0.48	0.17	-0.31
AC-HAP	typical	64	0.03	0	-0.03
		1518	0.09	0.01	-0.08
	worst-case	64	0.09	0.01	-0.08
		1518	0.20	0.04	-0.16
HAP-AC	typical	64	0.19	0.02	-0.17
		1518	0.40	0.07	-0.33
	worst-case	64	0.27	0.07	-0.20
		1518	0.47	0.16	-0.31

Table 5.5: Error statistics for the links between HAPs (HAP-HAP) and between HAPs and a ground station (HAP-OGS, OGS-HAP).

Link	Condition	Size	FER w/o FEC	FER with FEC	Change
HAP-HAP	typical	64	0.17	0.01	-0.16
		1518	0.43	0.05	-0.38
	worst-case	64	0.26	0.05	-0.21
		1518	0.49	0.12	-0.37
HAP-OGS	typical	64	0	0	-0.00
		1518	0	0	-0.00
	worst-case	64	0.00	0	-0.00
		1518	0.00	0	-0.00
OGS-HAP	typical	64	0	0	-0.00
		1518	0	0	-0.00
	worst-case	64	0.01	0	-0.01
		1518	0.03	0.01	-0.02

Table 5.6: Error statistics for the links near ground (NGND) and between UAVs and a ground station (UAV-OGS, OGS-UAV).

Link	Condition	Size	FER w/o FEC	FER with FEC	Change
NGND	typical	64	0.00	0.00	-0.00
		1518	0.00	0.00	-0.00
	worst-case	64	0.31	0.15	-0.16
		1518	0.46	0.23	-0.23
OGS-UAV	typical	64	0.03	0.00	-0.03
		1518	0.48	0.00	-0.48
	worst-case	64	0.54	0.32	-0.22
		1518	0.69	0.44	-0.25
UAV-OGS	typical	64	0.00	0.00	-0.00
		1518	0.00	0.00	-0.00
	worst-case	64	0.02	0.00	-0.02
		1518	0.05	0.01	-0.04

5.2.4 Selective-Repeat ARQ for Protection on Data Link Layer 2b

ARQ-SR is a well known ARQ variant, that has been under research since the 1960s [73, 74]. Information about the practical application of ARQ-SR can be found in The Internet Engineering Task Force's (IETF) request for comments (RFC) that deal with the extension of TCP/IP [75, 76] by ARQ-SR. Also tailored for the integration of new features into TCP/IP, the concepts presented in these RFCs can be used as general suggestions for the implementation of communication protocols. One has to keep in mind, that the presented concepts are not proposed in an optimum way, but in a way to integrate them into TCP/IP while keeping backward compatibility with older versions of the protocol. So modifications to the proposed implementations might be advisable when creating a new protocol that does not have the requirement of backward compatibility. The used RFCs are, besides others, RFC 1072 [77], RFC 1323 [78] and RFC 2018 [79]. An additional source of information is SCPS-TP [80] which is a transport protocol similar to TCP/IP, but developed for the protocol stack of (deep-)space RF communication systems. It bears some features for long-range links that can be useful for long-range OWC links, but it is optimized for the lower data rates (<1 Gbit/s) typically used in space communications. Based on the information given in these documents, the ARQ-SR optimized for OWC has been developed.

Requirements

The requirements for an ARQ-SR protocol for OWC have been investigated in [29, 16, 17]. The major requirements from these investigations are:

1. A sequence number of at least 32 bit for 1 Gbit/s.

2. Sufficient memory to support large buffers because of the large bandwidth-delay-product.

3. Functionality to limit the number of retransmission and implicitly setting an upper bound for the delay.

4. Explicit acknowledgement of received data by ACKs.

5. Frame format compatible with Ethernet (IEEE 802.3 [81]) (for practical reasons).

Frame Format

The IEEE 802.3 compliant Ethernet frame format is given in Figure 5.2. Elements evaluated by hubs, switches, or other low level networking devices

Figure 5.2: IEEE 802.3 compliant Ethernet frame format.

are the source and destination media access control (MAC) addresses, the optional virtual local area network (VLAN) tag, and the cyclic redundancy check (CRC). These elements have to be part of all ARQ-SR frames for a correct transport through an Ethernet network. The optional VLAN tag has only to be used if it is also present in the encapsulated Ethernet frames. If the Ethernet frames are VLAN tagged and this tag would not be copied to the ARQ-SR frames, some network devices might drop the ARQ-SR frames or output them to a wrong port. If the CRC of an Ethernet frame is invalid, the frame can be dropped. Therefore the ARQ-SR protocol should only encapsulate Ethernet frames with a valid CRC. If it is ensured at the receiver that the ARQ-SR protocol only passes the Ethernet frames from correctly transmitted ARQ-SR frames to higher layers, then the Ethernet CRC can be removed in the encapsulation step and added back to the Ethernet frame at the decapsulation step. The integrity of the received ARQ-SR frames can be ensured by using the CRC, which is anyway required to form a valid Ethernet frame. At this point it should be noted that the padding done by Ethernet on frames shorter than 64 B usually requires a length entry inside the embedded data for removing the additional bytes. Because the proposed error protection scheme uses an Ethernet input interface, it is ensured that all ARQ-SR frames are large enough and they will not be subject to padding when transmitted on Ethernet. Therefore a length entry is not required. In addition to the fields required for correct delivery, a crucial element is also the EtherType field. This field should be set according to the encapsulated protocol inside the Ethernet frame. For network security reasons some network devices implement frame filtering based on EtherTypes. For ARQ-SR it is not possible to use the same EtherType as the encapsulated Ethernet frame because this would result in an invalid higher layer packet if any device tries to decapsulate this frame. Therefore a specific EtherType for ARQ-SR has to be used and all filtering or frame processing devices have to be configured to forward these frames. Because ARQ-SR is intended to be placed on a dedicated device between the local Ethernet and the media converters of the

optical link, there should usually be no network device in between causing problems. The next element required is a sequence number (SN) for identifying frames for retransmission. Because of the large bandwidth-delay-products of OWC links, this field should be 32 bit. Finally, the timestamp has to be added to the frame. In order to be compatible with the timestamp option of TCP/IP this field should be 64 bit. Based on the given considerations, an ARQ-SR data frame, carrying an Ethernet frame, has the structure shown in Figure 5.3. The extra ARQType, sequence number and timestamp fields

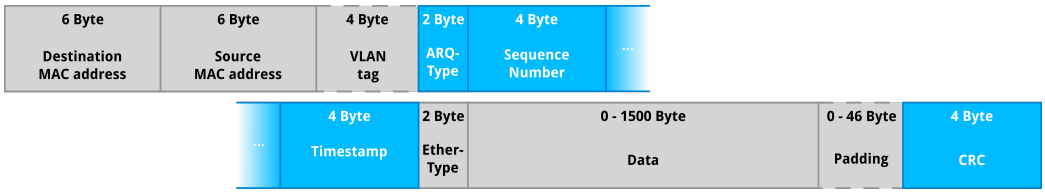

Figure 5.3: IEEE 802.3 compliant ARQ-SR data frame format, carrying an Ethernet frame.

add 10 B to the Ethernet frame. This overhead can result in ARQ-SR frames of up to 1532 B, were IEEE 802.3 has only specified Ethernet frames up to 1522 B, if the VLAN tag is used. Latest developments in networking technology include so called jumbo frames which can be up to 9000 B. Jumbo frames are not standardized by IEEE, but supported by most networking devices. In case hardware should be used that can not handle oversized Ethernet frames, the Ethernet frame embedded into ARQ-SR has to be split into two parts. In order to mark the two parts for reassembly, a field has to be added to the ARQ-SR data frame. In order to save some header bytes it is suggested to use additional ARQTypes for this purpose. For ARQ-SR there are now four different ARQTypes. One for frames that are not split (e.g 0x420D) and possibly oversized, one for the first part (0x420B) of a split frame, one for the second part (0x420C) and one for ACK frames (0x420A).
Each received ARQ-SR data frame has to be answered by an ARQ-SR ACK frame. For ARQ-SR the receiver is not only acknowledging received frames, but also signaling lost frames to the sender. This is done in the following way. On reception of a frame, the receiver checks the received SN and calculates the SN of the next frame that should be received. On reception of the next frame, the received SN and the expected SN are compared. If the received SN is larger than expected, the frames with a SN between both numbers have been lost. For ARQ-SR the receiver should store all received data frames and be able to fill the gaps in the received data stream by the reception of retransmitted frames. In order to trigger retransmission of lost frames, the receiver has to acknowledge all received data frames to the sender. This acknowledg-

ment is also an implicit negative acknowledgment for the lost frames. In an ACK frame, the first entry is the SN of the first missing frame, called the ACK-number. If no frames have been lost, this SN is the next expected SN at the receiver. Following the ACK-number, the timestamp of the ACKed frame is echoed in order to enable calculation of the round trip time (RTT). Finally, information about blocks of contiguous received SN is transmitted, called ACK blocks. Such an ACK block is defined by the SN of the first successfully received frame (left edge) and the SN of the next detected frame loss (right edge). The sender can use this information to retransmit all frames with SN between the blocks and to remove all frames form its buffers that have either a SN smaller or equal to the ACK-number or frames that have a SN belonging to one of the acknowledged blocks. In order to also use ACK frames for the detection of lost data frames, they also carry a SN. The SN of an ACK frame is the same SN as the next data frame would have, but the transmission of the ACK does not increase the SN count and therefore the next data or ACK frame will carry the same SN. By this, the receiver can still check the received and expected SN for frame loss, but lost ACK frames do not cause problems. If ACK frames would increase the SN count, lost ACK frames could be misinterpreted as lost data frames and break the data stream. For transmission of the ACK frame to the sender of the data frame, the ACK frame has to be addressed back to the sender, i.e. the destination and source MAC addresses from the received data frame are switched for the reply, and the frame has to carry the same VLAN-tag if the received data frame was tagged. Finally, the frame has to be closed by a CRC to form a valid Ethernet frame. Putting all this together results in the ACK frame structure shown by Figure 5.4.

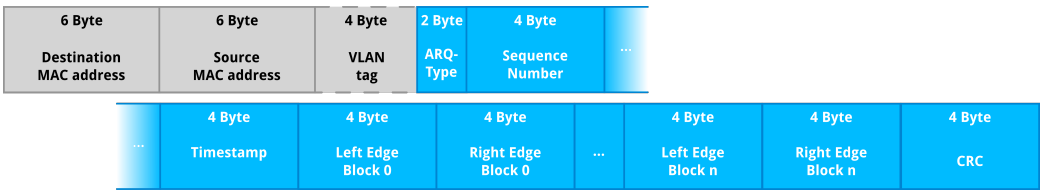

Figure 5.4: IEEE 802.3 compliant ARQ-SR ACK frame format.

Required Number of ACK Blocks in ACK Frames

The minimum size of 64 B for an IEEE 802.3 compliant Ethernet frame is large enough to hold information about five ACK blocks, where the maximum sized frame can hold 187 ACK blocks. If an ACK would carry only the ACK-number and no information about the other received frames, the protocol

would behave like a go-back-n ARQ. The same is true if there are more ACK blocks created at the receiver than the ACK frame can acknowledge. Therefore the number of blocks that can be acknowledged is a crucial number to keep the continuous data frame flow running. The actual number of blocks that an ACK frame should be able to acknowledge depends on the available memory for frame buffers and the FER on the channel. On a perfect channel there will be no losses and the ACK-number is sufficient for acknowledgment. With increasing FER the number of deleted frames increases, and with this the number of received blocks of data frames at the receiver as well. Because a new ACK block can only be created by a lost frame, the number of ACK blocks is related to FER and the number of all frames in-flight, i.e. the sum of all frames that are either on the optical link or kept in the receive buffer and not yet forwarded to a higher layer. The number of in-flight frames, in the following called round-trip time capacity C_{RTT}, can be calculated by [29]

$$C_{\mathrm{RTT}} = \frac{RTT \times D}{l + l'} \tag{5.1}$$

where D is the link data rate, l the size of the encapsulated data and l' the protocol overhead added to the frames. The round-trip time RTT can be approximated by

$$RTT = 2 \times \frac{L}{c} + t_{\mathrm{proc}} \tag{5.2}$$

where L is the link distance, c the speed of light and t_{proc} the processing time of the protocol stack. In order to estimate the worst-case number of created ACK blocks at the receiver, it can be assumed that each lost frame results in a new ACK block, i.e. frame erasures do not occur on two consecutive frames. The maximum number of ACK blocks (NB_{max}) can then be estimated by

$$NB_{\mathrm{max}} = C_{\mathrm{RTT}} \times FER \tag{5.3}$$

Following this rough estimation, several thousand ACK blocks have to be acknowledged for small frames and large FER in the scenarios from Section 4.3. For maximum sized frames the requirement is reduced to a few hundred ACK blocks. Nevertheless, under bad channel conditions it is more likely that two subsequent frames will be in error and it can be assumed that the high numbers of ACK blocks will only be required in very rare situations. Additionally, ACK frames for a few thousand ACK blocks will require jumbo frames for transmission and will require a large bandwidth on the back channel. Therefore it might be more efficient to accept a go-back-n behavior of the protocol in such rare situations and to limit the number of ACK blocks to a value less than NB_{max}. Since no exact statistical description of the

burstiness of frame erasures on OWC links is available, a good value for the number of ACK blocks limit should be determined by simulation.
A strategy to limit the protocol overhead for the acknowledgment of frames is to send ACKs with just a subset of all ACK blocks. The ACK-number in these frames is the same as it is in full sized frames and only advanced if the first gap in the received frames is closed, i.e. if the frame with SN equals ACK-number+1 is received or timed out. Instead of sending all ACK blocks inside a single ACK frame, it is sufficient to submit just a subset of the ACK blocks, due to the fact that an acknowledged frame can not be unacknowledged. The sender can work on these reduced ACK frames as usual and remove all acknowledged frames from its transmit buffer and timeout queue.

Memory Requirements

For the implementation of ARQ-SR an important value is the amount of memory required for the frame buffers at sender and receiver. Because the frame size varies on the channel and the actual memory required to store each frame depends on the implementation, all values are calculated in terms of frames, and the conversion into bytes is left to the implementer.
At the sender, all transmitted frames have to be buffered until they are either given lost and no longer have to be retransmitted, or acknowledged. Until the sender can receive the first acknowledgement from the receiver, there are at least C_{RTT} frames that have to be buffered. On reception of the first ACK, data will be removed from the buffer and new frames can be transmitted and buffered, or frames from the buffer will be retransmitted. So the minimum size of the transmission buffer is

$$B_{\mathrm{Tx}} = C_{\mathrm{RTT}} \tag{5.4}$$

For practical reasons B_{Tx} should be set slightly larger than C_{RTT}, for the following reasons. ACKs can get lost, and the sender will add new frames to the channel instead of removing ACKed frames. In addition frame retransmissions are timeout triggered, where the timeout will not fit exactly RTT. This mismatch will allow the sender to add new frames to the channel instead of retransmitting lost frames.
If a frame loss is detected at the receiver, all subsequent frames have to be buffered until a retransmission of the missing frame is received. If no upper bound is set on the number of retransmissions or the time that is waited for a successful reception of this frame, an infinite sized receive buffer B_{Rx} would be required. For the given requirements, there is a maximum delay $\Delta t_{\max}$ which limits the time that a frame is allowed to take for transmission

through the whole system. Taking the time into account that a frame has already spent within the system when the receiver detects its loss, B_{Rx} can be calculated by:

$$B_{\mathrm{Rx}} = \left(\Delta t_{\max} - \frac{RTT}{2} \right) \times FPS \tag{5.5}$$

Where FPS are the transmitted frames per second on the channel.
If any side of the link can not meet the given memory requirements, a window size has to be determined that limits the number of frames in-flight and with this B_{Tx} and B_{Rx}. TCP/IP uses a transmit window for flow control. If as many data is in flight as signaled by the window, TCP/IP reduces its throughput in order to reduce the load on the receiving process. TCP/IP is a connection on a higher layer between two processes. These processes can be slowed down by the host system, or have only limited memory access and therefore flow control is needed. On the physical layer however, all hardware parts should be designed to be able to process all incoming data, even if the link is fully loaded, and therefore usually no flow control is required on physical layer.

Processing of ACK Frames

When the sender receives an ACK frame, it has to process all ACK blocks contained within the ACK frame and to ensure that it does not retransmit these frames any more. Depending on the implementation this might require to remove the ACKed frames from some buffers, or to set a flag for the frame to drop it at the next retransmission attempt. In any case, the ACK blocks will be used to reduce the number of buffered data frames at the sender. The gaps between the ACK blocks could be used to trigger retransmission of the implicitly NACKed frames. This would reduce the delay for retransmitted data and improve overall latency. The problem with this approach is, that subsequent ACK frames might hold the same ACK blocks and also the same gaps. If the first ACK frame would trigger the retransmission of frames, there must be an algorithm that prevents the second ACK frame from triggering again the retransmission of the same frames. If the retransmission of some frames is blocked by an algorithm, there also has to be an algorithm that removes this retransmission block for the frames after a certain time in order to allow multiple retransmissions of data frames. The only time that could be used for this kind of blocking and unblocking of retransmissions is the RTT. So in case implicit NACKs would be used for triggering retransmissions, RTT would be required to prevent unnecessary retransmissions. Therefore

a simpler approach is to automatically retransmit frames that have not been ACKed after RTT and to ignore the implicit NACKs.

Setting the Timeouts

The smooth operation of ARQ-SR requires some timeouts that prevent the communication from breaking down due to lost frames. The first timeout is the retransmission timeout that is used for retransmitting unacknowledged frames. The second timeout is a timeout at the receiver to give data frames lost and to stop waiting for a successful retransmission of this frame. The third timeout is a timeout at the sender, that removes a data frame from the retransmission buffer without receiving an ACK for this frame. The third timeout can also be implemented by a retransmission counter that removes the frame from the buffer after a maximum number of retransmission attempts has been done.
For all timeouts an upper limit is given by the previously defined requirement to not delay the data flow by more than 100 ms. For the given scenarios a conservative estimate of RTT is 10 ms (if processing is done in user space). Adding an additional delay for the processing of retransmissions in the sender, this value allows for approximately eight retransmissions. The residual frame erasure rate FER_{res} after any number N of retransmissions is given by:

$$FER_{\text{res}} = FER^{N+1} \tag{5.6}$$

Using the results from Tables 5.4 to 5.6 it can be assumed that FER will never be larger than 0.5. Using (5.6) this indicates that a maximum of six retransmission attempts should be enough to achieve the targeted $FER_{\text{res}} \leq 0.01$. This value can be used by the sender to drop frames after the seventh transmission.
For setting the other two types of timeout, the RTT is required. In order to get an estimate of RTT, the sender can take the time when a data frame is sent and use the receiving time of the corresponding ACK frame for taking sampled RTT measurements s_i.

Setting the Retransmission Timeout (RTO)

For TCP/IP, the smoothed RTT, denoted as $SRTT_i$, and its variance $RTTVAR_i$ are used for calculating the retransmission timeout RTO_i [82]. Consecutive measurements of RTT are stored in the variable s_i.
When RTT is measured for the first time, i.e. s_0, the variables are initialized:

$$RTTVAR_0 = \frac{s_0}{2} \tag{5.7}$$

$$SRTT_0 = s_0 \tag{5.8}$$

$$RTO_0 = SRTT_0 + \max\left(G, K \times RTTVAR_i\right) \tag{5.9}$$

where G is the granularity of the system clock and $K = 4$. This calculation sets RTO_0 to the measured RTT and adds a margin to avoid early time outs. This margin is at least as large as the granularity of the system clock or four times the calculated variance of RTT. For subsequent measurements s_i, the calculation is done in the following way:

$$RTTVAR_i = (1-\beta)\, RTTVAR_{i-1} + \beta \left| SRTT_{i-1} - s_i \right| \tag{5.10}$$

$$SRTT_i = (1-\alpha)\, SRTT_{i-1} + \alpha s_i \tag{5.11}$$

$$RTO_i = SRTT_i + \max\left(G, K \times RTTVAR_i\right) \tag{5.12}$$

where $SRTT_{i-1}$ is the last calculated value of the smoothed RTT, $\alpha = 1/8$ and $\beta = 1/4$. α and β are smoothing factors for calculating the next estimate. A higher value of α gives more weight to the currently measured RTT against the previously calculated $SRTT_{i-1}$ and a higher value for β gives more weight to the measured variance against the previously calculated variance. RTO_i is calculated the same way as in the initial calculation, with the added early timeout margin. As it can be seen from 5.12 the added margin is relatively large and should be calculated in a different way for data transmissions requiring low delays.

The Problem with early Timeouts and Karn's Algorithm

One problem for the calculation of $SRTT_i$ arises from frame retransmissions. As soon as a frame has been retransmitted it is no longer possible to associate the ACK with a unique transmission of the corresponding frame. This is because ACKs usually do not carry any information to which transmission of the frame they belong to. For this reason Karn has formulated an algorithm for RTT calculation using only frames that have not yet been retransmitted [83]. This algorithm is also used for current TCP/IP implementations [82]. Also this algorithm leads to a better estimate of RTT, it creates a new problem if retransmissions are triggered before the ACK associated with the initial transmission of a frame has been received. For example, if the round trip delay suddenly increases by a larger amount, such early timeouts will occur and frame retransmission will start before an ACK could be received. Due to the limitation of Karn's algorithm on using only frames that have not yet

been retransmitted, RTO_i will never be updated again and each frame will be retransmitted the maximum number of times.
To prevent this situation from happening several solutions exist. TCP/IP implements the so called back-off mechanism [82]. Whenever a retransmission timeout occurs, RTO_i is doubled. For transmission of frames over the lossy optical channel, this back off is not feasible because high frame loss will lead to a large RTO_i and possibly indirectly violate the overall delay requirements. Another solution to the early timeout problem is the use of timestamps for frame transmissions [77, 84, 78] or to add any other flag that associates the ACKs with a single instance of a frame transmission. This solution renders the usage of Karn's algorithm obsolete. Preceding research has suggested that the timestamp feature does not improve communication quality on OWC links [29]. The setup of the simulations done at that time assumed rather good channel conditions. When redoing these simulations over links with higher BER, where most frames are retransmitted at least once, Karn's Algorithm prevents updates of RTO_i. Therefore, despite earlier research results, EPC for OWC should implement timestamps, eliminating the requirement to follow Karn's algorithm.

Giving Frames lost

Since TCP/IP is a reliable protocol, the receiver has to wait until a missing frame is successfully retransmitted before it can continue to pass data to higher layers. On the contrary to this, the proposed EPC for OWC has an upper limit for delay and therefore the receiver can not wait infinite time for successful retransmissions of lost frames. A timeout $FLTO_i$ is required at the receiver to give frames lost and continuing to forward received data to higher layers:

$$FLTO_i = N \times SRTT_i \tag{5.13}$$

Because Eq. (5.10) is designed to slightly overestimate RTT, Eq. (5.13) will set the timeout larger than actually required for the maximum number of retransmissions. Because of the upper limit for delay of 100 ms, the maximum allowed value for $FLTO_i$ is $0.1 - SRTT_i/2$ s.
One problem with Karn's algorithm is that in wired networks, RTT varies due to network congestion, multi-hop routing of packets, rerouting, and others. For the presented point-to-point OWC links, RTT varies mainly due to changes in link distance or buffer load at either end of the link. For example, if an airborne terminal flies past an OGS, RTT will first decrease while the aircraft is approaching the OGS and then increase when the aircraft has passed. The smoothing factor α in (5.10) will prevent an accurate estimation of RTT, the estimate will be too high as the aircraft approaches the

OGS and too low when the aircraft flies away. Therefore it is suggested to replace (5.10) by a predicting g-h-k-filter (also called α-β-γ-filter, but this could be confused with the other variables within this section). A g-h-k-filter is a linear estimator that tries to predict a sampled value based on its first and second derivative with respect to time. The fundamental assumption behind the following equations is that the second derivative of s_i is constant between measurements. Because of the high frame transmission rate in OWC systems, this assumption is generally valid. $SRTT_i$ can then be calculated by:

$$s_i = t_{\mathrm{ACK},i} - t_{\mathrm{tx},i} \tag{5.14}$$

$$\Delta t_{\mathrm{ACK}} = t_{\mathrm{ACK},i} - t_{\mathrm{ACK},i-1} \tag{5.15}$$

$$\Delta t_{\mathrm{tx}} = t_{\mathrm{tx},i} - t_{\mathrm{tx},i-1} \tag{5.16}$$

$$\widehat{s_i} = SRTT_{i-1} + \Delta t_{\mathrm{ACK}} \dot{SRTT}_{i-1} + \frac{\Delta t_{\mathrm{ACK}}^2}{2} \ddot{SRTT}_{i-1} \tag{5.17}$$

$$\dot{\widehat{s_i}} = \dot{SRTT}_{i-1} + \Delta t_{\mathrm{ACK}} \ddot{SRTT}_{i-1} \tag{5.18}$$

$$\ddot{\widehat{s_i}} = \ddot{SRTT}_{i-1} \tag{5.19}$$

$$e_{\mathrm{RTT},i} = s_i - \widehat{s_i} \tag{5.20}$$

$$SRTT_i = \widehat{s_i} + g\ e_{\mathrm{RTT},i} \tag{5.21}$$

$$\dot{SRTT}_i = \dot{\widehat{s_i}} + \frac{h}{\Delta t_{tx}}\ e_{\mathrm{RTT},i} \tag{5.22}$$

$$\ddot{SRTT}_i = \ddot{\widehat{s_i}} + \frac{2k}{\Delta t_{tx}^2}\ e_{\mathrm{RTT},i} \tag{5.23}$$

Where s_i is the current measurement of RTT, based on the timestamp for the transmission of the frame $t_{\mathrm{tx},i}$ and the timestamp for the reception of the corresponding ACK frame $t_{\mathrm{ACK},i}$. $\widehat{s_i}$ is the current estimate of RTT, $\dot{\widehat{s_i}}$ and $\ddot{\widehat{s_i}}$ are its first and second derivative over time. The same definition holds for $SRTT_i$ and its derivatives. $e_{\mathrm{RTT},i}$ is the error of the current estimation for RTT.

The g-h-k-filter uses s_i and timing information to predict $SRTT$ for the next received ACK frame. This variable is no longer just a smoothed value, but $SRTT_i$ is not renamed in order to reflect that the g-h-k-filter is a replacement for Eq. (5.10) in Karn's algorithm.

In order to fulfill the delay requirement, there is an upper bound on RTT (and in consequence on $SRTT$):

$$RTT_{\max} = \frac{0.1}{N + 0.5}\ \text{seconds} \tag{5.24}$$

Because the processing time of frames by the protocol stack is the dominating factor on RTT and signal propagation time is negligible in comparison, $RTT_{\max}$ does not limit the link distance, but sets a strict requirement for the processing speed of the protocol stack.
As initial values for the calculation of $SRTT_i$ the following values should be used:

$$SRTT_0 = RTT_{\max}$$
$$\dot{SRTT}_0 = 0$$
$$\ddot{SRTT}_0 = 0$$

A good value for β in Eq. (5.10) has to be determined by simulation. For $FLTO_i$ at the receiver, the initial values result in a maximum allowed delay for the transmission of unidirectional streams. Only if there is a data flow (i.e. not only ACK frames) from receiver to sender, $SRTT_i$ gets updated (optimized) and a lower $FLTO_i$ is set if possible. This directly results in a lower delay on the link. For this reason, the receiver of an unidirectional stream should send empty data frames from time to time in order to adjust $SRTT_i$ to the current link conditions.

5.3 Scintillation Loss and Compensation in Link Budgets

Most often, when the performance of communication protocols is discussed, the terms throughput (data rate used on link layer) and goodput (data rate available on higher layers) are used. It is commonly accepted, that goodput degrades with channel quality. I.e. if fading on an optical link increases, the user can transmit less data. From a quality of service point of view, this degradation of goodput is not acceptable, since each application has a certain required data rate that should be guaranteed by the transmission link. Therefore developers of OWC systems have to take this goodput degradation into account and adjust the link design accordingly, in order to guarantee a certain link quality for higher layers.
In [30] formulae were given to adjust τ_{Sci} from Equation (3.10) by the error protection used on the link. The introduction of EPC into an OWC system leads to a reduction of $P_{\text{Rx,Th}}$ at the cost of link capacity used by the EPC mechanisms. Therefore the scintillation loss for the case of EPC is given by

$$\tau_{\text{Sci,EPC}} = \tau_{\text{Sci}} \tau_{\text{EPC}} \tag{5.25}$$

5.3.1 Scintillation Loss and Compensation in Link Budgets for FEC

For the use of FEC as single EPC mechanism $\tau_{\mathrm{EPC,FEC}}$ is given by[30]:

$$\tau_{\mathrm{EPC,FEC}} = \frac{k}{n} \tag{5.26}$$

where k is the number of data symbols and n the code word length of the used code.
Using Equations (3.6), (3.10), (6.2) and (6.3) a new value for τ_{Sci} can be calculated, taking the application of FEC into account. For the used RS(255, 223) code and the Capanina receiver, $\tau_{\mathrm{Sci,FEC}}$ is approximately 1.7 (2.3 dB).

5.3.2 Scintillation Loss and Compensation in Link Budgets for ARQ

For the use of ARQ as single EPC mechanism $\tau_{\mathrm{EPC,ARQ}}$ is given in [30] without taking retransmissions into account. The number of retransmissions, which are required in order to compensate for frame losses, have to be included in these calculations in order to guarantee enough link capacity for higher layers. Therefore the formula from [30] is extended to include the average number of retransmissions per frame, in order to achieve the targeted value for FER_{res}.

$$\tau_{\mathrm{EPC,ARQ}} = \frac{1}{log_{FER}\left(FER_{\mathrm{res}}\right)\left(1 - FER_{\mathrm{res}}\right)} \tag{5.27}$$

Since ARQ should be able to recover for all errors, τ_{Sci} can be set to 1. $\tau_{\mathrm{Sci,ARQ}}$ depends on FER on the link. Tables 5.4, 5.5 and 5.6 predict an FER of up to 0.7 in the selected scenarios, therefore $\tau_{\mathrm{EPC,ARQ}}$ and respectively $\tau_{\mathrm{Sci,ARQ}}$, can be expected to be around 0.1 (-10 dB). This calculation illustrates that while ARQ-SR can eliminate the scintillation loss, but link designers have to take the additionally required link capacity for retransmissions into account.

5.3.3 Scintillation Loss and Compensation in Link Budgets for FEC and ARQ combined

For the link improvement by a combination of FEC and ARQ, first the effect of FEC has to be evaluated, because it influences FER, on which the calculation of $\tau_{\mathrm{EPC,ARQ}}$ depends on. Because approximation of FER after the application of FEC is difficult to calculate, an upper limit for $\tau_{\mathrm{Sci,FEC+ARQ}}$

can be calculated by multiplying $\tau_{\mathrm{Sci,FEC}}$ and $\tau_{\mathrm{Sci,ARQ}}$. This results in a factor of 0.17 ($-7.7\,\mathrm{dB}$) in the worst-case for the selected scenarios.
Looking at this result, one might think that applying ARQ and FEC is expensive in terms of link budget, but these $-7.7\,\mathrm{dB}$ are invested in converting the worst-case FER from about 0.7 down to less than 0.01. In case that no EPC is implemented, τ_{Sci} is calculated to be around 0.04 ($-14\,\mathrm{dB}$). This shows that despite its rather high cost, EPC results in a link budget gain of about 6 dB and is able to improve link quality by a vast amount. It should be noted that (5.27) assumes a possibly unlimited number of retransmissions. If the number of retransmissions is limited, $\tau_{\mathrm{EPC,ARQ}}$ will increase, but also FER_{res}.

Chapter 6

Implementation

In this chapter the implementation of the simulator is described in detail. A short description of the simulator and some simulation results have already been presented in [26]. As illustrated in Figure 6.1, the simulator implementation consists of four main components. The first component is the SimulationConfigurator which configures each other component for a simulation run. This component allows for batch simulation of several different communication scenarios without any user interaction during the simulation runs. The other components are the Sender, used for generating frames to transmit on the channel, the channel used for simulating the transmission path and the receiver used for recording the transmitted frames and to generate statistics about the communication path. These components are described in the following subsections in more detail.
The actual implementation of the simulator is done in C/C++, therefore some language specific elements e.g. pointers, might be used in the following descriptions, but the general simulator architecture should be realizable with any other programming language. A general design goal for the simulator architecture was to use generic interfaces between each module, in order to allow for easy reconfiguration of the communication path and the simulator setup, as well as to be able to distribute the simulator over several machines. For this, each component implements the EthernetFrameProcessor interface which defines a processFrame method and a nextProcessor field. The processFrame method accepts a pointer to an EthernetFrame object as argument, and can be used for implementing any action that should be taken on the reception of an EthernetFrame. After all actions on a received EthernetFrame have been done (which is not required to be at the end of processFrame, e.g. for the ARQ component) the component should forward an EthernetFrame pointer to the nextProcessor if this is defined. By this design, a chain of EthernetFrameProcessors can be linked together and it is possible to implement

some of the components on external hardware and adding a specialized EthernetFrameProcessor into the communication path for communication with this hardware. For performance reasons, all EthernetFrame objects are created in shared memory and only pointers to this memory are passed, as long as the target component runs on the same machine. The class diagram of the EthernetFrameProcessor interface is shown in Figure 6.2.

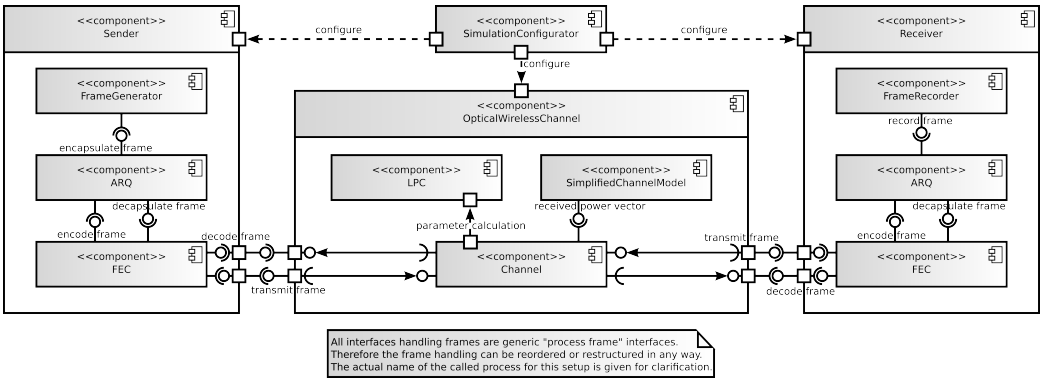

Figure 6.1: Component diagram for the implementation of a simulator for optical wireless communications

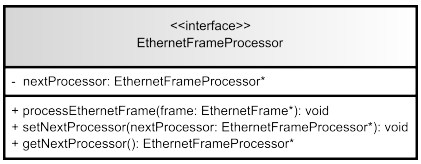

Figure 6.2: Class diagram for the EthernetFrameProcessor interface

6.1 Sender

The Sender consists of a FrameGenerator, an ARQ component and an FEC component. The ARQ and FEC components will be described in separate subsequent sections. The FrameGenerator is kept rather simple, it can be configured to generate Ethernet frames with defined size at a defined data rate. It is also possible to give the FrameGenerator a distribution for the size of generated frames, but this leads to a reduced generation performance. Each frame has a 32-bit sequence number in its data part in order to count received and lost packets at the receiver and a 64-bit timestamp counting in microseconds for delay and jitter measurements at the receiver. To distinguish the generated frames from other frames in Ethernet networks, the

EtherType field in the Ethernet header is set to C0DE (hexadecimal notation) which is not listed in the EtherType list maintained by the IEEE Registration Authority. For every generated frame, the FrameGenerator adds a log entry to a SQLite database.

6.2 OpticalWirelessChannel

The OpticalWirelessChannel component is implemented following the description in Chapter 4, particularly it is structured as proposed by Figures 3.4 and 4.1. The LPC component is used for calculating the link budget and channel parameters. The SimplifiedChannelModel component generates a value for P_{Rx} at simulation time t. The resolution of the generator clock depends on the sampling frequency f_{s} set for the Bessel filter. For the Bessel filter some parameters have been fixed; $n = 3$ and f_{s} =10 000 Hz. As input for the Bessel filter Gaussian distributed random numbers are generated with mean = 0 and variance = 1. Without the filtering step this set of numbers ($x(t)$) could be easily transformed to the desired log-normal distributed set of $P_{\mathrm{Rx}}(t)$ by applying $P_{\mathrm{Rx}}(t) = \exp[\mu + \sigma x(t)]$, but since the filtering affects the variance of the generated random numbers, this change has to be compensated. Using the given values for the Bessel filter, the following formula has been derived:

$$P_{\mathrm{Rx}}(t) = \exp\left[\mu + \frac{\sigma}{0.014532\sqrt{f_{\mathrm{c}}}} x(t)\right] \tag{6.1}$$

The Channel component implements the EthernetFrameProcessor interface and adds the number of generated symbol errors to each passed EthernetFrame. At this point the implementation deviates from Figure 4.1. For efficient simulation each EthernetFrame object carries additional information within its payload about the used FEC scheme of the physical layer, particularly the symbol size and the code word boundaries. This information does not increase the transmitted frames size, as it fits within the payload of a minimum sized Ethernet frame as defined by IEEE. For live simulation of single bit errors for gigabit communications, at least 10^9 random numbers have to be generated per second. In order to reduce the computational load of this process, the number of required random numbers is reduced by calculating the loss probability of an EthernetFrame based on code words. For each EthernetFrame the loss probability is equivalent to the probability of carrying more errors in any code word than the selected FEC scheme can correct. If a single code word of a frame can not be decoded, the whole frame is lost. For this simplification, first the symbol error probability $SEP(t)$ is

calculated from the simulated $BEP(t)$ and symbol size s.

$$SEP(t) = 1 - (1 - BEP(t))^s \tag{6.2}$$

Formula 6.2 is derived by remembering that a symbol error is defined as having at least one bit error within a symbol, so $SEP(t)$ is 1− the probability of having no error within a symbol. Based on $SEP(t)$ the probability of having a larger than δ number of symbol errors in a code word, i.e the code word error probability $CWEP(t)$, is given by:

$$CWEP(t) = 1 - \sum_{i=0}^{\delta} SEP(t)^i \times (1 - SEP(t))^{n-i} \times \binom{n}{i} \tag{6.3}$$

where n is the number of symbols of the code word. This approach does not only reduce the processing load for generating bit errors, it also allows for the simulation of FEC without actually implementing it. A small drawback of this approach is that FEC schemes like LDPC codes, can not be simulated because the error correction capability δ of these codes is not exactly known. Nevertheless, for Reed-Solomon codes this approach is well suited. The simplifications made imply that $BEP(t)$ does not change significantLY during the transmission duration of each code word, which is true for high transmission rates in the gigabit range and the used code word size of 255 B. The error estimation for each code word is done based on the simulation time t for every code word of the frame, the corresponding $P_{\mathrm{Rx}}(t)$ value from the SimplifiedChannelModel component and the provided receiver model as it is shown in Figure 3.4. The decision if a code word can be decoded is done by comparing a random number with the calculated $CWEP(t)$.

6.3 Receiver

Like the Sender, the Receiver component holds an ARQ and an FEC component for decoding/decapsulating the received EthernetFrames and for conducting the ARQ error correction. The ARQ component passes the successfully decapsulated EthernetFrames to an EthernetRecorder component which logs all information about the received frame into an SQLite database. The data gathered in this database can later be used for statistical analysis of the data transmission. The ARQ and FEC components are described in more detail in the following sections.

6.4 ARQ

The ARQ component consists mainly of three threads, where each of these threads manages a list of entries. The first thread handles all frames that are scheduled for transmission and takes care of the encapsulation of these frames in ARQ frames. The second thread tracks the timeouts for each transmitted ARQ frame and passes retransmission requests to the transmission thread. The third thread handles the received ARQ frames and the decapsulation of the EthernetFrames. This handling includes passing ACK transmission requests and retransmission requests for not acknowledged ARQ frames to the transmission thread and passing received ACKs to the timeout thread in order to cancel the retransmission timers for these frames. Operation on lists are generally not thread-safe and require the use of performance reducing locking mechanisms like semaphores. In order to realize thread-safe and lock-free communication between the threads, the following concept has been implemented. Base of this concept is that as long as there is only one reader and one writer, operations on ring buffers are thread-safe. By buffering communication between threads via dedicated ring buffers, thread-safe communication can be realized. Before a thread can communicate with another thread in order to request changes to its managed list, it has to request a ring buffer from this thread. The receiving thread will then create a ring buffer in a managed shared memory for efficient access by the other thread. From then on, the calling thread can put its requests into this ring buffer. The receiving thread will regularly check all its created ring buffers and process the given requests. The only thread accessing the list managed by a thread, is the thread itself and all requested operations on this list are buffered in a thread-safe way without requiring locks. Besides the improved performance due to the lock-free communication, another advantage of this communication architecture is that each thread can implement its own scheduler for the requests on its ring buffers and realize features like priorisation of retransmission requests over initial transmission requests.

6.5 FEC

As already mentioned in Section 6.2, the implementation of the FEC component is kept as simple as possible, in particular encoding and decoding of frames and the detection of erroneous bits are not realized in code, but implemented in a statistical way.
For encoding, the FEC information of the EthernetFrame is filled according to the scheme used in Section 5.2.3. The type of FEC code used can be set

by the SimulationConfigurator. If no FEC should be used for the simulation, the FEC component does not have to be removed from the Simulator. FEC can also be disabled by setting the symbol size to 1 and by setting the code word length as well as the data length entry equal to the frame size. These parameters indicate that the whole frame is a single code word with no redundancy and every bit is a symbol on its own. The EthernetFrame with the filled FEC information is then passed on to the OpticalWirelessChannel component.
For decoding the FEC component receives the EthernetFrame from the OpticalWirelessChannel component and reads the FEC and contained error information. Based on this information the component can decide if every code word can be decoded, or if it contains too many symbol errors. If a single code word can not be decoded, the whole EthernetFrame has to be considered lost. If the EthernetFrame can be decoded, it gets forwarded to the ARQ component, otherwise the frame is dropped and no further action is taken.

Chapter 7

Performance Analysis of Optical Wireless Communications

In order to evaluate the performance of OWC and the proposed EPC in the scenarios given in Section 4.3, the developed simulation system has been used to simulate the transmission of common internet traffic types in these environments. As common traffic types, voice over IP (VoIP), video streaming, online gaming, web browsing and file transfer have been selected.

7.1 Common Traffic Types used for Simulation

In order to setup simulations with realistic parameters, the network protocol analyzing software Wireshark [85] has been used to obtain the typical packet sizes and data rates used by well known network applications and web services. These applications and web services were Skype video and voice only calls, Microsoft Windows 7 Update, playing games on Facebook, file transfer using SCP, watching videos on YouTube and the media centers of German TV stations ARD and ZDF, browsing of news websites and using web based email services. The results from these measurements are given in Table 7.1. Unfortunately none of the service providers give quality of service requirements for the transmission of their service, therefore the QoS requirements previously compiled in [17] are used. It can be seen that these applications use typically two different packet sizes. 64 B, which are mainly packets of the back channel for transmitting acknowledgments and status information, and 1468 B which is the maximum packet size for most consumer broadband

Table 7.1: Typical packet sizes and data rates for selected internet services

Service	packet size in (B)	packet size out (B)	data rate in (Mbit/s)	data rate out (Mbit/s)
Video Streaming				
ARD	1468	64	2.37	0.05
YouTube	1468	64	1.08	0.03
ZDF	1468	64	2.78	0.05
Telecommunications				
Skype telephony	79	72	0.04	0.04
Skype videophony	652	707	0.62	0.65
File transfer				
SCP	1514	64	8.17	0.16
Windows Update	1468	64	0.28	0.01
Online gaming				
Facebook games	1468	64	0.09	0.01
Web browsing				
Web mailer	1468	64	0.11	0.01
News pages	1468	64	0.17	0.02

connections. The only exception is video telephony which uses packet sizes between 650 B and 700 B. Similar results can be obtained by using frame statistics of internet exchange points like the Amsterdam Internet Exchange (AMS-IX) [86] or from literature [87, 88].
For data rates used by the given services, SCP is the dominating one which will typically use up all available bandwidth the involved systems can provide. The same applies to web browsing services. Due to user inactivity while reading content, the average data rate is quite low, but when new content is loaded, most of the available bandwidth will be used. From all services, the service requiring the largest average data rate is video streaming. While the streaming services used for the given measurement did only provide streams at data rates below 3 Mbit/s, the required data rate will rise up with the introduction of 3D video streaming to approximately 12 Mbit/s [89].
Following this analysis, it was decided to conduct simulations for packets of size 64 B, 675 B and 1468 B for data rates of 1 Mbit/s and 12 Mbit/s. While OWC links can transport data rates of several Gbit/s, the data rate for the simulation is limited to the data rate of single streams in order to keep the generated data manageable. The results from the single stream simulations will then be extrapolated to higher data rates. During time of writing, Ultra-

HD or 4k video streams became available on streaming platforms, requiring data rates of about 25 Mbit/s [90]. The given resluts can also be extrapolated to this type of traffic.

7.2 Results

The basic findings about the feasibility of OWC in the given scenarios is illustrated by Figure 7.1. For each EPC mechanism, one of the given radar plot shows the simulated FER_{res} in each scenario at different P_{Tx}. P_{Tx} is varied between 0 W and 0.5 W. The colors indicate the FER_{res} based on scenario and P_{Tx}. Green indicates good channel conditions (FER$\leq$ 0.001). Yellow indicates acceptable channel conditions (FER$\leq$ 0.01) which fulfill the given requirements by ITU [62]. Light red indicates bad channel conditions on which some types of communications might still be possible (FER$\leq$ 0.1) and red indicates that no commonly used type of communication will be possible (FER$>$ 0.1). It can be seen that on links in the near ground scenario and between a HAP and an OGS, no EPC is required at all for fulfilling the given FER requirements. In the UAV to OGS scenario the downlink from the UAV to OGS is also possible without any type of EPC. The uplink to the UAV should be protected using FEC or a combination of FEC and ARQ. A general observation is that by using ARQ and higher power levels, communications can be realized in all scenarios. If power levels should be limited for some reason, using the combination of FEC and ARQ will allow to communicate at lower power levels. Therefore EPC mechanisms can also be used for extending the feasible communication ranges in the given scenarios.
When taking a look at the efficiency of the different EPC methods, FEC is most effective in the uplink from ground to UAV where it outperformes ARQ, while ARQ performs better in all other scenarios. This indicates a different type of fading in the ground to UAV scenario. Most likely the small receiving aperture and the high velocity of the receiving terminal lead to fast fading which is better compensated by FEC than ARQ.
Although FER is an important indicator for the evaluation if a certain type of communication is implementable on a selected link, other constraints might also impede successful communications. In order to give a more precise answer on the question if OWC is implementable in each scenario, a closer look on all relevant channel performance parameters like FER, delay and jitter as well as on all relevant EPC characteristics like coding gain, bandwidth and resource usage is given in the following section.

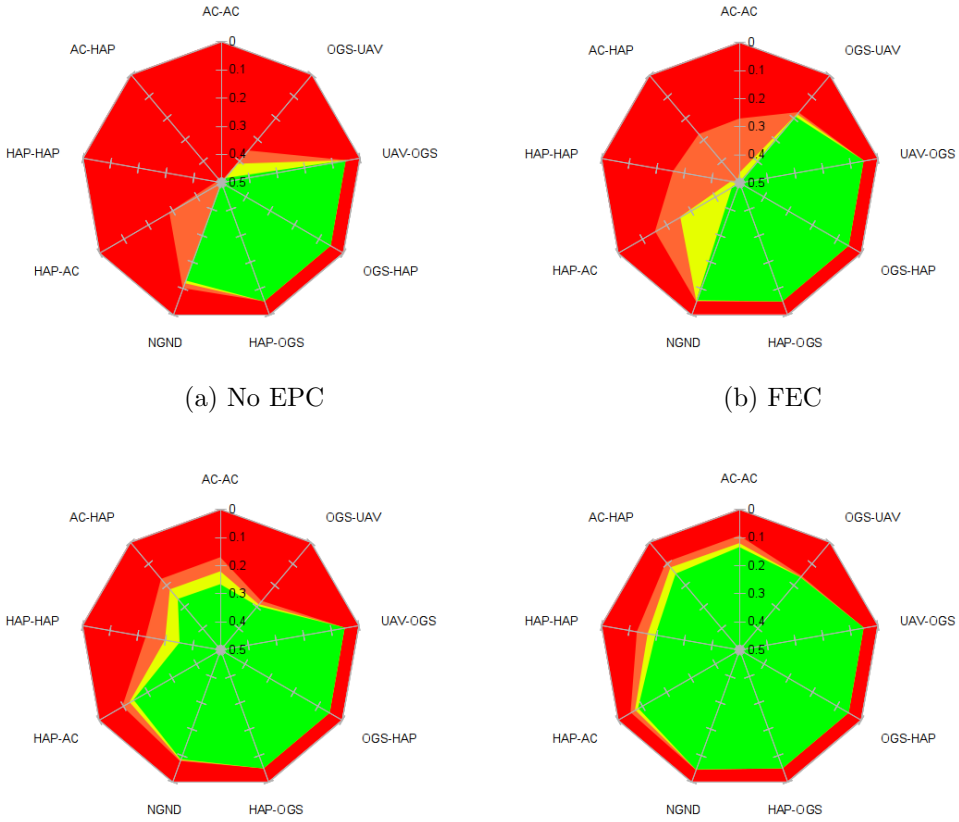

(a) No EPC (b) FEC

(c) ARQ (d) ARQ and FEC

Figure 7.1: Link quality for the different EPC mechanisms within each scenario. Each axis of the radar plots shows P_{Tx}, the colors indicate link quality based on FER_{res}. Green$\leq$ 0.001, yellow$\leq$ 0.01, light red$\leq$ 0.1 and red$>$ 0.1.

7.2.1 Residual Frame Erasure Rate

Figure 7.2 and Figure 7.3 show the FER_{res} based on channel FER. The y-axis is limited to an FER of 0.1 for giving a better view on the area which fulfills the given system requirements. For applying only FEC it can be seen that in some scenarios (NGND, OGS-UAV, UAV-OGS, OGS-HAP, HAP-OGS) this already enables successful communications even under severe channel conditions. Whereas in other scenarios (AC-AC, AC-HAP) FEC improves communications, but can not give a guarantee for successful communications. For the HAP-HAP scenario it can be seen, that in the case of using 1468 B frames, FEC does not improve communications at all. This observation illustrates the weakness of FEC for not being channel aware. To alleviate this

problem, modern communication systems have added channel monitoring, which senses for P_{Rx} and adjust the applied coding strength according to measured channel conditions. The drawback of these solutions is, that both ends of the communication link have to be synchronized for changing the used type of coding on the fly, which increases cost of components and leads to interruptions on the link while coding parameters are changed. In addition, the variation of the used coding parameters also varies the available bandwidth for user data, which might cause problems on higher communication layers, which are sensitive to this type of change.

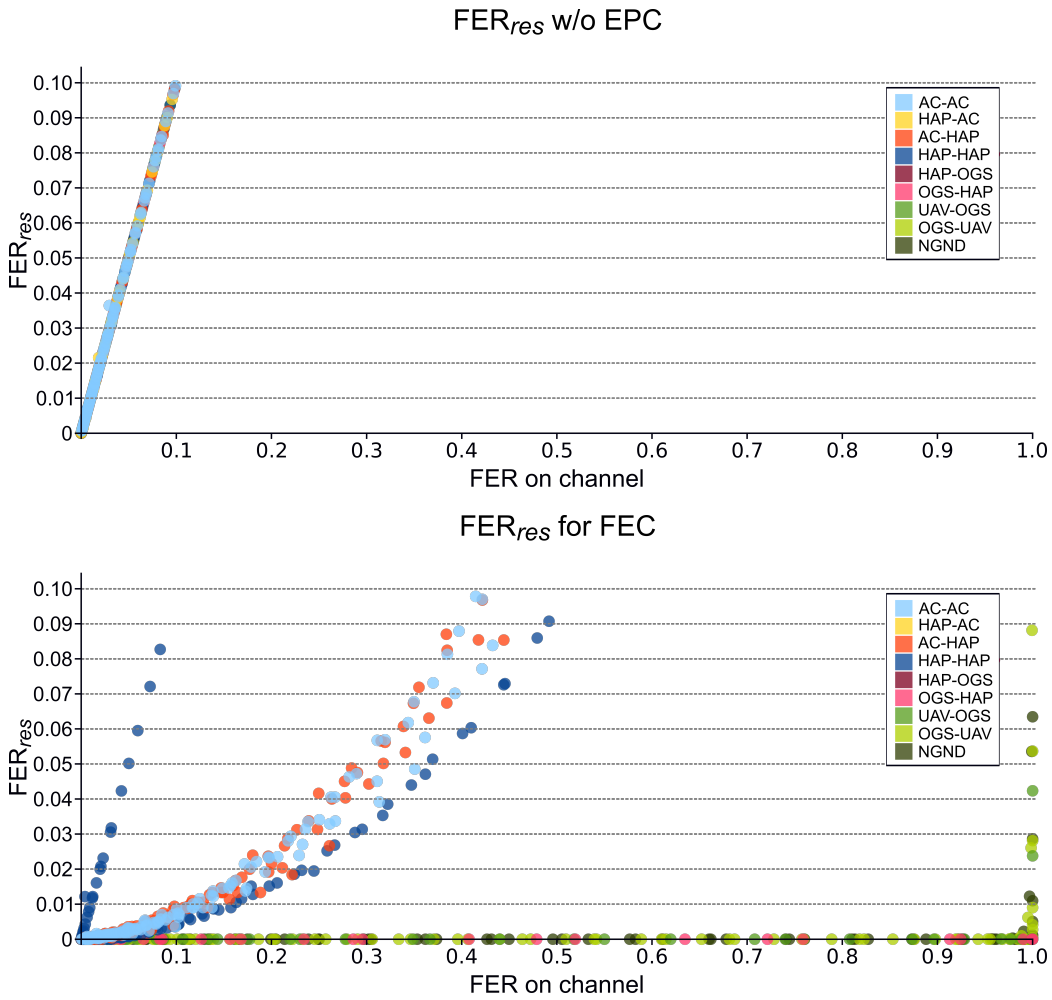

Figure 7.2: Detailed view of FER_{res} for communications over OWC links using no EPC method or ARQ. The y-axis is limited to 0.1 for focusing on the region where some types of internet communications are still functional.

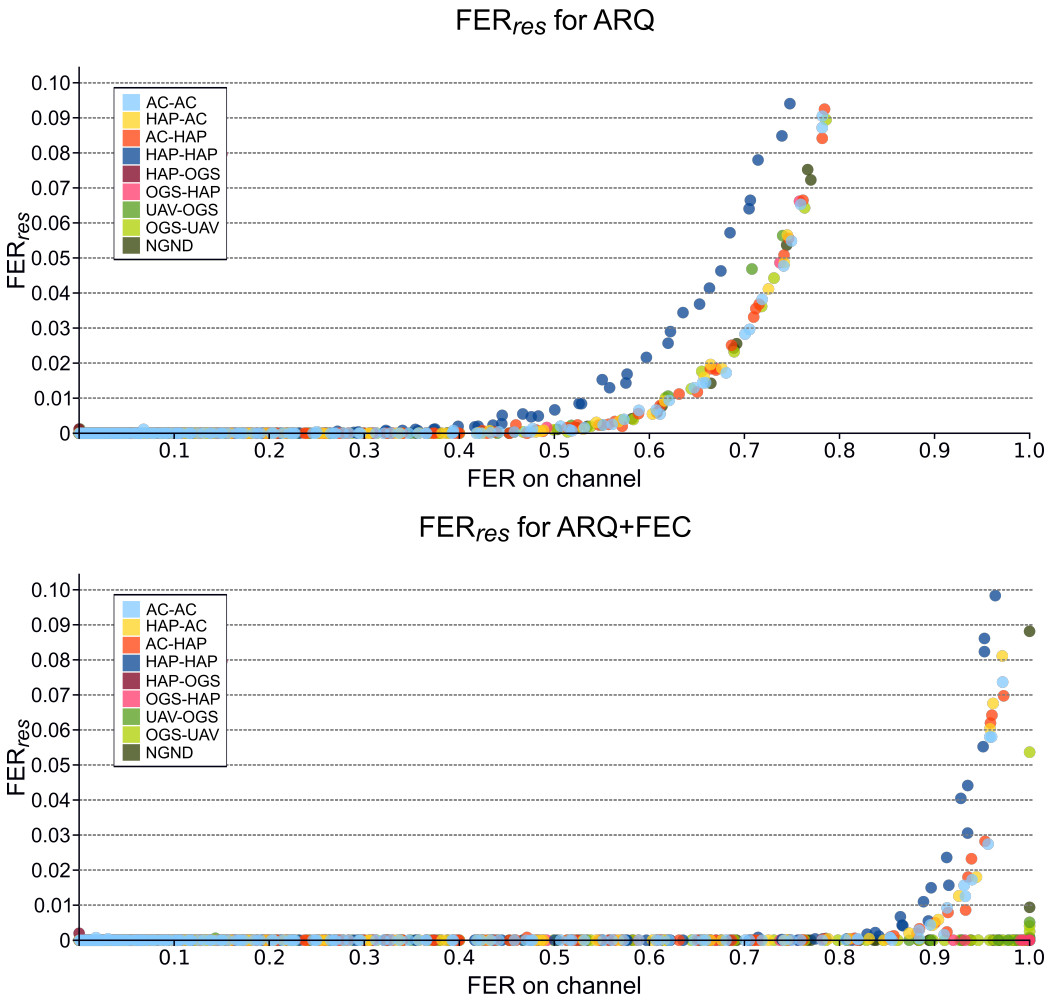

Figure 7.3: Detailed view of FER$_{res}$ for communications over OWC links using ARQ or ARQ with FEC. The y-axis is limited to 0.1 for focusing on the region where some types of internet communications are still functional.

7.2.2 Delay and Jitter caused by ARQ

For real time communications, like VoIP or video conferencing, delay and jitter are important channel characteristics. For jitter, no upper limit has been given in this work so far. Most communication equipment manufacturers implement jitter compensation techniques for systems which would be otherwise sensitive to jitter. So there is no common requirement for jitter on the communication channel, it mostly depends on the used systems. For compensating for jitter, data is usually buffered within the communication chain at the receiver side and forwarded with smoothed jitter. Therefore

jitter compensation adds additional delay to the communication link and should be as low as possible. As hard limit it can be said that delay plus jitter should not violate the 100 ms limit previously given for maximum delay. Experience gained with commercial communication systems has shown, that most systems can handle jitter in the order of a few ms. For jitter and delay evaluations, it is assumed that FEC adds constant delay to the data stream without noticeable jitter. Therefore delay and jitter are only of interest for EPC mechanisms which involve ARQ. Figure 7.4 shows the average experienced jitter depending on channel FER. It can be seen, that the average jitter introduced by retransmissions of the ARQ protocol, is less than 2 ms. Taking also a look at Figure 7.5 it can bee seen that delay reaches the 100 ms limit only under severe channel conditions with FER above 0.9. For this type of channel conditions it has already been shown in Figure 7.2 that even with ARQ and FEC applied, the requirement of having an $\mathrm{FER}_{res} \leq 0.01$ can not be met. Therefore it can be concluded that delay and jitter requirements will always be met by the presented EPC methods, if the communication system fulfills the FER_{res} requirements. For Figure 7.5 it has to be noted that the delay of the link is dominated in the shown simulations by the processing time of each frame within the communication stack and not by the propagation delay of the signal between partners. For this reason it is possible to include delay values from each scenario within a single plot.

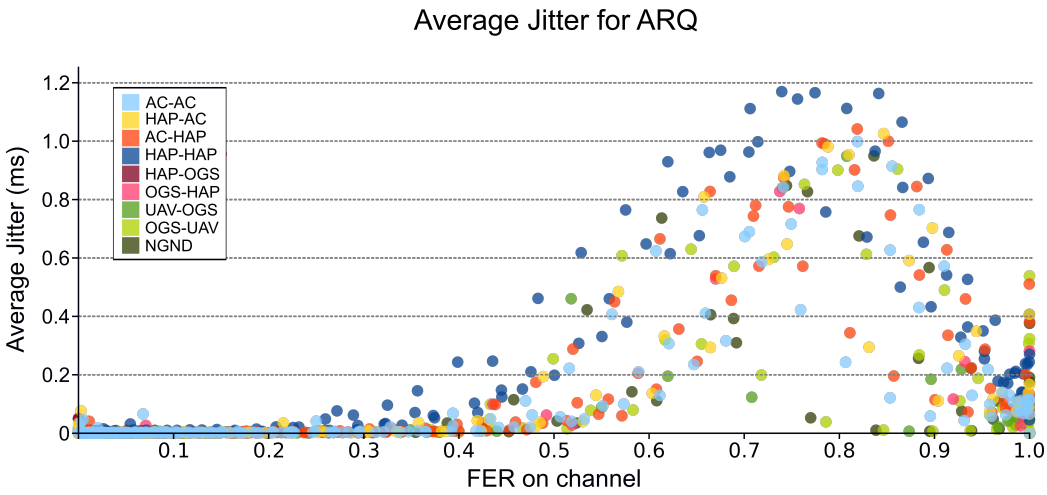

Figure 7.4: Delay for communication secured by ARQ depending on channel FER

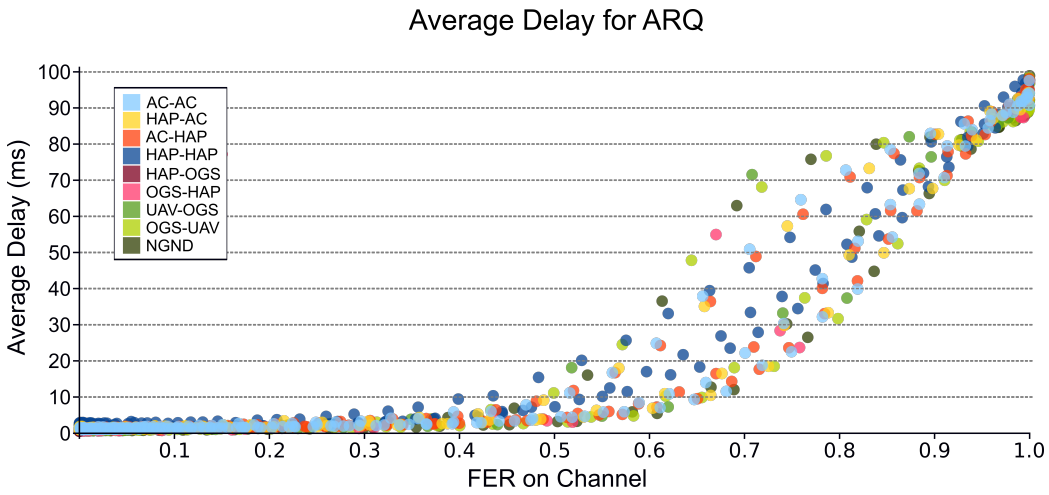

Figure 7.5: Delay for communication secured by ARQ depending on channel FER

7.2.3 Coding Gain of Error Protection and Correction methods for Optical Wireless Communications

Coding gain is an often used measure for evaluating the amount of signal energy that can be saved by the use of any type of coding. For evaluation of coding gain for EPC methods, usually the signal to noise ratios at the receiver are compared at selected BER levels. Because for this work the receiver is modeled as part of the simulator, this definition can not be used. The further, BER on its own is a bad measure for channel quality of OWC as the correlation in time between bit errors has strong influence on communication quality on higher layers. Therefore P_{Rx} is compared at selected FER_{res} levels for each EPC mechanism in order to determine the coding gain of the proposed EPC mechanisms. The most important FER_{res} level for this, is the level of $FER_{\mathrm{res}} = 0.01$, which is defined as the level where communication will begin to fail. Figure 7.6 shows the receiver performance by means of FER_{res} in dependency of P_{Rx} for simulations in all scenarios. It can be seen that using no EPC is the worst performing type of communication (as expected), ARQ performs better than FEC (as predicted in section 5.1.2) and best performance is achieved by applying ARQ and FEC to the communication. The area, where the curve for ARQ and the curve for FEC overlap, indicates the region where FEC is more efficient than ARQ. The possible coding gain for EPC is mainly depending on the type of fading present in each communication scenario which is illustrated in Figure 7.7, where the average coding gain simulated at the level of $\mathrm{FER}_{res} = 0.01$ is shown for each

scenario. This plot shows that for scenarios with good channel conditions,

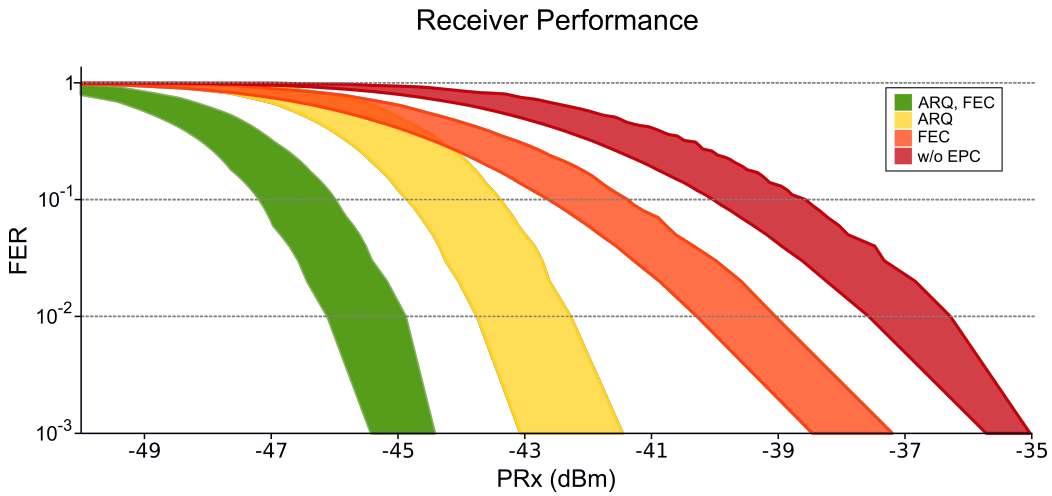

Figure 7.6: FER experienced for the selected receiver at different levels for P_{Rx}

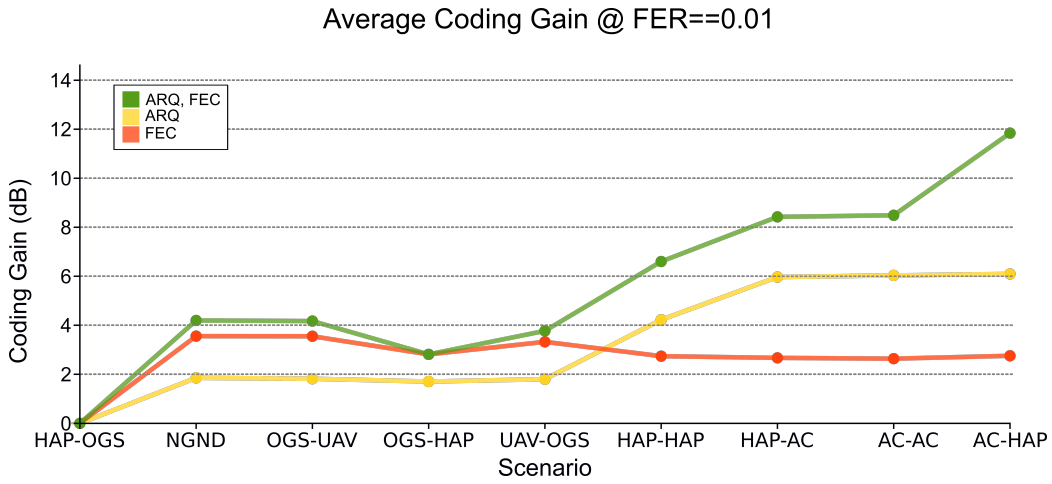

Figure 7.7: Average Coding Gain experienced for the selected receiver in the given scenarios

applying FEC is more efficient than applying ARQ, while the combination of both EPC methods will always bring best results. It can also be seen that the coding gain is higher than the gain predicted in subsection 5.3.3. This is because the used definition for the coding gain does not take the used bandwidth by retransmissions into account.

7.2.4 Bandwidth Usage

Both EPC methods, FEC and ARQ, add redundancy to the transmitted data and reduce the available user bandwidth. For FEC the added redundancy is fixed by the used code. For the selected RS(255, 223) code, the bandwidth usage is increased by 1.50, 1.19 and 1.15 for the simulated packet sizes of 64 B, 675 B and 1468 B.
For ARQ the redundancy depends on the number of retransmissions required for each successful transmission and therefore scales with channel quality. Additionally some protocol information is added to each packet, which also uses bandwidth for transmission. The bandwidth usage on the forward channel is illustrated in Figure 7.8. It can be seen that on forward channel the required bandwidth is increased by a factor of up to 11 under severe channel conditions. When taking the bandwidth used by acknowledgement frames into account, this factor is close to 12 (Figure 7.9). From Figure 7.2 it can be

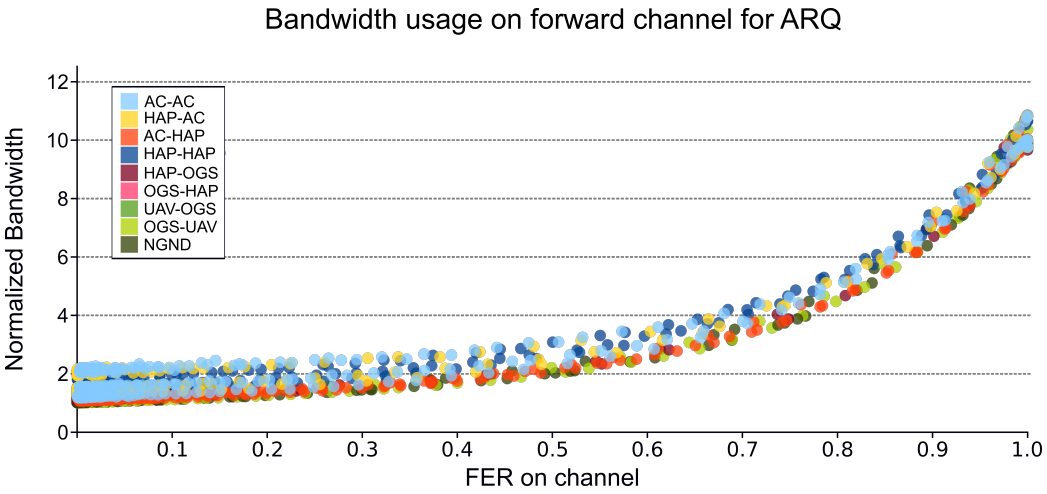

Figure 7.8: Bandwidth usage on forward channel for ARQ, normalized by bandwidth usage without EPC

seen that the presented implementation of ARQ can only fulfill the communication requirements over links with an FER less than 0.7. For this region the bandwidth usage is increased by a factor of 4 (only forward channel) or 6 (forward + backward channel). In Section 5.2.3 it has been calculated, that when FEC is used, as it is the case with the presented EPC method, then FER on the link should always be better than 0.5. This implies, that the increase of bandwidth requirements will always be less than 4. At this point it should be noted that the ARQ implementation used for simulations has not been optimized for reduced bandwidth usage. For example acknowl-

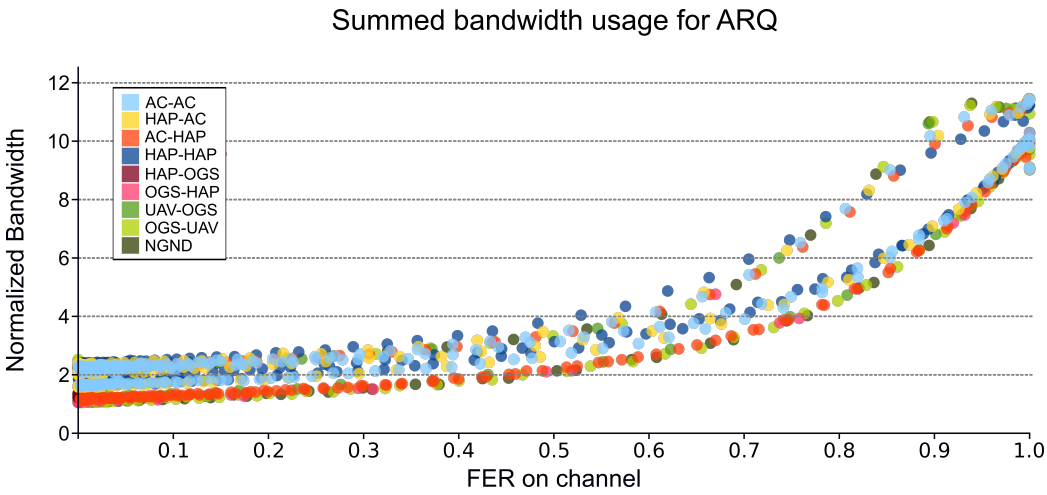

Figure 7.9: Added up bandwidth usage (forward + reverse channel) for ARQ, normalized by bandwidth usage without EPC

edgments could be piggy backed on data frames in bidirectional scenarios or ACKBlocks could be split over several frames. In addition, the implementation of the protocol stack was done in user space and not within the kernel of the operating system or even in hardware. This also increases bandwidth requirements, because of the reduced processing speed. In addition, the timings within the protocol stack in user space are subject to relatively strong jitter. This jitter causes problems for the calculation of RTO and in consequence, early timeouts. This jitter can be reduced by implementing the protocol in kernel space, FPGA or similar. From Tables 5.4 to 5.6 it had been derived, that FER in all scenarios will never be larger than 0.5. Therefore a factor of 4 can be assumed as upper limit for increased bandwidth requirements under worst-case conditions.

7.2.5 Memory Requirements

The memory required depends mainly on frames which have to be buffered at the sender and receiver. On the sender side, frames are buffered for possible retransmission. On the receiver side, frames have to be buffered while waiting on reception of frames missing at an earlier position within the data stream. For each frame some additional information has to be stored, in order to manage retransmission and reassembly of the data stream. Therefore the memory requirements depend on the transmitted data rate and the frame rate on the channel. In the following, the number of buffered frames will be normalized by the transmitted frame rate, in order to achieve comparability

of the results between different link types. The maximum number of frames buffered (NFB_{max}) at sender and receiver normalized by the transmitted frame rate on the link are shown in Figure 7.10. Note, the relatively high

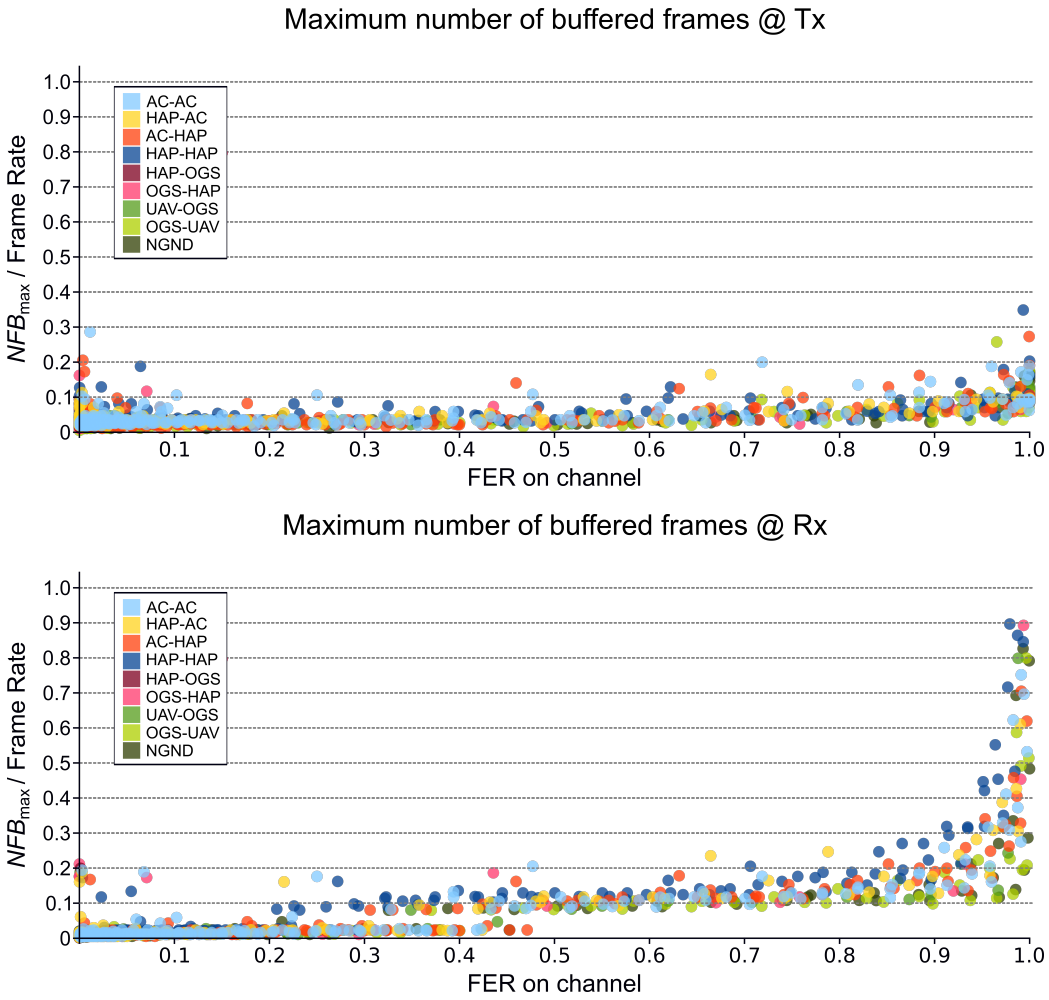

Figure 7.10: Maximum sizes for Tx and Rx buffers normalized by the frame rate for all simulations

value at the beginning of each curve in Figure 7.10 is due to the implementation of the buffer management and should not be taken into account for evaluation. For faster frame processing, frames that get acknowledged are not immediately removed from the retransmission queue. They are kept in the buffer until they time out. Once they time out, they get deleted instead of retransmitted. In case of good channel conditions, this leads to all frames being buffered at least for the duration of RTO. When retransmissions occur, the timeout queue is checked more often for outdated frames.

When taking a look at Figure 7.10, one can see, that the maximum number of buffered frames is largest at the receiving buffer. This is because the receiver does not know if the sender is still retransmitting the missing frame. Therefore it has to wait and buffer data for the maximum allowed retransmission delay. As mentioned before, it is expected that the systems do not have to operate over channels worse than a FER of 0.5, therefore it is possible to limit the maximum number of frames that can be buffered at each side to 20 % of the link frame rate.
From statistics of AMS-IX [86] one can derive that the average frame size for backbone traffic is about 770 B. When scaling simulation results up to the average load of AMS-IX of 3.3 Tbit/s, memory requirements go up to 413 GB for each buffer. If OWC links should be used as backbone links, this memory requirement should be matched, for typical link speeds of 10 Gbit/s, buffer sizes of 1.25 GB should be sufficient.

7.2.6 Number of ACK Blocks

In Chapter 5.2.4 it has been mentioned, that for $NB_{\max}$ only an upper limit can be given and it is more appropriate to determine an estimated value by simulation. Analysis of simulation results has confirmed, that $NB_{\max}$ is de-

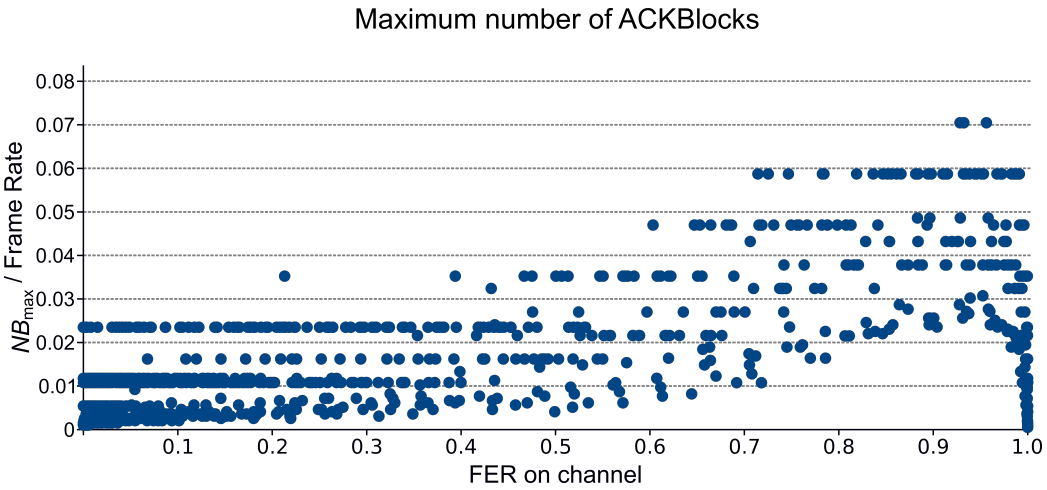

Figure 7.11: Maximum number of ACKBlocks normalized by the frame rate on the link

pending on frame rate and channel FER. The burstiness of bit errors causes $NB_{\max}$ to increase with FER. In order to derive an estimate of expectable values for $NB_{\max}$, the simulation results for $NB_{\max}$ have been normalized by the frame rate in each simulation run. Figure 7.11 shows that for all

conducted simulations, an upper limit of $NB_{\max}$ is at 7 % of the frame rate. For high data rate OWC links this shows that a large number of acknowledgement blocks should be expected. E.g. for backbone traffic of 1 Gbit/s, $NB_{\max}$ will be around 10300 blocks of missing frames. When assuming that channel FER will never be worse than 0.5, $NB_{\max}$ will be about 4 % of the link frame rate which is approximately 6800 blocks. For such high numbers, either huge ACK frames filled up with ACKBlocks will reduce available bandwidth for data transmission, or limitation of ACKBlocks per ACK frame will also reduce achievable transmission rates. Therefore optimizations like splitting the signaling of ACKBlocks over several ACK frames or piggybacking ACK frames on data frames should be added to EPC. Another optimization would be the implementation of EPC not for link traffic as a single stream, but separate for each transmitted data stream.

7.2.7 Summary

The presented simulation results show that OWC is feasible in all scenarios described in chapter 4.3.
The most favorable scenarios are the near ground links, downlinks from UAVs and links between a ground station and a high altitude platform. These are also the scenarios where optical links are mostly deployed at the time of writing.
For forward error correction it has been shown that it can be implemented in a simple and cost efficient way and therefore it should be implemented in all link scenarios for increased link robustness.
For scenarios involving only flying platforms, like links between aircrafts, additional error protection and correction schemes are required in order to overcome link errors. For selective repeat ARQ it has been shown that it can be used for establishing reliable optical links even under worst-case channel conditions, at the cost of additional memory requirements and reduced user data rate. For common single link speeds, the memory requirements can be met by modern hardware. The additional required bandwidth for retransmissions and acknowledgments can not easily be compensated for. When developing an OWC system, one has to define a guaranteed user data rate and then design the system in order to achieve a link data rate of four times the guaranteed user data rate, which might be challenging for link speeds in the range of 100 Gbit/s. The given factor of four includes the signaling of missing data frames in a straight forward implementation, which leads to high load on the back channel by acknowledgment frames. Therefore putting some effort in a more efficient way of communicating lost frames between receiver and sender will allow to reduce the required link data rate.

When including error protection and correction into link budget calculations, no specific formula can be given as to many factors influence the efficiency of EPC mechanisms. As a rule of thumb it can be said that under worst-case conditions, the given FEC adds a gain of 3 dB, ARQ adds 6 dB and the combination of both adds 12 dB. Since this gain is generated out of the correction of errors, this gain will be reduced as soon as better channel conditions are present. For typical channel conditions with FER of a few percent, gains of 2 dB (FEC or ARQ) and 4 dB (FEC+ARQ) seem to be reasonable.

Chapter 8

Conclusion

8.1 Discussion

The focus of this dissertation is the description of a simplified channel model that is suitable for the computer based simulation of higher layer communication in optical communication systems (using intensity modulation with direct detection) and on the description of error protection and correction mechanisms required to implement optical wireless communication systems in a wide range of scenarios
The presented channel model has been developed based on theoretical descriptions of the optical channel and a larger amount of measurements. Measurements and theory have been put together in order to derive a stochastic description of the optical channel which masks the true complexity of all physical processes influencing the laser beam within the atmosphere. It further has been shown that this reduced complexity results in a model which is accurate enough for the simulation of higher layer communication, but it should not be used for simulation of the laser propagation by itself.
In order to allow for the practical application of the simulation model, several parameter sets for different communication scenarios have been given.
For the evaluation of error protection and correction methods for OWC systems, it has been shown how the well known methods of forward error correction and selective repeat ARQ can be integrated into optical communication systems based on intensity modulation with direct detection and interfacing to other communication devices using IEEE 802.3 Ethernet.
In order to illustrate how the developed system can be practically used, a feasibility study for the implementation of OWC in several different communication scenarios has been done. For this, the developed channel model as well as the described error protection and correction scheme has been imple-

mented within a computer based simulation. The study has shown that by using FEC and ARQ, OWC can be implemented in a wide range of scenarios, overcoming practical and physical limitations imposed on the quality of the OWC physical layer. The results also indicate the amount of effort one has to put into making OWC work in each scenario. Based on these findings, system developers can optimize their systems for new areas of application. All formulae and models described within this work can be seen as a frame work for system developers that supports them in the development of new systems.

8.2 Future Work

The presented work has shown that implementation of OWC is possible in all inner atmospheric scenarios. The focus was laid on compatibility of the presented EPC methods with available OWC systems, leading to a system that is not optimal in terms of cost and transmission efficiency. In order to extend the application of OWC, the presented channel model can be used to develop FEC schemes optimized for the characteristics of the atmospheric optical channel.
It also has been shown that the signaling of lost data for selective repeat ARQ is driving costs for the implementation of reliable OWC links and heavily influences the achievable user data rates. The straight forward implementation of acknowledgment frames requires a lot of bandwidth on the back channel, which should be reducible by the implementation of a more sophisticated acknowledgment scheme.
The further, the given parameterization of the channel model is limited to inner atmospheric links. Other fields of application for OWC are underwater links or inter planetary links. For these links the stochastic description from the channel model should be adjusted in order to be able to simulate also this type of communication.
Finally, since the presented channel model and its parameters are based on measurements, the information from this thesis should be used to reevaluate the channel model and given parameter sets based on new measurements.

Bibliography

[1] H. Henniger, B. Epple, and H. Haan, "Maritime mobile optical-propagation channel measurements," in *Communications (ICC), 2010 IEEE International Conference on*, Cape Town, May 2010, pp. 1–5.

[2] J. Horwath, M. Knapek, B. Epple, M. Brechtelsbauer, and B. Wilkerson, "Broadband backhaul communication for stratospheric platforms: the stratospheric optical payload experiment (stropex)," *Free-Space Laser Communications VI*, vol. 6304, no. 1, p. 63041N, 2006.

[3] J. Horwath and C. Fuchs, "Aircraft to ground unidirectional laser-communications terminal for high-resolution sensors," *Free-Space Laser Communication Technologies XXI*, vol. 7199, no. 1, p. 719909, 2009.

[4] L. B. Stotts, L. C. Andrews, P. C. Cherry, J. J. Foshee, P. J. Kolodzy, W. K. McIntire, M. Northcott, R. L. Phillips, H. A. Pike, B. Stadler, and D. W. Young, "Hybrid optical rf airborne communications," *Proceedings of the IEEE*, vol. 97, no. 6, p. 1109, 2009.

[5] L. C. Andrews, R. L. Phillips, R. Crabbs, D. Wayne, T. Leclerc, and P. Sauer, "Atmospheric channel characterization for orca testing at nttr," in *Proceedings of the SPIE*, 2010, p. 758809.

[6] T. Jono, Y. Takayama, and N. Perlot, *Report on DLR-JAXA Joint Experiment - The Kirari Optical Downlink to Oberpfaffenhofen (KIODO)*. Japan Aerospace Exploration Agency, Apr 2007.

[7] D. M. Boroson, "Free-space optical communications comes of age," *Photonics Spectra*, vol. 51, no. 5, pp. 38–43, May 2017.

[8] L. M. Wasiczko, "Techniques to mitigate the effects of atmospheric turbulence on free space optical communication links," Ph.D. dissertation, University of Maryland, College Park, Md., Oct 2004.

[9] R. Purvinskis, D. Giggenbach, H. Henniger, N. Perlot, and F. David, "Multiple-wavelength free-space laser communications," *Free-Space Laser Communication Technologies XV*, vol. 4975, no. 1, pp. 12–19, 2003.

[10] A. Biswas and S. Lee, "Ground-to-ground optical communications demonstration," Jet Propulsion Laboratory, Pasadena, CA, Telecommunications and Mission Operations Progress Report 42-141, May 2000.

[11] X. Zhu and J. M. Kahn, "Free-space optical communication through atmospheric turbulence channels," *Communications, IEEE Transactions on*, vol. 50, no. 8, pp. 1293–1300, Aug 2002.

[12] J. H. Churnside, "Aperture averaging of optical scintillations in the turbulent atmosphere," *Applied Optics*, vol. 30, no. 15, pp. 1982–1994, May 1991.

[13] H. Henniger, F. David, D. Giggenbach, and C. Rapp, "Evaluation of fec for the atmospheric optical im/dd channel," in *Society of Photo-Optical Instrumentation Engineers (SPIE) Conference Series*, ser. Presented at the Society of Photo-Optical Instrumentation Engineers (SPIE) Conference, G. S. Mecherle, Ed., vol. 4975, Jul 2003, pp. 1–11.

[14] H. Henniger, "Packet-layer forward error correction coding for fading mitigation," in *Society of Photo-Optical Instrumentation Engineers (SPIE) Conference Series*, ser. Presented at the Society of Photo-Optical Instrumentation Engineers (SPIE) Conference, vol. 6304, Sep 2006.

[15] S. Trisno, I. I. Smolyaninov, S. D. Milner, and C. C. Davis, "Characterization of time delayed diversity to mitigate fading in atmospheric turbulence channels," in *Society of Photo-Optical Instrumentation Engineers (SPIE) Conference Series*, ser. Presented at the Society of Photo-Optical Instrumentation Engineers (SPIE) Conference, D. G. Voelz and J. C. Ricklin, Eds., vol. 5892, Aug 2005, pp. 388–397.

[16] B. Epple, H. Henniger, and C. Serrano Solsona, "An error protection protocol for user-transparent bridging of fast ethernet data transmission over the optical fading channel in an aeronautical environment," in *Proceedings of the SPIE 6877*, ser. Presented at the Society of Photo-Optical Instrumentation Engineers (SPIE) Conference, S. Mecherle, Ed., vol. 6877, Mar 2008, p. 68770.

[17] B. Epple and C. Serrano Solsona, "Implementation concepts for a bridging protocol for the high data rate slow-fading free-space optical

channel," in *Proceedings of the SPIE 6877*, ser. Presented at the Society of Photo-Optical Instrumentation Engineers (SPIE) Conference, S. Mecherle, Ed., vol. 6877, Mar 2008, p. 687709.

[18] J. Fleck, J. Morris, and M. Feit, "Time-dependent propagation of high energy laser beams through the atmosphere," *Applied Physics A: Materials Science & Processing*, vol. 10, no. 2, pp. 129–160, 1976.

[19] R. Frehlich, "Simulation of laser propagation in a turbulent atmosphere," *Appl. Opt.*, vol. 39, no. 3, pp. 393–397, Jan 2000.

[20] L. Sjöqvist, M. Henriksson, and O. Steinvall, "Simulation of laser beam propagation over land and sea using phase screens: a comparison with experimental data," in *Proceedings of SPIE*, ser. Presented at the Society of Photo-Optical Instrumentation Engineers (SPIE) Conference, D. H. Titterton, S. M. Kirkpatrick, R. Stoian, R. Appleby, J. M. Chamberlain, and K. A. Krapels, Eds., vol. 5989, Nov 2005, p. 59890.

[21] B. Epple, "Impact of ground profile on scintillation index for high-altitude optical wireless links," in *GLOBECOM Workshops (GC Wkshps), 2010 IEEE*, Dec 2010, pp. 1057–1061.

[22] B. Epple, H. Henniger, S. Kurz, and H. Haan, "Rural optical-propagation measurements," *Radioengineering*, vol. 20, no. 1, pp. 49–54, 2011.

[23] B. Epple, "Simplified channel model for simulation of free-space optical communications," *Journal of Optical Communications and Networking*, vol. 2, no. 5, pp. 293–304, May 2010.

[24] D. Giggenbach, B. Epple, J. Horwath, and F. Moll, *Optical Satellite Downlinks to Optical Ground Stations and High-Altitude Platforms*, ser. Lecture Notes in Electrical Engineering. Springer, Oct 2008, vol. 16, pp. 331–349.

[25] B. Epple and H. Henniger, "Discussion on design aspects for free-space optical communication terminals," *IEEE Communications Magazine*, vol. 45, no. 10, pp. 62–69, Oct 2007.

[26] B. Epple, "Performance analysis of optical wireless communications on long-range links," in *Free-Space and Atmospheric Laser Communications XI*, vol. 8162. SPIE, 2011, pp. 81 620H–81 620H–8.

[27] C. Fuchs, H. Henniger, B. Epple, D. Giggenbach, M. Amirfeiz, M. Jentile, G. Di Nepi, F. Mazzi, and G. Martini, "Broadband communications for aeronautical networks: The atenaa outer optical link validation," *Proceedings of 1st CEAS European Air and Space Conference*, Sep 2007.

[28] M. Knapek, J. Horwath, F. Moll, B. Epple, N. Courville, H. Bischl, and D. Giggenbach, "Optical high-capacity satellite downlinks via high-altitude platform relays," *Proc.SPIE*, vol. 6709, pp. 6709–6709, 2007.

[29] B. Epple, "Performance optimization of free-space optical communication protocols based on results from fso demonstrations," *Free-Space Laser Communications VII*, vol. 6709, no. 1, p. 670915, 2007.

[30] S. D. Milner, S. Trisno, C. C. Davis, B. Epple, and H. Henniger, "A cross-layer approach to mitigate fading on bidirectional free space optical communication links," in *Military Communications Conference, 2008. MILCOM 2008. IEEE*, Nov 2008, pp. 1–6.

[31] H. Henniger, B. Epple, S. D. Milner, and C. C. Davis, "Coding techniques to mitigate fading on free-space optical communication links," in *Proceedings of the SPIE 7091*, ser. Presented at the Society of Photo-Optical Instrumentation Engineers (SPIE) Conference, vol. 7091, Aug 2008.

[32] H. Henniger, B. Epple, and D. Giggenbach, "Mobil fso activities in europe and fading mitigation approaches," in *2007 17th International Conference Radioelektronika*, Apr 2007, pp. 1–6.

[33] L. C. Andrews, *Field Guide to Atmospheric Optics*. SPIE Publications, Jan 2004, vol. FG02.

[34] L. C. Andrews and R. L. Phillips, *Laser Beam Propagation Through Random Media*, 2nd ed., ser. Press Monograph Series. P.O. Box 10, Bellingham, WA 98227-0010: SPIE Optical Engineering Press, 2005, vol. PM152.

[35] L. C. Andrews, R. L. Phillips, and C. Y. Hopen, *Laser Beam Scintillation with Applications*, ser. SPIE Press monograph. P.O. Box 10, Bellingham, WA 98227-0010: SPIE Optical Engineering Press, 2001, vol. PM99.

[36] B. E. A. Saleh and M. C. Teich, *Fundamentals of photonics*, 3rd ed., ser. Wiley Series in Pure and Applied Optics, J. W. Goodman, Ed. New York, NY: John Wiley & Sons, Inc., 1991.

[37] A. K. Majumdar, "Free-space laser communication performance in the atmospheric channel," *Journal of Optical and Fiber Communications Research*, vol. 2, no. 4, pp. 345–396, 2005.

[38] I. I. Kim, B. McArthur, and E. J. Korevaar, "Comparison of laser beam propagation at 785 nm and 1550 nm in fog and haze for optical wireless communications," *Optical Wireless Communications III*, vol. 4214, no. 1, pp. 26–37, 2001.

[39] D. Atlas, "Optical extinction by rainfall." *Journal of Meteorology*, vol. 10, pp. 486–486, Dec 1953.

[40] R. M. Rasmussen, J. Vivekanandan, J. Cole, B. Myers, and C. Masters, "The estimation of snowfall rate using visibility," *Journal of Applied Meteorology*, vol. 38, no. 10, pp. 1542–1563, 1999.

[41] I. I. Kim and E. J. Korevaar, "Availability of free space optics (fso) and hybrid fso/rf systems," in *Optical Wireless Communications IV*, E. J. Korevaar, Ed., vol. 4530. SPIE, 2001, pp. 84–95.

[42] I. Toselli, R. L. Phillips, L. C. Andrews, and D. T. Wayne, "Impact of ground profile on scintillation: 50km and 200km slant paths from airplane to antelope peak," *Atmospheric and Oceanic Propagation of Electromagnetic Waves IV*, vol. 7588, no. 1, p. 75880, 2010.

[43] F. Strömqvist Vetelino, C. Young, and L. C. Andrews, "Fade statistics and aperture averaging for gaussian beam waves in moderate-to-strong turbulence," *Applied Optics*, vol. 46, no. 18, p. 3780, Jun 2007.

[44] L. C. Andrews and R. L. Phillips, "Measured statistics of laser-light scattering in atmospheric turbulence," *J. Opt. Soc. Am.*, vol. 71, no. 12, pp. 1440–1445, 1981.

[45] G. Parry, "Measurement of atmospheric turbulence induced intensity fluctuations in a laser beam," *Journal of Modern Optics*, vol. 28, no. 5, pp. 715 – 728, May 1981.

[46] M. A. Al-Habash, L. C. Andrews, and R. L. Phillips, "Mathematical model for the irradiance probability density function of a laser beam propagating through turbulent media," *Optical Engineering*, vol. 40, no. 8, pp. 1554–1562, Aug 2001.

[47] N. Perlot and D. Fritzsche, "Aperture-averaging - theory and measurements," in *Proceedings of the SPIE*, G. S. Mecherle, C. Y. Young, and J. S. Stryjewski, Eds., vol. 5338, Jun 2004, pp. 233–242.

[48] A. K. Majumdar and J. C. Ricklin, Eds., *Free-space laser communications : principles and advances*, ser. Optical and Fiber Communications Reports. New York: Springer, Dec 2008, vol. 2.

[49] N. D. Chatzidiamantis, H. G. Sandalidis, G. K. Karagiannidis, and M. Matthaiou, "Inverse gaussian modeling of turbulence-induced fading in free-space optical systems," *Lightwave Technology, Journal of*, vol. 29, no. 10, pp. 1590–1596, May 2011.

[50] L. C. Andrews and R. L. Phillips, *Mathematical Techniques for Engineers And Scientists*, ser. SPIE Press monograph. Bellingham, WA, USA: SPIE Press, 2003, vol. PM118.

[51] R. R. Parenti, S. Michael, J. M. Roth, and T. M. Yarnall, "Comparisons of cn2 measurements and power-in-fiber data from two long-path free-space optical communication experiments," *Free-Space Laser Communications X*, vol. 7814, no. 1, p. 78140, 2010.

[52] D. T. Wayne, "The pdf of irradiance for a free-space optical communications channel: a physics based model," Ph.D. dissertation, University of Central Florida, 2010.

[53] V. I. Tatarskii, *Wave Propagation in a Turbulent Medium.* New York: McGraw-Hill, 1961.

[54] A. Ishimaru, *Wave Propagation and Scattering in Random Media.* New York: Academic, 1978.

[55] G. I. Taylor, "The spectrum of turbulence," in *Proceedings of The Royal Society of London. Series A, Mathematical and Physical Sciences (1934-1990)*, vol. 164, no. 919, 1938, pp. 476–490.

[56] F. David, "Scintillation loss in free-space optic im/dd systems," in *Free-space laser communication technologies XVI*, ser. Proceedings of the SPIE, G. S. Mecherle, C. Y. Young, and J. S. Stryjewski, Eds., vol. 5338. Bellingham, WA, USA: SPIE Society of Photo-Optical Instrumentation Engineers, Jan 2004, pp. 66–75.

[57] F. Moll and M. Knapek, "Free-space laser communications for satellite downlinks: Measurements of the atmospheric channel," in *Proceedings of IAC2011*, 2011, pp. IAC–11–B2.6.2.

[58] L. M. Wasiczko, C. I. Moore, H. R. Burris, M. Suite, M. Stell, J. Murphy, G. C. Gilbreath, W. Rabinovich, and W. Scharpf, "Characterization of the marine atmosphere for free-space optical communication," in *Proceedings of SPIE*, no. 06. SPIE, 2006, pp. 621 501–621 501.

[59] F. S. Vetelino, K. Grayshan, and C. Y. Young, "Inferring path average c2n values in the marine environment," *Journal of the Optical Society of America A*, vol. 24, no. 10, pp. 3198–3206, Oct 2007.

[60] A. Papoulis and S. U. Pillai, *Probability, Random Variables, and Stochastic Processes*, 4th ed. Mc-Graw Hill, 2002.

[61] U. G. Gujar and R. J. Kavanagh, "Generation of random signals with specified probability density functions and power density spectra," *Automatic Control, IEEE Transactions on*, vol. 13, no. 6, pp. 716–719, Dec 1968.

[62] Telecommunication Standardization Sector of ITU, "Itu-t recommendation y.1541: Network performance objectives for ip-based services," International Telecommunication Union (ITU), Tech. Rep. Y.1451, Feb 2006.

[63] Telecommunication Standardization Sector of ITU, "Itu-t recommendation g.1050: Network model for evaluating multimedia transmission performance over internet protocol," International Telecommunication Union (ITU), Tech. Rep. G:1050, Mar 2011.

[64] B. Epple, "Using a gps-aided inertial system for coarse-pointing of free-space optical communication terminals," in *Free-Space Laser Communications VI*, A. K. Majumdar and C. C. Davis, Eds., vol. 6304, no. 1. SPIE, 2006, p. 630418.

[65] X Development LLC, "Project loon," https://x.company/loon/, Oct 2017.

[66] internet.org by facebook, "Connectivity lab," https://info.internet.org/en/story/connectivity-lab/, Oct 2017.

[67] H. A. Pike, L. Stotts, P. Kolodzy, and M. Northcott, "Parameter estimates for free space optical communications," in *Applications of Lasers for Sensing and Free Space Communications*. Optical Society of America, Jul 2011, p. LWB3.

[68] F. G. Walther, G. A. Nowak, S. Michael, R. Parenti, J. Roth, J. Taylor, W. Wilcox, R. Murphy, J. Greco, J. Peters, T. Williams, S. Henion, R. Magliocco, T. Miller, and A. Volpicelli, "Air-to-ground lasercom system demonstration," in *MILITARY COMMUNICATIONS CONFERENCE, 2010 - MILCOM 2010*, Nov 2010, pp. 1594–1600.

[69] H. Henniger and A. Gonzalez, "Transmission scheme and error protection for simplex long-distance atmospheric fso systems," *The Mediterranean Journal of Electronics and Communications*, vol. 2, no. 3, pp. 118–126, Jul 2006.

[70] Telecommunication Standardization Sector of ITU, "Itu-t recommendation g.114: Transmission systems and media : General recommendations on the transmission quality for an entire international telephone connection : One-way transmission time," International Telecommunication Union (ITU), Tech. Rep. G.114, 1994.

[71] IEEE 802.11 Working Group, *Wireless LAN Medium Access Control (MAC) and Physical Layer (PHY) Specifications*, 3 Park Avenue, New York, NY 10016-5997, USA, Mar 2012.

[72] Telecommunication Standardization Sector of ITU, "Itu-t recommendation g.9960: Unified high-speed wireline-based home networking transceivers – system architecture and physical layer specification," International Telecommunication Union (ITU), Tech. Rep. G.9960, Dec 2011.

[73] R. Stuart, "An insert system for use with feedback communication links," *IEEE Transactions on Communications Systems*, vol. 11, no. 1, pp. 142–143, Mar 1963.

[74] R. Benice and A. Frey, "An analysis of retransmission systems," *IEEE Transactions on Communication Technology*, vol. 12, no. 4, pp. 135–145, Dec 1964.

[75] J. Postel, "Internet protocol," Internet Engineering Task Force, Request for Comments 791, Sep 1981, updated by RFCs 1349, 2474.

[76] J. Postel, "Transmission control protocol," Internet Engineering Task Force, Request for Comments 793, Sep 1981, updated by RFCs 1122, 3168, 6093, 6528.

[77] V. Jacobson and R. T. Braden, "Tcp extensions for long-delay paths," Internet Engineering Task Force, Request for Comments 1072, Oct 1988, obsoleted by RFCs 1323, 2018, 6247.

[78] V. Jacobson, R. Braden, and D. Borman, "Tcp extensions for high performance," Internet Engineering Task Force, Request for Comments 1323, May 1992.

[79] M. Mathis, J. Mahdavi, S. Floyd, and A. Romanow, "Tcp selective acknowledgment options," Internet Engineering Task Force, Request for Comments 2018, Oct 1996.

[80] CCSDS Secretariat, "Space communications protocol specification - transport protocol," The Consultative Committee for Space Data Systems, National Aeronautics and Space Administration, Washington, DC 20546, USA, Recommended Standard 2, Oct 2006, cCSDS 714.0-B-2 Blue Book.

[81] IEEE 802. 3 Working Group, *Carrier Sense Multiple Access with Collision Detection (CSMA/CD) Access Method and Physical Layer Specifications*, 3 Park Avenue, New York, NY 10016-5997, USA, Dec 2008.

[82] V. Paxson, M. Allman, J. Chu, and M. Sargent, "Computing tcp's retransmission timer," Internet Engineering Task Force, Request for Comments 6298, Jun 2011.

[83] P. Karn and C. Partridge, "Improving round-trip time estimates in reliable transport protocols," *SIGCOMM Comput. Commun. Rev.*, vol. 17, no. 5, pp. 2–7, Aug 1987.

[84] V. Jacobson, R. T. Braden, and L. Zhang, "Tcp extension for high-speed paths," Internet Engineering Task Force, Request for Comments 1185, Oct 1990, obsoleted by RFC 1323.

[85] G. Combs, "Wireshark," http://www.wireshark.org/, Dec 2017.

[86] Amsterdam Internet Exchange, "Frame size statistics," http://web.archive.org/web/20170809160044/https://ams-ix.net/technical/statistics/sflow-stats/frame-size-distribution, Aug 2017.

[87] R. Palit, K. Naik, and A. Singh, "Anatomy of wifi access traffic of smartphones and implications for energy saving techniques," *International Journal of Energy, Information and Communication (IJEIC)*, vol. 3, no. 1, pp. 1–16, Feb 2012.

[88] T. Bujlow and J. M. Pedersen, "Obtaining application-based and content-based internet traffic statistics," in *Signal Processing and Communication Systems (ICSPCS), 2012 6th International Conference on*, 2012, pp. 1–10.

[89] Netflix Inc., "Internet connection speed recommendations," http://web.archive.org/web/20131206141904/https://support.netflix.com/en/node/306, Dec 2013.

[90] Netflix Inc., "Internet connection speed recommendations," http://web.archive.org/web/20170606171719/https://help.netflix.com/en/node/306, Jun 2017.